AD-A067 289 DREXEL UNIV PHILADELPHIA PA F/G 11/4
CERTIFICATION OF COMPOSITE AIRCRAFT STRUCTURES UNDER IMPACT, FA--ETC(U)
JAN 78 A S WANG N62269-76-C-0378
UNCLASSIFIED NADC-78259-60-PT-3 NL

1 OF 1
AD A067 289

END
DATE FILMED
6-79
DDC

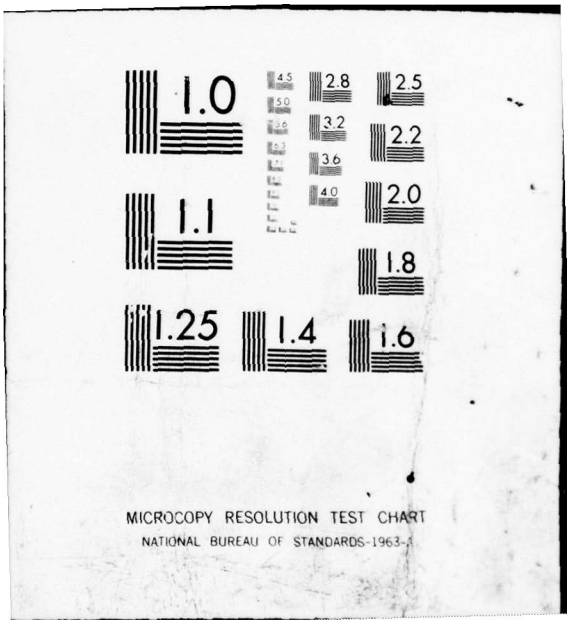
1.0
1.1
1.25
1.4
1.6
1.8
2.0
2.2
2.5
2.8
3.2
3.6
4.0
4.5
5.0
5.6
6.3
MICROCOPY RESOLUTION TEST CHART
NATIONAL BUREAU OF STANDARDS-1963-A

REPORT NO. NADC-78259-60

LEVEL II

12

CERTIFICATION OF COMPOSITE AIRCRAFT STRUCTURES UNDER IMPACT, FATIGUE AND ENVIRONMENTAL CONDITIONS

PART III

ENVIRONMENTAL EFFECTS ON COMPRESSIVE STRENGTH

Albert S. D. Wang
DREXEL UNIVERSITY
Philadelphia, Pennsylvania 19104

JANUARY 1978

FINAL CONTRACT REPORT
1 July 1976 - 31 December 1977
CONTRACT NO. N62268-76-C-0378

APPROVED FOR PUBLIC RELEASE; DISTRIBUTION UNLIMITED

Prepared for
NAVAL AIR DEVELOPMENT CENTER
Warminster, Pennsylvania 18974

NOTICES

REPORT NUMBERING SYSTEM - The numbering of technical project reports issued by the Naval Air Development Center is arranged for specific identification purposes. Each number consists of the Center acronym, the calendar year in which the number was assigned, the sequence number of the report within the specific calendar year, and the official 2-digit correspondence code of the Command Office or the Functional Directorate responsible for the report. For example: Report No. NADC-78015-20 indicates the fifteenth Center report for the year 1978, and prepared by the Systems Directorate. The numerical codes are as follows:

CODE	OFFICE OR DIRECTORATE
00	Commander, Naval Air Development Center
01	Technical Director, Naval Air Development Center
02	Comptroller
10	Directorate Command Projects
20	Systems Directorate
30	Sensors & Avionics Technology Directorate
40	Communication & Navigation Technology Directorate
50	Software Computer Directorate
60	Aircraft & Crew Systems Technology Directorate
70	Planning Assessment Resources
80	Engineering Support Group

PRODUCT ENDORSEMENT - The discussion or instructions concerning commercial products herein do not constitute an endorsement by the Government nor do they convey or imply the license or right to use such products.

APPROVED BY: Edward J. Sturm DATE: 17 November 1978

(12)

UNCLASSIFIED

(19)

REPORT NO. NADC-78259-60-PT-3

(18)

(6)

CERTIFICATION OF COMPOSITE AIRCRAFT STRUCTURES UNDER IMPACT, FATIGUE AND ENVIRONMENTAL CONDITIONS.

PART III.

ENVIRONMENTAL EFFECTS ON COMPRESSIVE STRENGTH.

(9) Final rept. 1 Jul 76 - 31 Dec 77,

(10) Albert S. D. Wang
DREXEL UNIVERSITY
Philadelphia, Pennsylvania

(11) Jan[redacted]78

(12) 93 p.

(15) N62269-76-C-0378

Prepared for
NAVAL AIR DEVELOPMENT CENTER
Warminster, Pennsylvania 18974

UNCLASSIFIED

UNCLASSIFIED

SECURITY CLASSIFICATION OF THIS PAGE (When Data Entered)

REPORT DOCUMENTATION PAGE		READ INSTRUCTIONS BEFORE COMPLETING FORM
1. REPORT NUMBER NADC-78259-60	2. GOVT ACCESSION NO.	3. RECIPIENT'S CATALOG NUMBER
4. TITLE (and Subtitle) Certification of Composite Aircraft Structures Under Impact, Fatigue and Environmental Conditions. Part III-Environmental Effects on Compressive Strength		5. TYPE OF REPORT & PERIOD COVERED Final Contract Report July 1 1976 - Dec. 31 1977 6. PERFORMING ORG. REPORT NUMBER
7. AUTHOR(s) A.S.D. Wang		8. CONTRACT OR GRANT NUMBER(s) N62269-76-C-0378
9. PERFORMING ORGANIZATION NAME AND ADDRESS Drexel University Philadelphia, PA 19104		10. PROGRAM ELEMENT, PROJECT, TASK AREA & WORK UNIT NUMBERS
11. CONTROLLING OFFICE NAME AND ADDRESS Aircraft and Crew Systems Technology Directorate Naval Air Development Center Warminster, PA 18974		12. REPORT DATE January 1978 13. NUMBER OF PAGES 84
14. MONITORING AGENCY NAME & ADDRESS(if different from Controlling Office)		15. SECURITY CLASS. (of this report) UNCLASSIFIED 15a. DECLASSIFICATION/DOWNGRADING SCHEDULE

16. DISTRIBUTION STATEMENT (of this Report)

Approved for Public Release; distribution unlimited.

17. DISTRIBUTION STATEMENT (of the abstract entered in Block 20, if different from Report)

18. SUPPLEMENTARY NOTES

19. KEY WORDS (Continue on reverse side if necessary and identify by block number)

Graphite-Epoxy Composites and Laminates
Compressive Strength
Temperature and Humidity Effects
Microbuckling Failure

20. ABSTRACT (Continue on reverse side if necessary and identify by block number) The compressive behavior of a graphite/epoxy (AS-3501-6) composite system is studied here experimentally and analytically. First, a test method is developed using a flat-end specimen. Tests are then performed for six (6) different composite laminates. In each case, the variation of the test temperature ranges from -12°C to 121°C while the variation of the moisture content in the specimens ranges from dry to saturated-wet. Two cases of dry/wet/dry conditioned specimens are also studied. An analytical model which is based on the concept of microbuckling is developed to predict the compression strength of unidirectional laminates. The analytical results compare well with experiment. The rule-of-mixture method is shown to predict the compressive strength of laminates of complex lay-ups.

DD FORM 1 JAN 73 1473

UNCLASSIFIED

SECURITY CLASSIFICATION OF THIS PAGE (When Data Entered)

Table of Contents

Foreword

This is part III of the final technical report for Contract No. N62269-76-C-0378, which is sponsored by the Naval Air Development Center, Warminster, Pa. The work was performed during the period of July 1, 1976 through December 30, 1977. Mr. Lee W. Gause was the contract monitor.

The contracted study is under the title "Certification of Composite Aircraft Structures under Impact, Fatigue and Environmental Conditions "; parts I and II of the study are under the supervision of Dr. P.C. Chou, while part III is under Dr. A.S.D. Wang, both of Drexel University.

This report concerns the environmental effects on the compressive strength of a graphite-epoxy laminate; both analytical and experimental results are presented and discussed herein.

The author would like to thank Dr. Edward J. McQuillen, Dr. James L. Huang and Mr. Lee W. Gause for the frequent technical discussions. The author would also like to thank Mr. James Alper who helped conducting the experiments.

1. Introduction

Recent years have seen increased attention on the material response of fibrous composites under compressive loads. This is due, in part, to the increased application of composites in primary aircraft structural components. Unlike tensile load which can be taken up by the reinforcing fibers alone, compressive load must be borne by the fiber and matrix together, with the fiber/matrix bonding serving a key link in the load-sharing mechanism. It is known that the mechanical properties of a polymeric matrix are intrinsically susceptible to environmental degradation. Similar degrading characteristics will ultimately manifest themselves in the interface bonding properties and hence the behavior of the composite. The degradation of compressive strength due to temperature and moisture has been one of the major concerns in the application of polymer-based composite systems.

A considerable amount of effort has been devoted during the past decade to the study of compression behavior of composites. A survey of the field however, shows that the state of the art is uncertain. There exists not only the lack of a clear understanding of the load-sharing mechanism between matrix and fiber during loading of the composite, but also the lack of a standard test procedure by which one can establish experimentally the compressive strength of the material.

Early studies have been concerned with the compressive strength of unidirectional composites, i.e. load is applied parallel to the fibers. It is generally acknowledged that Dow and Gruntfest [1] were the first to suggest that local fiber buckling (microbuckling) causes failure of unidirectional composite under compression. Rosen [2] and Schuerch [3] applied this concept to describe microbuckling of fibers using a two-dimensional model of columns on an elastic foundation. For composite systems having high fiber content ($V_f > \cdot 2$), a shear-mode microbuckling usually controls the failure. The critical composite compressive strength depends essentially on the elastic shear modulus of the matrix, G_m:

$$\sigma_c = G_m/V_m \qquad (1)$$

where $V_m = 1 - V_f$, is the matrix volume content.

It has generally been observed that Eq. (1) over estimates experimentally obtained values, sometimes by an order of magnitude. Especially for composites with small-diameter fibers, such as graphite systems, the discrepancy between the theory and experiment is very wide.

Other experimental studies on composites having low fiber shear moduli have observed the formation of an in-plane shear-band (Kink-band) prior to failure [4,5]. By a method of generalized plane stress and an energy argument [6,7,8], the shear-mode of failure is shown to occur when the compressive stress approaches the in-plane shear modulus of the composite, G_{LT}:

$$\sigma_c = G_{LT} \qquad (2)$$

Eq. (2) was earlier derived independently by a Russian author [9]. This result appears to be an improvement over Eq. (1) in that G_{LT} not only reflects the properties of the matrix but also the properties of the fiber.

In addition, if G_{LT} is determined experimentally, it could also reflect the characteristics of the fiber/matrix interface. However, for composites having $G_f >> G_m$, as is generally the case, Eq. (2) reduces to Eq. (1).

In fact, from a recent experiment by Davis [10], there is the evidence that the shear modulus G_{LT} of a boron epoxy system is a function of the axial compressive stress; i.e. G_{LT} decreases as σ_c increases, suggesting a nonlinear behavior. No analytical effort was made to explicitly establish this function, however.

Recognizing the fact that most polymeric matrix systems are highly nonlinear in shear, it was suggested in [3] that G_m in Eq. (1) be replaced by the inelastic tangent shear modulus $\bar{G}_m$ of the matrix. Lager and June [11] tested a boron-epoxy system and found that an arbitrary coefficient of 0.63 must be used to multiply $\bar{G}_m$ in order to forge an agreement between prediction and experiment. This practice however lacks a theoretical foundation.

DeFerran and Harris [12] observed in their experiment using a polyester resin reinforced by steel wires, that the fibers appeared to buckle into a three-dimensional helix rather than a planar curve. They suggested that the result expressed in Eq. (1) could possibly be modified by a three-dimensional microbuckling model. Actually, such an analyses have been attempted by several authors [13,14,15]; but they considered only a single fiber embedded in an infinite matrix. A more realistic case of multiple fibers was considered by Greszczuk [16], who also performed experiments in which aluminum and steel wires were used as reinforcement. Although good correlation was obtained, the analytical result could not be generalized to predict the failure of boron or graphite fibrous systems.

The existence of initial fiber deflection and its effect on composite compressive strength has been investigated by Lanir and Fung [15], Hawasaki and Hasegawa [16] and more recently by Davis [17]. It was found that initial fiber deflection considerably reduces the compressive strength as predicted by either Eq. (1) or Eq. (2). When the matrix nonlinear shear stress-strain relation is also included in the analysis [16,17], the predicted strength agrees more closely with experiments.

But the initial fiber deflection is essentially a statistical quantity; it is not clear how it can be determined conveniently as a basic material property. Davis [17] used a micrographic method and measured the averaged initial fiber deflection of a boron epoxy system. It was found that the ratio between the amplitude and the wave length of the initial deflection is in the order of 10^{-2}.

Compression tests on unidirectional graphite/epoxy composites show several different modes of failure [18], including; end crushing, split by transverse tension, delamination and fiber/matrix debonding, etc. It is not clear, however, whether interface debonding or fiber length-wise cracking precedes fiber microbuckling. It was shown in Ref. [15] that separation of fiber and matrix by transverse tension could occur if the Poisson ratio of the fiber is less than the matrix's. This is certainly the case for most graphite/epoxy systems. It seems also that transverse tension, though secondary in nature, would weaken the fiber/matrix bonding strength which would in turn induce premature shear-mode microbuckling.

This latter inference was recently advanced in a paper by Kulkarni, Rice and Rosen [19], who introduced in their analysis an interface bonding parameter, K. The value of K is bounded by $-(1 - V_f)/V_f$ and 1.

When K equals to the lower bound, it corresponds to the case of total debonding, i.e. the composite is no more than a loose bundle of fibers and hence the compressive strength is essentially null. On the other hand, when K=1, it corresponds the case of perfect bonding. In this case, the compressive strength is predicted by Eq. (2). Kulkarni, et al. reasoned that in actual composites, the parameter K is somewhere in between the bounds, and the compressive strength of the composite is therefore somewhere between zero and G_{LT}. The difficulty in this model is how to determine K which is a measure of the fiber/matrix bonding characteristics. The Kulkarni model does not include the nonlinear shear property of the matrix.

Complicating the development of a unified theory for predicting the compressive strength of unidirectional composites is that there is no generally accepted compression test procedure. Although ASTM has recently issued a test standard [20], various other test methods have simultaneously been developed and used (see [21] for discussion).

Generally speaking, there are two types of compressive test methods which have been widely used: the flat-end specimen and the sandwich beam specimen. And, even among these tests, the geometrical dimensions are not unified. With a given composite system, different test methods usually yield different results. Moreover, the associated mode of failure may also be different. It is probably appropriate to state that the ultimate compressive strength of a composite is not a precise term, but rather, it is primarily one of definition.

This difficulty in identifying a unique way to determine the compressive strength and the associated mode of failure complicates the situation even more since any workable theory must be developed based on the actual mechanism of failure.

The problem of including environmental effects, viz temperature and humidity, has been necessitated by practical requirements. Extensive experiments with controlled temperature and/or humidity have been conducted in recent years in order to establish a design data bank (see, e.g. [22],[23]). However, a predictive model for the compressive strength taking into account environmental factors has not been available, at least in the open literature.

Since a full understanding in the compressive behavior of unidirectional composite is basic to the understanding of composite laminates, it seems that continued effort should be made in studying unidirectional composites.

The objectives of the present work concern the compressive behavior of a graphite/epoxy (AS/3501-6) composite system and its various laminates. Temperature and humidity factors are also included in the study. Emphasis is placed on both experimental and theoretical development. The main features of the present study may be summarized as follows:

1. A test method is developed using a flat-end specimen. This method causes the specimen to fail in the form of transverse splitting which is also associated with end crushing and sometimes shear crippling. The average value for the compressive strength of the U.D. laminate obtained by this method compares well with the results obtained in the literature and other independent tests. The scatter of the test values also falls within ranges found elsewhere.
2. Several lamination patterns were selected for experimentation. These are U.D. laminates, $(0/90)_{2s}$, $(\pm 45)_{2s}$, $(0/90/\pm 45)_s$, $(0/\pm 45/90)_s$ and $(\pm 45/90/0)_s$. These lamination patterns are considered basic elements of more practical laminations, and an understanding of the basic elements will be helpful in understanding the more complicated ones.

3. Variation of temperature ranges from 10°F(-12°C) to 250°F(121°C); humidity conditioning ranges from ambient dry (stored in ambient after curing) to saturated wet. In each case, three to four intermediate temperature and moisture conditionings were selected. Two cases of wet/dry treatments on the test specimens were also selected, to see if wetting causes any permanent damages in the specimens.

4. A nonlinear microbuckling model is developed to predict the strength of the U.D. laminates, including temperature and humidity factors. This model bases on the knowledge of the entire in-plane shear stress-strain curve of the composite, which is derived from the test results of the $(\pm 45)_{2s}$ laminates. In addition, the model assumes fibers alignment imperfection in the form of sinesoidal waves. The amplitude to wave length ratio is a statistical material property, which is determined based on experiment.

   Temperature and/or humidity effects are reflected in the in-plane shear stress-strain curve of the conditioned specimens. In the same light, any possible damage to the fiber/matrix interface and the associated degradation in properties are also expected to manifest themselves in the shear stress-strain curve. It is noted that initial fiber alignment imperfection is independent of environmental condition (except due to residual stresses, the effect of which is considered secondary compared to the applied compressive load).

   The model developed herein is shown to correlate satisfactorily with the experiment, considering the fact that the test method causes different modes of failure and that the test values are scattered.

5. It was found that, for all practical purposes, the rule of mixture theory may be applied to predict the strength of other laminates. This is checked, at least in the three types of quasi-isotropic laminates tested.

In this report, the experiments are described in Chapter 2; the development of the nonlinear mibrobuckling model is presented in Chapter 3. Presentation of the experimental and theoretical results are contained in Chapter 4. A final chapter is included for concluding discussions.

2. Description of Experiment

The scope of experiments in this study program was limited to the following specific aspects:

1. To establish a test procedure which, on one hand, is relatively easy to deploy so that a large number of tests may be processed within a limited time period; and, on the other hand, yields consistent and acceptable test results;
2. To test the specimens in conditioned temperature and humidity environments in order to study hygrothermal effects on the compressive behavior of the specimens. Complete load-displacement curves are recorded, from which complete stress-strain curves are deduced. Temperature variation ranges from -12°C (10°F) to 121°C (250°F) and moisture conditioning ranges from ambient-stored to water saturated. These represent approximately the extreme ranges of anticipated service conditions.
3. To test specimens made of different lamination patterns. (0°) and $(\pm 45)_{2s}$ laminates are considered "basic" laminations. They are tested in relatively large numbers. $(0/90)_{2s}$ laminate is chosen to see the cross-ply effects as manifested by edge stresses and ply-induced residual stresses; three different quasi-isotropic laminates are chosen for the same reasons. In addition, test results from the quasi-isotropic laminates also serve to correlate the results from a predictive model which uses the results from the "basic" laminations. A (90°) laminate is also "basic", but was not tested in this program. Information concerning the compression behavior of (90°) laminates made of the same material system may be found in Ref. [24]. All laminates are of 8-ply symmetric construction.

Material Selection and Specimen Fabrication

The material system chosen for this program is Hercules Magnamite AS/3501-6. It comes in prepreg form, and laminates are fabricated per specified curing processes*. All in-coming material was subjected to a quality-control procedure involving short-beam shear tests and unidirectional tension tests.

The cured specimens displayed a fiber content ranging from 60% to 65%; average ply-thickness was about 0.017 cm (0.0068 inch). The void content of the specimens was not determined. Six (6) laminations were selected: $(0°)$, $(0/90)_{2s}$, $(\pm 45)_{2s}$, $(0/90/\pm 45)_s$, $(0/\pm 45/90)_s$ and $(\pm 45/90/0)_s$, all 8-plies thick.

Test specimens were then cut, using a diamond saw, from cured laminated plates whose size was 30cm x 30cm (1 ft x 1 ft). Such a plate yields approximately 150 test specimens. After cutting a given plate into test specimens, they were then mixed in random and post-cured in an oven at a temperature of 93°C (200°F) for 48 hours. Specimens treated in this manner were considered "reference" specimens. Any subsequent treatments were referred to this "reference" state.

The shape of the test specimen is a flat-ended rectangular coupon of dimensions 1.9cm (0.75 inch) wide, 3.2cm (1.25 inch) high and 0.4cm (0.055 inch) in thickness. Tolerance of geometrical deviation was set at less than 0.0025cm (0.001 inch).

---

* All Q.C. and fabrication routines were conducted using NADC facilities. Cutting of specimens and all tests were conducted at Drexel University.

Test Fixture and Test Procedures

All tests were performed with a closed-loop Instron hydralic test machine which is equipped with an environmental chamber. The chamber can provide a temperature environment from -23°C (-10°F) to 296°C (500°F) with accuracy to within ± 0.5°C (± 1°F).

The test fixture used is a simple, self-aligning device which is depicted in Fig. 1. The flat ends of the specimen rest against a mild-steel pad in order to avoid premature end-crushing during loading. The specimen is wedged tightly at both ends to avoid premature end-blooming. There is only 0.5cm (3/16 inch) unsupported clearance. Thus, structural buckling failure is also avoided. The clearance space facilitates the mounting of strain-gages; in this case, a 1/8 inch-size 90°-rosette was used.

The entire test fixture can be placed inside the environmental chamber, so that the desired temperature/moisture level can be maintained during the test.

All tests were performed with a fixed cross head displacement rate. The rate chosen in this program is 0.025cm/min (0.01 in/min). A typical specimen fails within 30 to 60 seconds.

The environment in the test chamber simulated as closely as possible the environment in which the specimens were pre-conditioned. This was done to minimize possible moisture loss during the time of specimen mounting and loading, which takes five to ten minutes.

Moisture Conditioning

In this study, moisture absorption in a given specimen is assumed "uniform" throughout the specimen. That is, no moisture gradient should exist in the solid. To this end, the following procedures were followed to make sure that moisture content in the solid was "uniform", or at least as "uniform" as possible.

a. for low moisture content: post-cured specimens were placed in an ambient environment of approximately 60% R.H. and 24°C (75°F) room temperature. These specimens were tested after at least four months in ambient. The average moisture gain during this period was approximately 0.05%. Since such a moisture level is very low, it is considered as being essentially dry.

b. for intermediate levels of moisture content: one batch of specimens were placed in an environmental chamber in which the temperature was maintained at 27°C (80°F) and the humidity at 99% R.H. The moisture gain in the specimens was then monitored and recorded periodically until an equilibrium gain was reached. For the one batch of specimens, it took more than 8 weeks to gain an average moisture content of 0.5%.

Similar procedures were followed to treat other two batches of specimens. In one case, the specimens were submerged in 24°C (75°F) water for more than 7 weeks; 0.75% moisture gain was then reached. In the other case, the specimens were stored in an environment with 71°C (160°F) temperature and 90~95% R.H. for more than 15 weeks. A moisture gain of 1% was finally reached.

c. for saturated moisture gain: one batch of specimens was stored in 82°C (180°F) hot water for 10 weeks; the final equilibrium moisture gain averaged about 1.4%. This is considered the maximum possible moisture gain for the material system used.

d. for dry/wet/dry treatments: two batches of specimens were subjected to dry/wet/dry treatments. In one case, post-cured specimens were submerged in 27°C (80°F) water for 7 weeks to gain a moisture content of 0.75%;

they were then dried in 121°C (250°F) oven to rid all the absorped moisture; these specimens were then stored at ambient conditions before being tested. In the other case, post-cured specimens were placed in 180°F hot water until saturation; they were then dried to rid all moisture content, and were stored at ambient conditions before test. In all, there were seven (7) cases of moisture conditioning; namely, ambient dry, 0.5%, 0.75%, 1.0%, 1.4%, dry/wet/dry #1 and dry/wet/dry #2.

Temperature Conditioning

Not all of the seven batches of specimens tested were subjected to the same test temperature levels. For these specimens whose final moisture state was dry or ambient-dry, the following test temperatures were selected: -12°C (10°F), room-temperature (~24°C), 93°C (200°F) and 121°C (250°F). However, for the ambient-dry 0°-laminates only, additional temperature levels of 65°C (150°F) and 149°C (300°F) were also selected; and for dry/wet/dry #2 all laminates were tested at 65°C (150°F).

The remaining specimens, whose moisture contents were equal or greater than 0.5%, were subjected to the following test temperatures: -12°C (10°F), R.T., 65°C (150°F) and 93°C (200°F). By limiting the test temperatures below 100°C (210°F), the desired moisture condition inside the test chamber could be maintained during testing.

Test Matrix

To summarize the above described test parameters, a test matrix is presented in Table 1. It is seen that, in this test program, a total of 169 test cases were conducted. In each test case, an average of 5 specimens were tested resulting in more than 800 individual data points for this test program.

Temp / Moisture	10°F -12°C	R.T.(75°F) 24°C	150°F 65°C	200°F 93°C	250°F 121°C	300°F 149°C
Ambient Dry	All 6 laminations	All 6 laminations	0°-laminates only	All 6 laminations	All 6 laminations	0°-laminates only
0.5% mc	All 6 laminations	All 6 laminations	All 6 laminations	All 6 laminations	None	None
0.75% mc	All 6 laminations	All 6 laminations	All 6 laminations	All 6 laminations	None	None
1.0% mc	All 6 laminations	All 6 laminations	All 6 laminations	All 6 laminations	None	None
1.4% mc	All 6 laminations	All 6 laminations	All 6 laminations	All 6 laminations	None	None
D/W/D #1	All 6 laminations	All 6 laminations	None	All 6 laminations	All 6 laminations	None
D/W/D #2	All 6 laminations	All 6 laminations	All but 0°-laminates	All 6 laminations	All 6 laminations	None

Laminations - (0), $(0,90)_{2s}$, $(\pm 45)_{2s}$, $(0/90/\pm 45)_{s}$, $(\pm 45/90/0)_{s}$, $(0/\pm 45/90)$.

Test Matrix: D/W/D #1 - wet to 0.75%m and then dry to ~0%m.

D/W/D #2 - wet to 1.4%m and then dry to ~0%m.

3. A Nonlinear Shear-Mode Microbuckling Model

Development of Analytical Model for Unidirectional Laminates

The development of the analytical model for unidirectional laminates is based upon the following major assumptions:

1. that the fibers in the composite are not initially straight;
2. that the composite in-plane shear stress-strain relation is essentially nonlinear;
3. that an application of an incremental compressive load amplifies the deflection of the fibers which causes a rise in the in-plane shear-stress; due to the nonlinear nature of shear, a rise in shear stress decreases the shear stiffness, which in turn induces additional fiber deflection under the same compressive load; and
4. that compression failure of the composite occurs at the applied load which causes an unstable increase in fiber deflection.

Additional minor assumptions are also invoked which will be discussed as the development of the theory is presented.

Consider the plane view of a unidirectional composite, whose fibers are initially deflected, Fig. 2. Assume the initial fiber deflection is characterized by

$$y_0(x) = f_0 \sin \frac{\pi x}{\ell} \qquad (1)$$

where f_0 is the amplitude and ℓ is the half wave length of the deflection. Here, the quantity f_0/ℓ is considered a statistical material property which must be given along with other properties such as Young's modulus, Poisson ratio, etc.

When the material is compressed by a uniform compressive stress σ_c, the fiber deflection is then amplified to assume the form

$$y(x,\sigma_c) = f(\sigma_c)\sin\frac{\pi x}{\ell} \tag{2}$$

Here, y depends only implicitly on σ_c.

Now, let us consider the local deformation of a representative composite element when the composite is loaded by σ_c, Fig. 3. The shear strain of the element which is caused as a result of additional fiber deflection, is given by

$$\gamma_{LT} = \frac{d}{dx}(y-y_0), \tag{3}$$

while a balance of moments of the composite element yields

$$dM + Vdx - \sigma_c A_c\, dy = 0 \tag{4}$$

where dM is the induced element bending moment, V is the induced in-plane shear resultant, and A_c is the area of the element on which σ_c is applied.

Assume that the element bending obeys a simple-bending relation,

$$M = -E_c I_c \frac{d^2}{dx^2}(y-y_0) \tag{5}$$

where $E_c I_c$ is the bending rigidity of the element.

For the moment, assume also that shear resultant V can be expressed as

$$V = A_c\, \tau_{LT} = A_c\, G_{LT}\, \gamma_{LT} \tag{6}$$

where τ_{LT} is the in-plane shear stress of the composite element, and G_{LT} is the shear modulus.

Substitution of (1),(2),(3),(5),(6) into (4) yields

$$\frac{f(\sigma_c)}{f_0} = \frac{\sigma_c}{\dfrac{E_c I_c \pi^2}{A_c \ell^2} - \sigma_c + G_{LT}} + 1 \tag{7}$$

Using (7), the amplitude of the in-plane shear stress can be calculated by

$$\tau_{LT} = \left[\frac{\pi G_{LT} \sigma_c}{\dfrac{E_c r_c^2 \pi^2}{\ell^2} - \sigma_c + G_{LT}}\right] \frac{f_0}{\ell} \tag{8}$$

where r_c is the radius of gyration of the composite element, shown in Fig. 3.

At this point, it is recognized that the quantity r_c/ℓ should be several order of magnitude smaller than unity, especially for small diameter fibers such as graphite. Thus, omitting the term with r_c/ℓ, Eq. (8) reduces to

$$\tau_{LT} \sim \frac{\pi G_{LT} \sigma_c}{G_{LT} - \sigma_c} \cdot \frac{f_0}{\ell} \quad . \tag{9}$$

Let us now return to Eq. (6), which assumes a linear shear stress-strain relation. Actual shear behavior, however, is essentially nonlinear, such as depicted by Fig. 4. In what follows, we shall approximate the shear stress-strain curve by piece-wise linear segments, Fig. 4. Within a given linear segment, an incremental increase $\Delta\sigma_c$ corresponds approximately an incremental increase $\Delta\tau_{LT}$ in the following manner:

$$\Delta\tau_{LT} \sim \frac{\pi \bar{G}_{LT}^2}{(\bar{G}_{LT} - \sigma_c)^2} \frac{f_0}{\ell} \Delta\sigma_c \tag{10}$$

where $\bar{G}_{LT}$ is the local slope of the segment.

A computational scheme is then devised as follows:

1. One begins with a small increment of compressive stress $\Delta\sigma_c$, such that only a small shear stress is induced. This shear stress increment is computed using (10), along with the initial shear modulus from the shear stress-strain curve. Let us assume this calculation has advanced the shear stress level in the composite to point A in Figure 4. Now, using a new value of $\bar{G}_{LT}$ determined between points A and B, and increasing σ_c by an additional $\Delta\sigma_c$ the shear stress is increased to point B. Successive iterations in this manner eventually bring up the shear stress to point F, where the state of stress in the composite results in a shear-mode micro-instability.
2. In each load increment, similar computations may be carried out for the accumulative deflection $f(\sigma_c)$ in (7). As the computation progresses to point F in Fig. 4, the value of f will increase indefinitely without additional increase of σ_c. When this occurs the composite has microbuckled and thus defines the ultimate σ_c which can be applied to the composite, see Fig. 5.

Of course, if we regard $\bar{G}_{LT}$ in (10) as the tangent shear modulus and if we can express $\bar{G}_{LT}$ in terms of τ_{LT}, Eq. (10) may be integrated directly along the shear stress-strain curve for σ_c ultimate. The computational scheme described in the proceeding is essentially a piece-wise integration procedure.

It is noted that the foregoing derivation gives the Rosen [2] result directly when fiber initial deflection is infinitesimal (see Eq. (9)); that is, shear-mode deformation occurs when $\sigma_c \to G_{LT}$.

In actual composites, however, the quantity f_0/ℓ is finite. Davis [17] for example, found for a Boron/Epoxy System, the value of f_0/ℓ is in the order of 10^{-2}. It is conceivable that for graphite fibers whose diameter is much smaller than boron's, the value of f_0/ℓ is at least equal or greater than 10^{-2}.

The advantage of including the fiber imperfection is that it enables the computational model to incorporate the instantaneous nonlinear shear behavior of the composite. And, in turn, the composite shear behavior can reflect not only the properties of the fiber, the matrix, the fiber/matrix interface, but also the effects of environmental factors which so far have not been included explicitly in the analytical model.

Thus, the model relies on two types of material input; the quantity f_0/ℓ and the complete shear stress-strain curve of the unidirectional composite. From Eq. (8), it is seen that the value of f_0/ℓ is crucial in the evaluation of the induced shear stress level, which is in turn crucial in defining the value of the local shear modulus. But, unfortunately, f_0/ℓ is, at best, a statistical quantity and it is not clear how it may be defined for a given composite. The determination of the complete in-plane shear stress-strain behavior, including variations of environmental conditions, presents practical difficulties. In what follows, we shall describe briefly how these difficulties were handled in this study.

Determination of Initial Fiber Deflection and Composite Shear Property.

In this study, the U.D. lamina shear stress-strain curves were generated from uniaxial compressive tests on $(\pm 45°)_{2s}$ laminates.

The accuracy of this approach has been discussed by Hahn [25] where it is shown that for a $\pm$ 45°-laminate loaded axially, the tangent (local) shear modulus of the lamina (in the principal material coordinates LT) may be approximated by:

$$\bar{G}_{LT} \doteq \frac{\bar{E}_x}{2(1 + \bar{\nu}_{xy})} \tag{11}$$

provided that the laminate Poisson ratio $\bar{\nu}_{xy}$ remains constant throughout the loading history.

In Eq. (11), $\bar{E}_x$ is the local axial modulus of the $\pm$ 45°-laminate when loaded in the axial x-direction. Thus, the complete stress-strain curve obtained by testing the $\pm$ 45°-laminate axially can be inverted directly to obtain a complete shear stress-strain curve for the U.D. lamina, noting

$$\tau_{LT} = \frac{1}{2} \sigma_x$$

$$\gamma_{LT} = e_x - e_y.$$

In order to define $\bar{\nu}_{xy}$, it is also necessary to measure the transverse strain e_y as a function of σ_x. In the present study, the value of $\bar{\nu}_{xy}$ found for all cases tested ranged from 0.92 to 0.98.

Once the complete U.D. lamina shear stress-strain curve is obtained under a given environmental condition, say ambient dry, one can use the analytical model to calculate the compressive strength of the U.D. lamina by assuming a value for f_0/ℓ.

To determine f_0/ℓ, tests on unidirectional lamina under compressive axial load were performed and a statistical mean value for the ultimate σ_c was obtained. Next, a value for f_0/ℓ was selected by trial-and-error such that the predicted σ_c agreed with the experimental σ_c. This value of f_0/ℓ was then regarded as a material property of the composite system regardless of whatever subsequent environmental conditions the composite may be exposed to.

In the present study, f_0/ℓ was determined using the results of a shear stress-strain curve generated by compressing seven replicas of $(\pm 45°)_{2s}$ specimens and the statistical mean σ_c of nine replicas of 0°-laminates. All tests were performed for ambient-dry conditioned specimens in room temperature. It should be noted that little, if any, scatter in results was found for the seven $\pm$ 45°-specimens, while some scatter was present in the results for the nine 0°-laminates. The latter scatter, however, was comparable to the 0°-tensile scatter for the same composite system [26].

The value of f_0/ℓ found in this study is 0.0108, which is in the same order of magnitude as that determined for a boron/epoxy system by Davis [17].

4. Discussion of Results

Mode of Failure

In the present study, there were six categories of laminates which were tested under various temperature and humidity conditions. For each category of laminates, regardless of their environmental conditioning history, the compression failure appearances were similar. No effort, however, was made in this study to examine the failure surfaces using any electronic and/or optical instruments. Thus, it is not possible to describe with certainty the exact modes under which the various specimens failed.

Fig. 6 through Fig. 8 show the typically failed specimens for each of the six categories of laminates. In the case of the 0°-laminates, it is seen that the final appearance of failure is one of end-crushing and transverse fiber splitting. Failure of these specimens occurred rather suddenly without any noticeable pre-failure weakening. The axial stress-strain curve is essentially linear all the way to failure, although some softening of the material was detected when failure was imminent. This softening phenomena occurred early for those specimens tested under higher temperature and/or with higher moisture content. Thus, it is not known whether end-crushing or fiber splitting occurs first in the process of failure. In the analytical model, however, fiber splitting is preferred. In this case, it may be postulated that the splitting action is a result of the elastic microbuckling of the fibers (although the model is based on a nonlinear shear behavior of the composite, the fibers are considered elastic throughout the loading history).

The second picture in Fig. 6 shows the typical final failure appearance of the $(\pm 45°)_{2s}$ laminates. Surface ply-delamination and surface ply-shearing along fibers are observed. With this particular laminate type, the axial compressive behavior is one of excessive ductility, see Fig. 9, for example. In this case, surface ply-shearing along fibers usually occurs while the load is ascending; surface ply-delamination appears when final failure is imminent. Between the first ply-shearing and the final delamination the applied load can, sometimes, increase a little and, other times, decrease some depending on the environmental condition of the specimens. However, the corresponding axial strain can be as large as $40\text{x}10^{-3}$ to $50\text{x}10^{-3}$. Since the axial stress-strain curves of the $(\pm 45)_{2s}$ laminates can be readily converted into the in-plane shear stress-strain curves for the U.D. lamina, see Eq. (11), the highly nonlinear nature shown by the curves in Fig. 9 reflects essentially the highly nonlinear nature of the shear behavior of the U.D. lamina.

The first picture in Fig. 7 depicts a typical failed specimen of the $(0/90)_{2s}$ laminates. Extensive delamination and fiber breakage are seen to occur within the gage-section of the specimen. Delaminations within a single ply are observed throughout the thickness of the specimen. This failure mode may be explained by the presence of a σ_z edge stress (see, e.g., Wang and Crossman [27]). This particular edge stress effect definitely influences the compressive strength of the specimen, as will be discussed later in this section. However, one cannot be certain about the exact degree of influence this edge stress effect possesses.

Pictures in Fig. 7(b), and Fig. 8 show failed specimens for the three types of quasi-isotropic laminates. It is seen that all had failure occur within the gage-section of the specimen, although in the two cases where the 0°-ply is on the outside surface, there is also surface ply-delamination.

Further more, in these two cases, surface ply-delamination occurred before failure, and a somewhat decreased load continued to be carried by the rest of the plies, resulting in somewhat greater ductility. This is not the case, however, for the other type of laminate with the $\pm$ 45° plies on the outside. There the failure occurred rather suddenly with a higher strength than the other two. This latter observation may also be explained by edge stress effects [27].

Compression Behavior of $(\pm 45°)_{2s}$ Laminates

Figures 9 through 15 show the axial stress-strain curves for the $(\pm 45°)_{2s}$ laminates that were subjected to seven different moisture conditionings. In each case four or five temperature levels were selected beginning from -12°C (10°F). Aside from the material nonlinearity which was exhibited more or less in all cases shown, other features also deserve discussion. It should first be pointed out that each of the curves shown in these seven figures represents the typical results obtained from at least five (sometimes seven) specimens. No noticeable scatter was observed in the test results and therefore each of the curves is essentially reproducible.

1. Temperature effect: the fact that temperature softens the material stiffness and decreases the ultimate load-carrying capacity of the specimen is generally valid in all moisture-treated cases; the influence on the load-carrying capacity is perhaps the more pronounced one. Clearly, temperature increases the nonlinearity response of the laminate. Temperature also has a subtle effect on the failure mode. See, for example, the curves associated with -12°C (10°F). Load-bearing capacity of the specimens increases sharply to a maximum value, at which point surface

ply-shearing along fibers is observed to occur, and it then decreases rather significantly to a lower value when final failure occurs with additional surface delamination. This phenomena disappears when test temperature increases beyond room temperature.

This peculiar behavior associated with cold temperature may be attributed to the fiber/matrix interface stiffening caused by the low temperature.

2. Moisture effects: Comparisons of the curves shown in Fig. 9-13 also reveal the effects of moisture. In general, an increase in moisture content in the specimen both softens the material stiffness and lowers somewhat the load bearing capacity, although there are a couple of cases where the stiffness and/or strength are slightly increased by humidity. It is not clear whether or not this slight deviation is actually experimental error. The suggestion that moisure absorption has an equivalent effect as temperature exposure seems to be applicable.

Further, the load increase and then decrease phenomena which was seen in the drier specimens under cold temperature e.g. -12°C (10°F), is seen to disappear when moisture content is increased. This too is similar to the increase of temperature. No effort was made however, to determine numerically the equivalence between the humidity and temperature effects.

In order to answer the question of whether moisture exposure actually damages the integrity of laminated structure, let us examine the two cases shown in Fig. 14 and 15. The dry/wet/dry No. 1 refers to specimens that absorbed 0.75% of moisture and were then dried;

dry/wet/dry No. 2 refers to specimens that had 1.4% (saturated) moisture and were then dried. It is seen that curves in D/W/D No. 1 compare closely with those originally dry specimens, shown in Fig. 8. All features that are unique to this situation are preserved. On the other hand, D/W/D #2 specimens show noted difference in the ultimate load-carrying capacity and a slight but noticeable decrease in the stiffness. These combined conditions influence the ultimate compressive strength of the U.D. lamina, which will be discussed later. Thus, it appears that the D/W/D #2 specimens have been damaged by moisture exposure.

The above results are summarized in Fig. 16 and 17. It is seen that the influence on strength by humidity treatment is insignificant as compared to the influence by temperature, Fig. 16. The influence of humidity on the stiffness of the laminates is significant, Fig. 17, which displays the initial axial modulus E_1 as influenced both by moisture and temperature. Under colder temperature, there exists a wide difference between dry and wet specimens. The difference narrows, however, as temperature increases beyond 65°C (150°F).

Compression Behavior of 0°-Laminates

Experimental results obtained for the compressive strength of 0°-laminates that were tested under the seven different moisture conditionings are shown in Fig. 18 through Fig. 24. In the case of ambient-dry specimens, six temperature levels ranging from -12°C (10°F) to 149°C (300°F) were selected. This was done to check the analytical microbuckling model in a wider temperature range. For the remaining six moisture cases, only four temperature levels were selected. In general, three to five replica specimens were tested; their averaged values and their range of scatter are shown in the figures. In the case of ambient-

dry specimens tested under room temperature, nine replicas were used in order to make certain that the averaged value obtained represents reasonably well the statistical mean value of the compressive strength.

The scatter in the compressive strengths under a given test condition appears to be quite large. However, when compared to the tensile strength distribution of the same material system [26], the compressive strength scatter is about the same as in the tension strengths. This lack of uniformity is thought to be caused by material imperfections rather than the method used in conducting the experiments.

Temperature effect on the compressive strength is considerable. From room temperature to 121°C (250°F), the strength may decrease by 30%. This degrading effect is enhanced with moisture content. The effect of moisture absorption on the compressive strength is also significant. This is in contrast with the $(\pm 45°)_{2s}$ laminates where moisture has only a minimal effect on the strength but a larger effect on the stiffness.

These two effects are best observed in the display in Figs. 25 and 26. In Fig. 25, it is also seen that specimens subjected to moisture saturation appear to have been damaged, since a drying process did not return the specimens to the performance level of the un-treated specimens. Fig. 26 shows the σ_c versus moisture content relation when temperature is held constant. It is seen that moisture absorption can reduce noticeably the compressive strength.

The effects of temperature and/or moisture on the stiffness of the 0°-laminates was minimal. The only exception is the group of specimens which were moisture saturated ($m \sim 1.4\%$), see Fig. 27. The stiffness of this group was not influenced by temperature. It is not clear what mechanism causes the

decrease in stiffness. It should be recalled that the moisture saturated 45°-laminates also had a noticeable stiffness degradation due to moisture absorption. It is possible that the fiber/matrix interface bonding is weakened by excessive moisture absorption, so that premature fiber-buckling takes place resulting in structural stiffness degradation in the laminate.

Let us now return to the analytical microbuckling model developed earlier. From the axial stress-strain curves obtained for the $\pm$ 45°-laminates, lamina shear stress-strain curves were calculated for each of the seven moisture-treatments and the various temperature test conditions (i.e., from the curves in Figs. 9-15). A value for f_0/ℓ (see Eq. (7)) was then selected, in this case $f_0/\ell = 0.0108$, such that the computed room temperature compressive strength for the ambient-dry specimens agrees with the averaged value obtained experimentally, (see Fig. 18). This $f_0/\ell = 0.0108$ value was used in predicting the theoretical compressive strengths for all test cases. The comparisons between theory and experiment are depicted in Fig. 18 through Fig. 24. The agreement between theory and experiment is satisfactory, considering the scatter of the experimental results. Again, the only exception is the case of the moisture saturated specimens where the prediction over-estimates the experiment by about 40%.*

3

---

* The analytical model tends to over-estimate the strength of specimens conditioned under high temperature (65°C and above) and with some moisture absorption. It is suspected that the lamina shear stress-strain curves derived from the ($\pm$ 45°) laminates may be inaccurate; or at least, it is not accurate enough under high temperature and humidity conditions.

Compression Behavior of $(0/90)_{2s}$-Laminates

Results for the $(0/90)_{2s}$ laminates are presented in Fig. 28 through Fig. 34. In general, increasing temperature reduces the strength, except under very low temperature, see, e.g., Fig. 28. A combined edge effect and thermal residual stress effect is blamed for the lower compression strength at low temperature (see, e.g., discussions in [28]). This combined effect existed in all moisture conditioned specimens.

Moisture increase lowers uniformly the compressive strength. Notice the excessive drop in strength for the case of moisture saturated specimens, Fig. 33. The degrading effect of moisture tends to be minimized by increase of temperature.

Notice also the considerable scatter in strength caused by various moisture treatments. The scatter narrows, however, at higher temperature. This, too, may be attributed to the edge/residual thermal stress effects, which complicate the failure mechanisms. At higher temperature, these effects are reduced.

As for the stiffness of the $(0/90)_{2s}$ laminates, temperature does not seem to have any noticeable effect. The effect of moisture is also insignificant, except in the case of moisture saturated specimens whose stiffnesses are uniformly lower. This pattern is consistent with the previously discussed $(\pm 45°)_{2s}$ and 0°-laminates.

To attempt to predict the strength of the $(0/90)_{2s}$ laminates, the simple rule-of-mixture was used. Since the compressive data for a pure 90°-laminate was not compiled in this program, we used the results generated by Verette [24], who tested 90°-laminates made of the same AS/3501 graphite/epoxy system. Fig. 35 shows the Verette results for ambient dry and moisture

saturated cases. The contribution to compression strength of the 90°-lamina for various moisture streatments may be extrapolated between the curves in Fig. 35.

It is seen that the rule-of-moisture predicts rather well the strength of the (0/90) laminates, except for low temperature conditions. The lower temperature results could be accommodated if the edge effect and the thermal residual stress effect were included in the prediction.

It is also noted that the prediction by rule-of-mixture in this case is based primarily on the results of the 0°-lamina. The curves shown in Figs. 28 through 32 are calculated using the predicted strength for the 0°-lamina rather than the actual experimental values for the 0°-lamina. Recall that the predictions for the 0°-lamina under moisture saturated conditions were higher than from the experiments. The same discrepancy between theory and experiment is again evident in the results for the (0/90) laminates under the same moisture condition, Fig. 32. But, when the experimental values for the 0°-lamina are used in the rule-of-mixture calculation, the agreement is almost perfect, Fig. 32.

Compression Behavior of Quasi-isotropic Laminates

Experimental results for the three types of quasi-isotropic ($\pi/4$) laminates are shown in Fig. 36 through Fig. 46. Strength versus temperature plots for the various moisture treatments are depicted in Figs. 36 to 40. It is seen that the degrading effects of temperature and moisture are noticeable but not great. Some edge effect and thermal residual stress effects are also present at the low temperature test condition. Edge effects can be seen from the differences in strength for the three types of laminates.

It appears that $(0/90/\pm 45)_s$ has the lowest compressive strength and $(\pm 45/90/0)_s$ the highest. This difference in strength disappears when the temperature is increased beyond 65°C (150°F). It is interesting to note that an independent test in tension indicates tensile strength difference in the three types of laminates, with the order in strength reversed.

Use of the rule-of-mixture, by considering the 0°, 90°, and $\pm$ 45° laminae as basic elements, yields good agreement with the experiment in this case. Of course, the rule-of-mixture does not recognize the lamination sequence and differences due to lamination sequence (edge effect) do show in the experimental data.

Figs. 41, 42, and 43 summarize the averaged experimental values of the compressive strength for the three types of laminates. It is seen that the strengths of the laminates are sensitive to the moisture treatment only at temperatures equal to or lower than room temperature.

Figs. 44, 45 and 46 depict the averaged experimental values of the axial stiffness E_1 for the three types of laminates. Here again, the influence of temperature is minimal, while the influence of moisture is significant only for the case of moisture saturation.

5. Conclusions

In this report, we have presented the results of a comprehensive experimental program in which the compression behavior of some basic composite laminates was examined under a wide range of environmental conditions. A nonlinear microbuckling model was developed to predict the compressive strength of a unidirectional laminate. It was also found that the rule-of-mixture is generally applicable for other types of laminates, except in a few special cases where edge effects and thermal residual stress are important.

Experimental determination of the lamina shear stress-strain curve by testing a $\pm$ 45°-laminate in compression is generally satisfactory, although the accuracy of this approach is open to question when high temperature and moisture are present in the specimen. This aspect needs further examination.

The assumption of initial fiber deflection in the lamina is justified, but the determination of this deflection for this report was empirical. Confirmation of the existence of this initial deflection and its statistical magnitude needs further research.

Experimental failure modes in the unidirectional lamina do not indicate explicitly fiber microbuckling as it was assumed in the predictive model; nor do they preclude such a failure mode.

Despite these uncertainties, the fact that the predictive model yielded good agreement with a large number of test cases (total 30 cases with more than 120 specimens) tends to support the fiber microbuckling assumption.

The microbuckling model presented in this report does not include explicitly the parameters of temperature and moisture. Rather, these factors are implicit in the lamina shear stress-strain relation which serves as input information in the calculation. It is conceivable, as a future research subject, that the shear stress-strain relations generated under various temperature/moisture test conditions may be represented by a single master curve with temperature/moisture shift functions built in. This approach has been shown applicable in some viscoelastic behavior of composites [29]; it is also worthwhile trying in this case.

The test fixture used in the present study is, for all practical purposes, satisfactory.

References

[1] Dow, N.F. and Gruntfest, I.J., "Determination of Most Needed Potentially Possible Impreovements in Materials for Ballistic and Space Vehicles," TIS 60SD389. General Electric Co., Space Science Lab., Valley Forge, Pa. (1960).

[2] Rosen, B.W., "Mechanics of Composite Strengthening," in Fiber Composite Materials. Chapt. 3, Amer. Soc Metals (1965).

[3] Schuerch, H., "Prediction of Compressive Strength in Uniaxial Boron Fiber, Metal Matrix Composite Materials," AIAA Jour. Vol. 4, (1966) p. 102.

[4] Zaukelis, D.A., "Observation of Slip in Nylon 66 and 610 and Its Interpretation in Terms of A New Model," Jour. Appl. Phys., Vol. 33 (1962), p. 2797.

[5] Seto, T. and Tajima, Y., "Observation of Kink Bands in Oriented Polyethylene," Japan Jour. Appl. Phys., Vol. 5 (1966) p. 534.

[6] Foye, R.L., "Compression Strength of Unidirectional Composites," AIAA Paper No. 66-143 (1966).

[7] Chung, W. and Testa, R.B., "The Elastic Stability of Fibers in A Composite Plate," Jour. Comp. Matls., Vol. 3 (1969) p. 58.

[8] Greszczuk, L.B., "Analysis of the Test Methods for Unidirectional Composites," ASTM STP 521 (1973).

[9] Guz, O.M., "Determination of A Theoretical Ultimate Compression Strength of Reinforced Materials," FTD-HC-23-197-70, Translated from Russian, Foreign Tech. Div. WP-AFB, Dayton, Ohio (1970).

[10] Davis, J.G., "Compressive Instability and Strength of Uniaxial Filament-Reinforced Epoxy Tubes," NASA TN D5697 (1970).

[11] Lager, L.R. and June, R.R., "Compressive Strength of Boron-Epoxy Composites," Jour. Composite Matls., Vol. 3 (1969) p. 48.

[12] DeFerran, E.M. and Harris, B., "Compression Strength of Polyester Resin Reinforced with Steel Wires," Jour. Composite Matls., Vol. 4 (1970) p. 62.

[13] Sadowsky, M.A., Pu, S.M. and Hussain, M.A., "Buckling of Microfibers," Jour. Appl. Mech. Vol. 34 (1967) p. 1011.

[14] Herrman, L.R., Mason, W.E. and Chan, S.T., "Behavior of Compressively Loaded Reinforcing Wires," Jour. Comp. Matls., Vol. 1 (1967) p. 212.

[15] Lanir, J. and Fung, Y.C.B., "Fiber Composite Columns Under Compression," Jour. Comp. Matls., Vol. 6 (1972) p. 387.

[16] Hanasaki, S. and Hasegawa, Y., "Compressive Strength of Unidirectional Fiber Composites," Jour. Comp. Matls., Vol. 8 (1974) p. 306.

[17] Davis, J.G., "Compressive Strength of Fiber-Reinforced Composite Materials," ASTM STP 580 (1975) p. 364.

[18] Greszczuk, L.B., "Failure Mechanics of Composites Subjected to Compressive Loading," AFML-TR-72-107 (1972).

[19] Kulkarni, S, Rice, J, and Rosen, B., "An Investigation of the Compressive Strength of Kevlar 49/Epoxy Composites," Composites Vol. 6, (1975) p. 217.

[20] "Standard Method of Test for Compressive Properties of Oriented Fiber Composites," ASTM, Designation #D3410-75,

[21] Ryder, J.T., "Ascertainment of the Effect of Compressive Loading on the Fatigue Life-Time of Graphite Epoxy Laminates for Structural Applications." AFML-TR-76-241 (1976). p. 27.

[22] Hofer, K.E., Larson, D. and Humphreys, V.E., "Development of Engineering Data on the Mechanical and Physical Properties of Advanced Composite Materials." AFML-TR-74-266 (1975).

[23] Shen, C.H. and Springer, G.S., "Environmental Effects on the Elastic Moduli of Composite Materials," Jour. Comp. Matls., Vol. 11 (1977) p. 249.

[24] Verette, R.M., "Temperature/Humidity Effects on the Strength of Graphite/Epoxy Laminates," Jour. Aircraft, Vol. 14 (1977), p. 90.

[25] Hahn, H.T., "A Note on Determination of the Shear Stress-Strain Response of Unidirectional Composites," Jour. Comp. Matls., Vol. 7 (1973), p. 383.

[26] Chou, P.C., "Statistical Failure Analysis of Composite Materials," in Mechanics of Composite Review, (1977) Bergamo Center, Dayton, Ohio p. 124.

[27] Wang, A.S.D. and Crossman, F.W., "Some New Results on Edge Effects in Symmetric Composite Laminates," Jour. Comp. Matls., Vol. 11 (1977) p. 92.

[28] Wang, A.S.D. and Crossman, F.W., "Edge Effects on Thermally Induced Stresses in Composite Laminates," Jour. Comp. Matls., Vol. 11 (1977) p. 301.

[29] Wang, A.S.D. and Liu, P.K., "Humidity Effects on the Creep Behavior of An Epoxy-Graphite Composite," AIAA Jour. Vol. 14 (1977), p. 383.

List of Figures

21 Compressive strength versus temperature with 1.0% moisture content; 0°-laminates

22 Compressive strength versus temperature with 1.4% moisture content; 0°-laminates

23 Compressive strength versus temperature-Dry/wet/dry No. 1 0°-laminates

24 Compressive strength versus temperature-Dry/wet/dry No. 2 0°-laminates

25 Compressive strength versus temperature-All moisture conditions 0°-laminates

26 Compressive strength versus moisture content-All temperatures; 0°-laminates

27 Stiffness E_1 versus temperature-All moisture conditions; 0°-laminates

28 Compressive strength versus temperature-ambient dry condition; $(0/90)_{2s}$

29 Compressive strength versus temperature-with 0.5% moisture content; $(0/90)_{2s}$

30 Compressive strength versus temperature-with 0.75% moisture content; $(0/90)_{2s}$

31 Compressive strength versus temperature-with 1.0% moisture content; $(0/90)_{2s}$

32 Compressive strength versus temperature-with 1.4% moisture content; $(0/90)_{2s}$

33 Compressive strength versus temperature-all moisture conditions; $(0/90)_{2s}$

34 Stiffness E_1 versus temperature-all moisture conditions; $(0/90)_{2s}$

35 Compressive strength versus temperature - 90°-laminates.

36 Compressive strength versus temperature-Ambient dry condition; $\pi/4$ laminates

37 compressive strength versus temperature-with 0.5% moisture content; $\pi/4$ laminates

38 Compressive strength versus temperature-with 0.75% moisture content; $\pi/4$ laminates

39 Compressive strength versus temperature-with 1.0% moisture content; $\pi/4$ laminates

40 Compressive strength versus temperature-with 1.4% moisture content; $\pi/4$ laminates

Figure

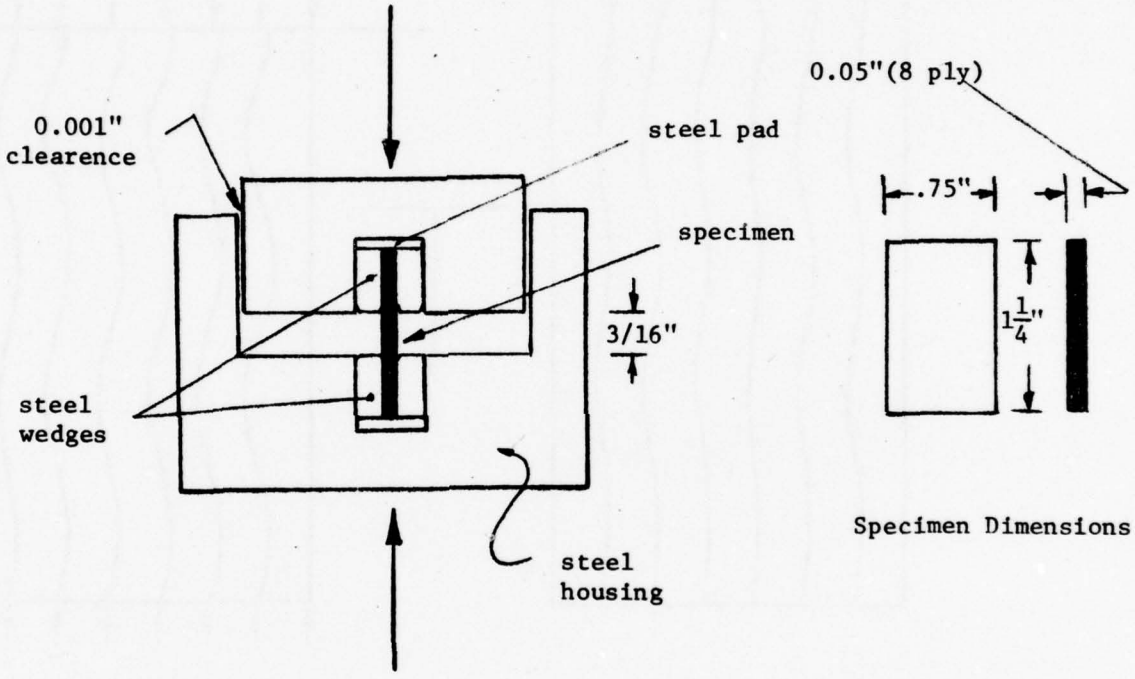

Front-view of Test Fixture

1" = 2.54 cm

Fig. 1 Compression Test Fixtures

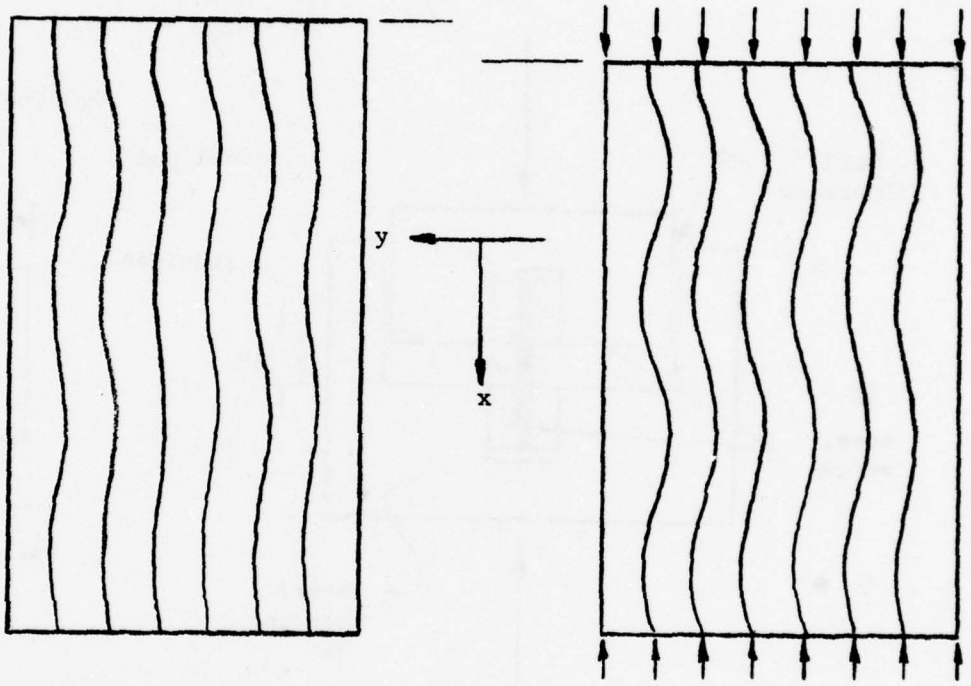

Fig. 2 U. D. Composite With Initial Fiber Deflection

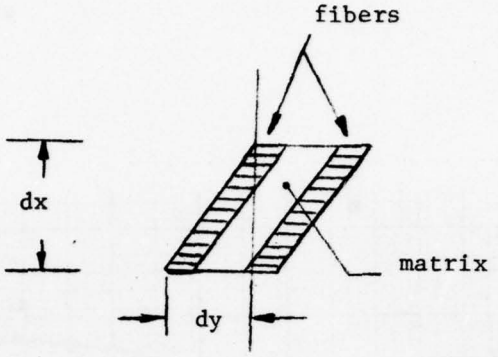

(A)

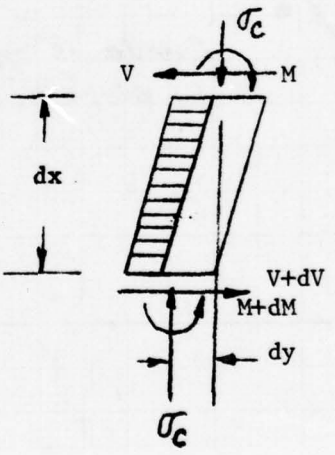

(B)

Fig. 3 Local Load-deformation Relations;
(a) Shear Deformation of A Composite Element.
(b) Force Equilibrium of A Composite Element.

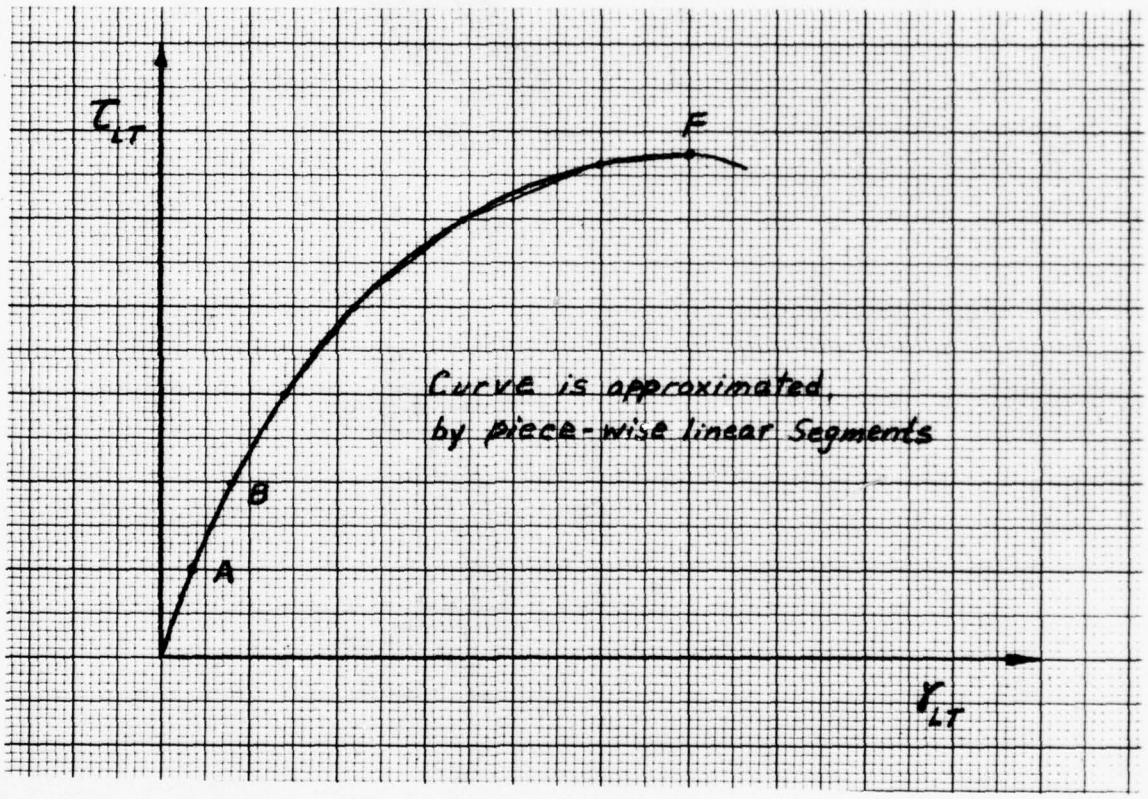

Fig. 4 A Hypothetical Shear Stress-strain Curve for U.D. Composite

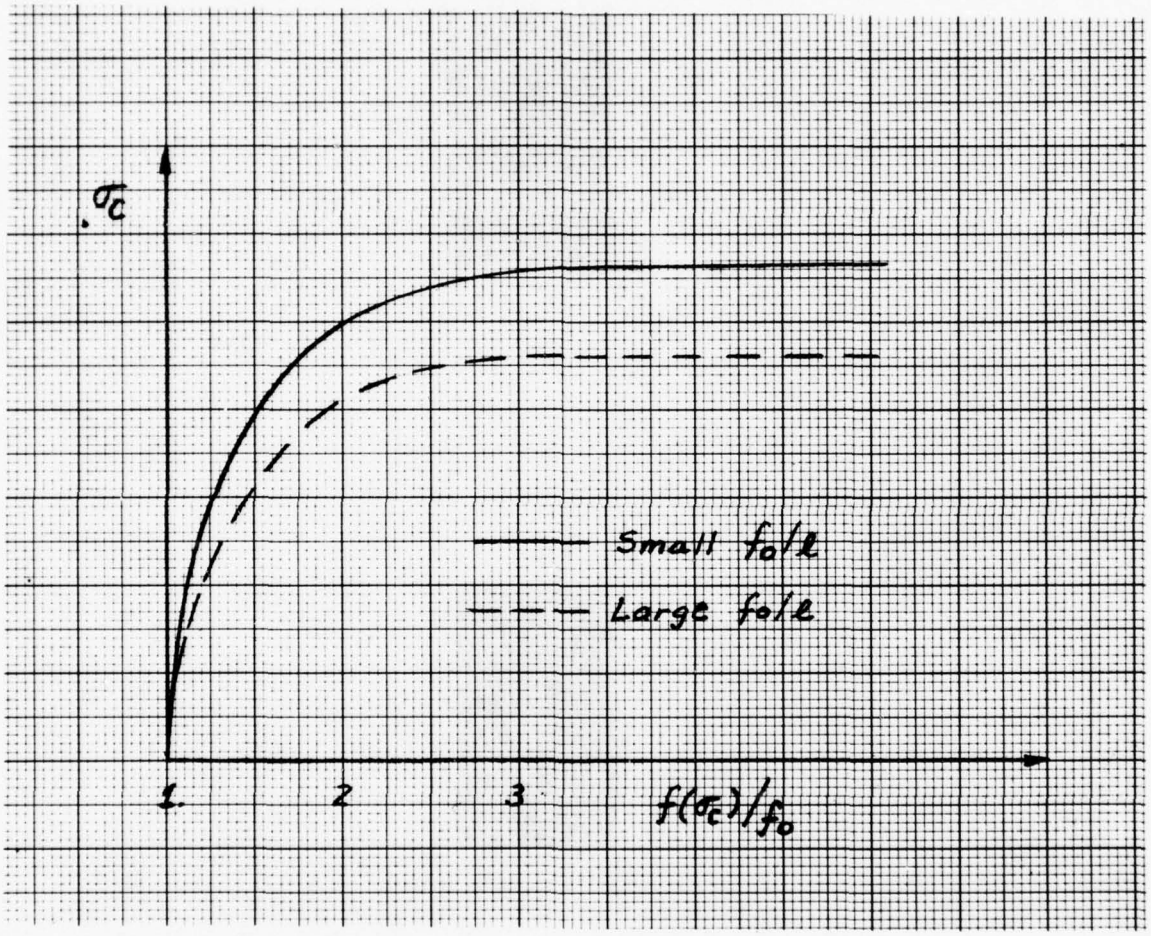

Fig. 5 A Hypothetical σ_c versus Lateral Fiber Deflection

AA1 (0° 8plies)

AA2 $(\pm 45)_{2s}$

Fig. 6 Final Failure Appearance; (a) 0°-laminate, and (b) $(\pm 45)_{2s}$ laminate.

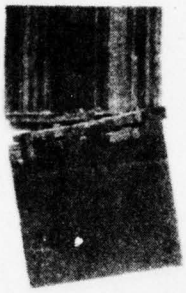

AA3 $(0/90)_{2s}$

B1 $(0/90/\pm45)_{s}$

Fig. 7 Final Failure Appearance; (a) $(0/90)_{2s}$ laminate, and (b) $90/90/\pm45)_{s}$ laminate.

B2 $(0/\pm 45/90)_s$

B3 $(\pm 45/90/0)_s$

Fig. 8 Final Failure Appearance; (a) $(0/\pm 45/90)_s$ laminate, and (b) $(\pm 45/90/0)_s$ laminate.

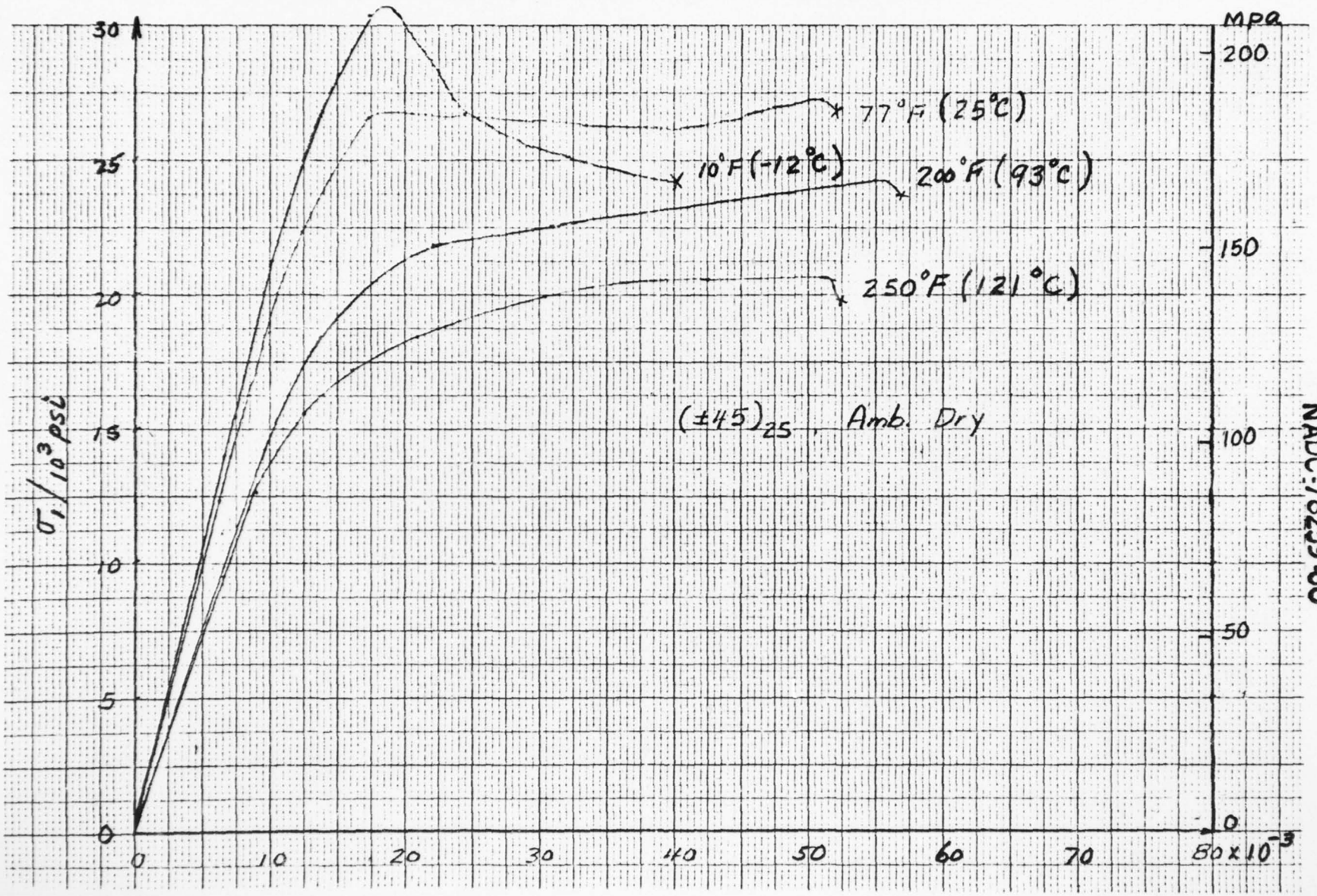

Fig. 9 Axial Stress-strain Curves for $(\pm 45)_{2s}$ Laminates Under Various Temperatures.

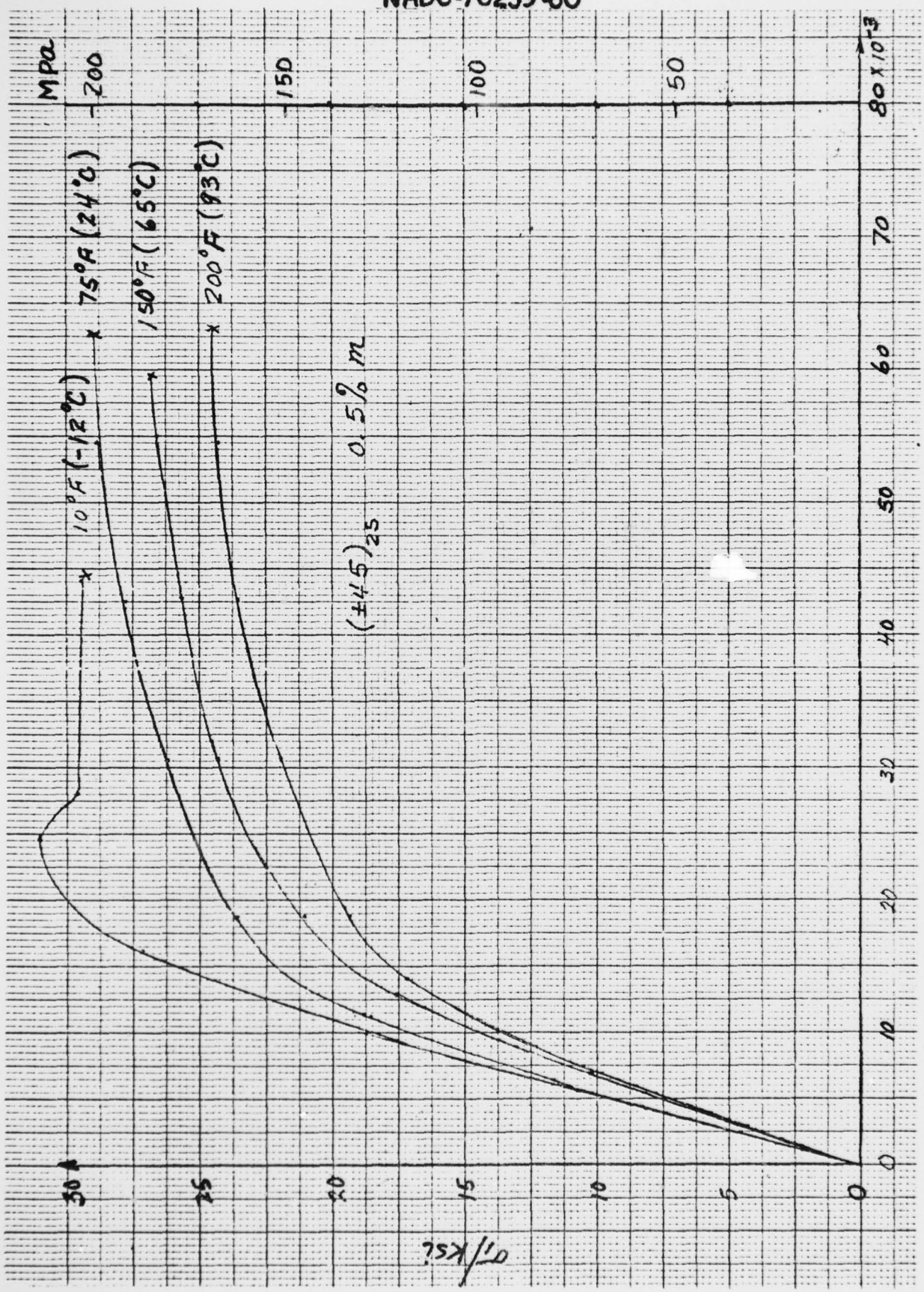

Fig. 10 Axial Stress-strain Curves for $(\pm 45)_{2s}$ Laminates Under Various Temperatures.

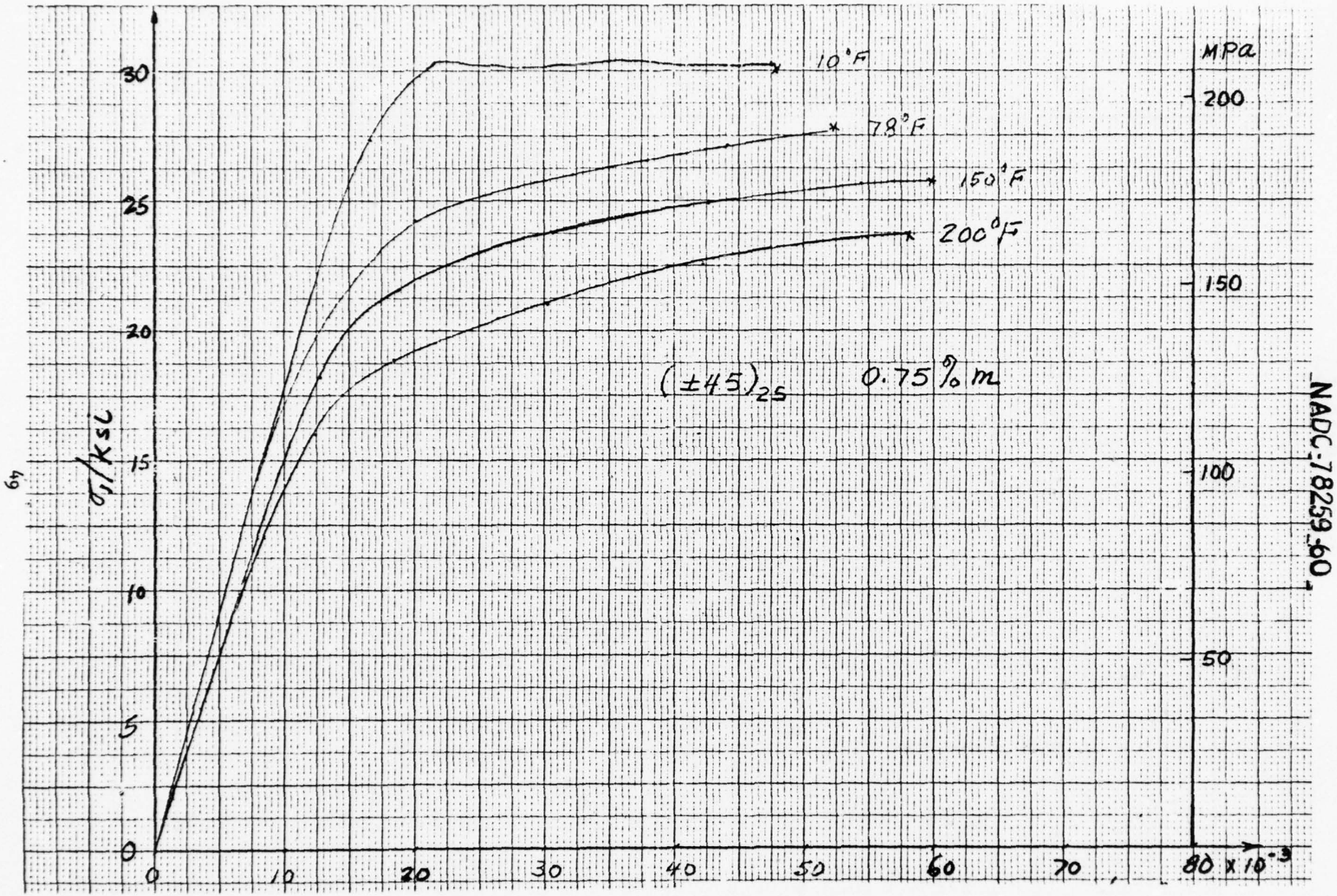

Fig. 11 Axial Stress-strain Curves for $(\pm 45)_{2s}$ Laminates Under Various Temperatures.

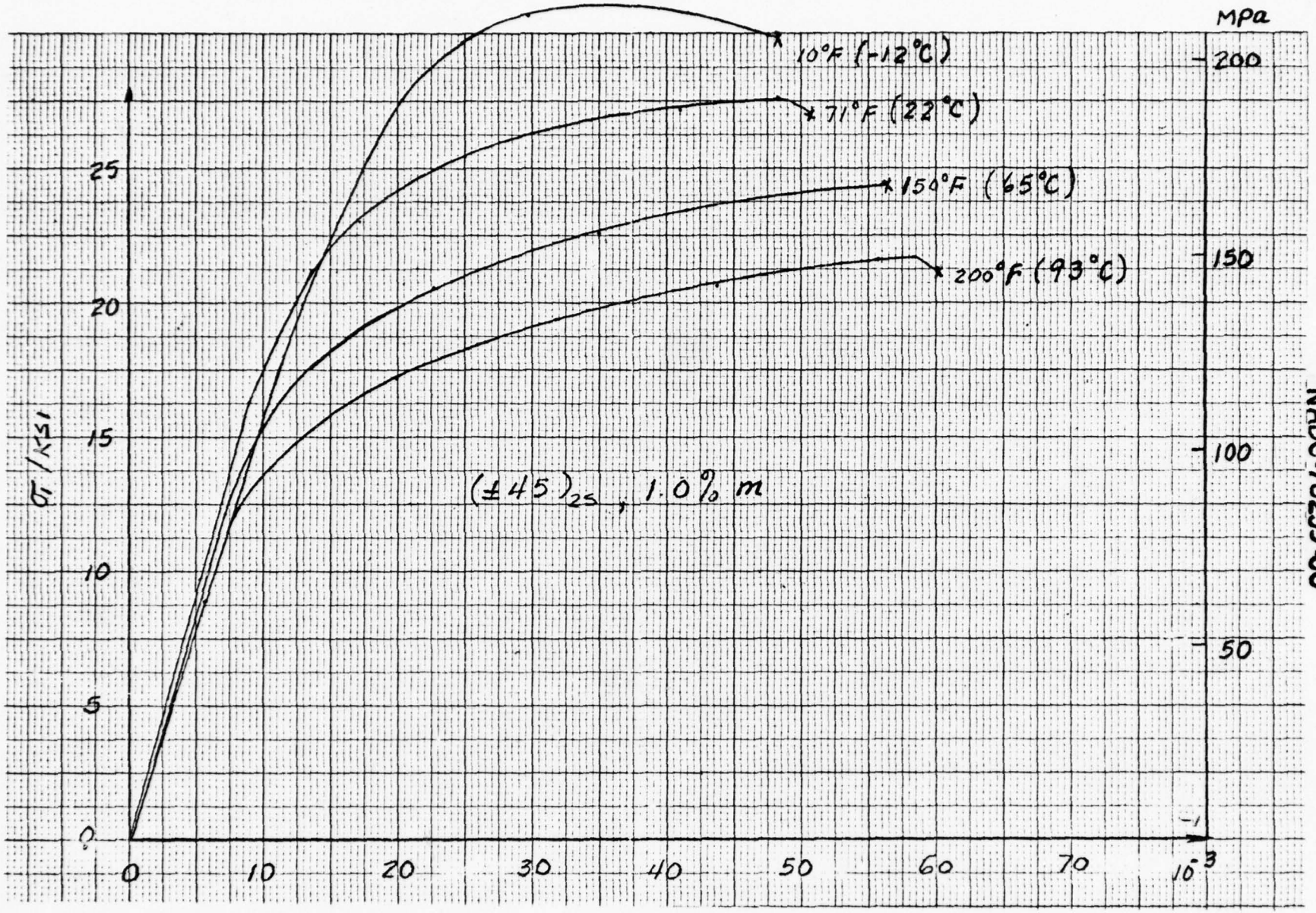

Fig. 12 Axial Stress-strain Curves for $(\pm 45)_{2s}$ Laminates Under Various Temperatures.

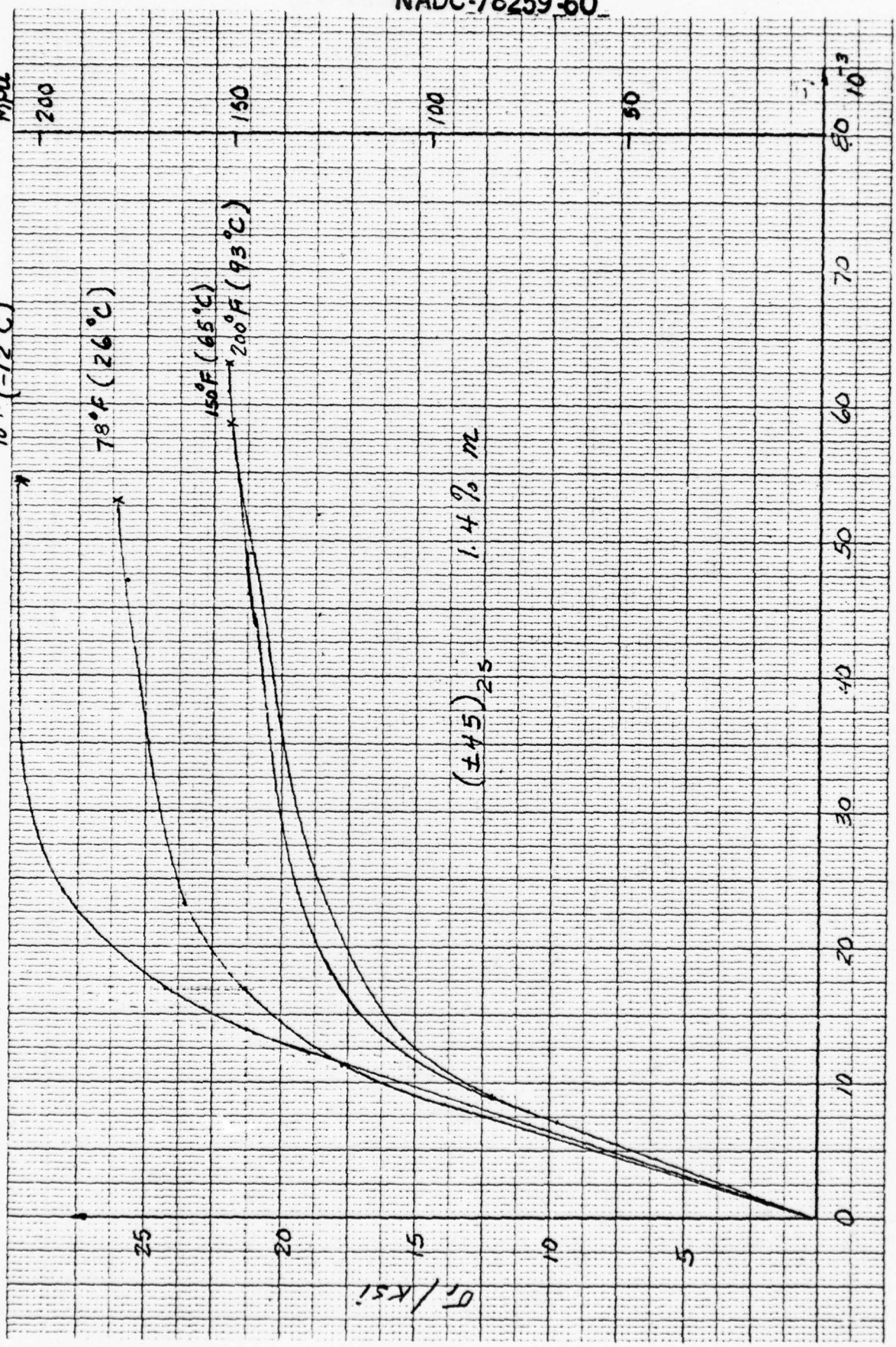

Fig. 13 Axial Stress-strain Curves for $(\pm 45)_{2s}$ Laminates Under Various Temperatures.

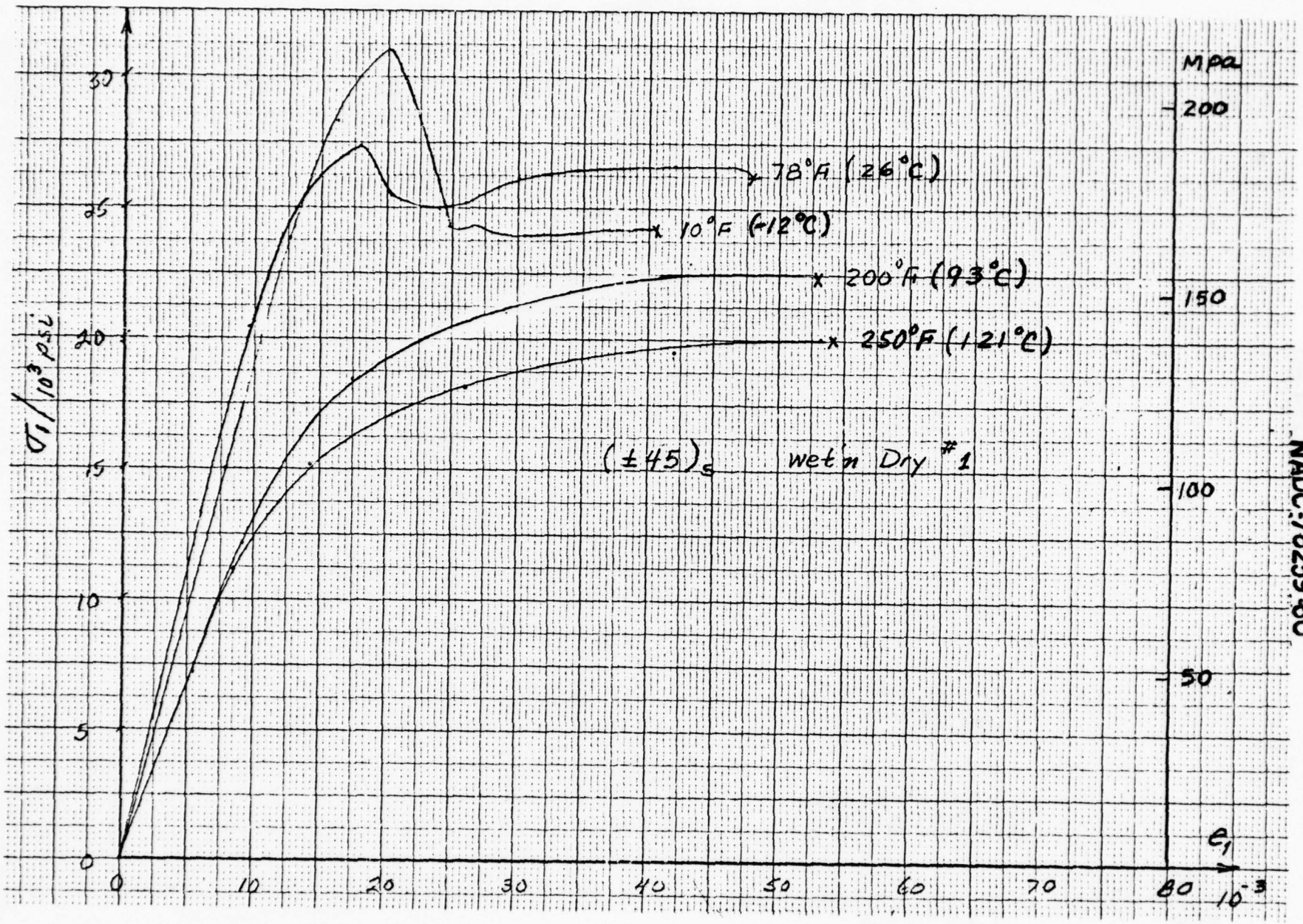

Fig. 14 Axial Stress-strain Curves for $(\pm 45)_{2s}$ Laminates Under Various Temperatures.

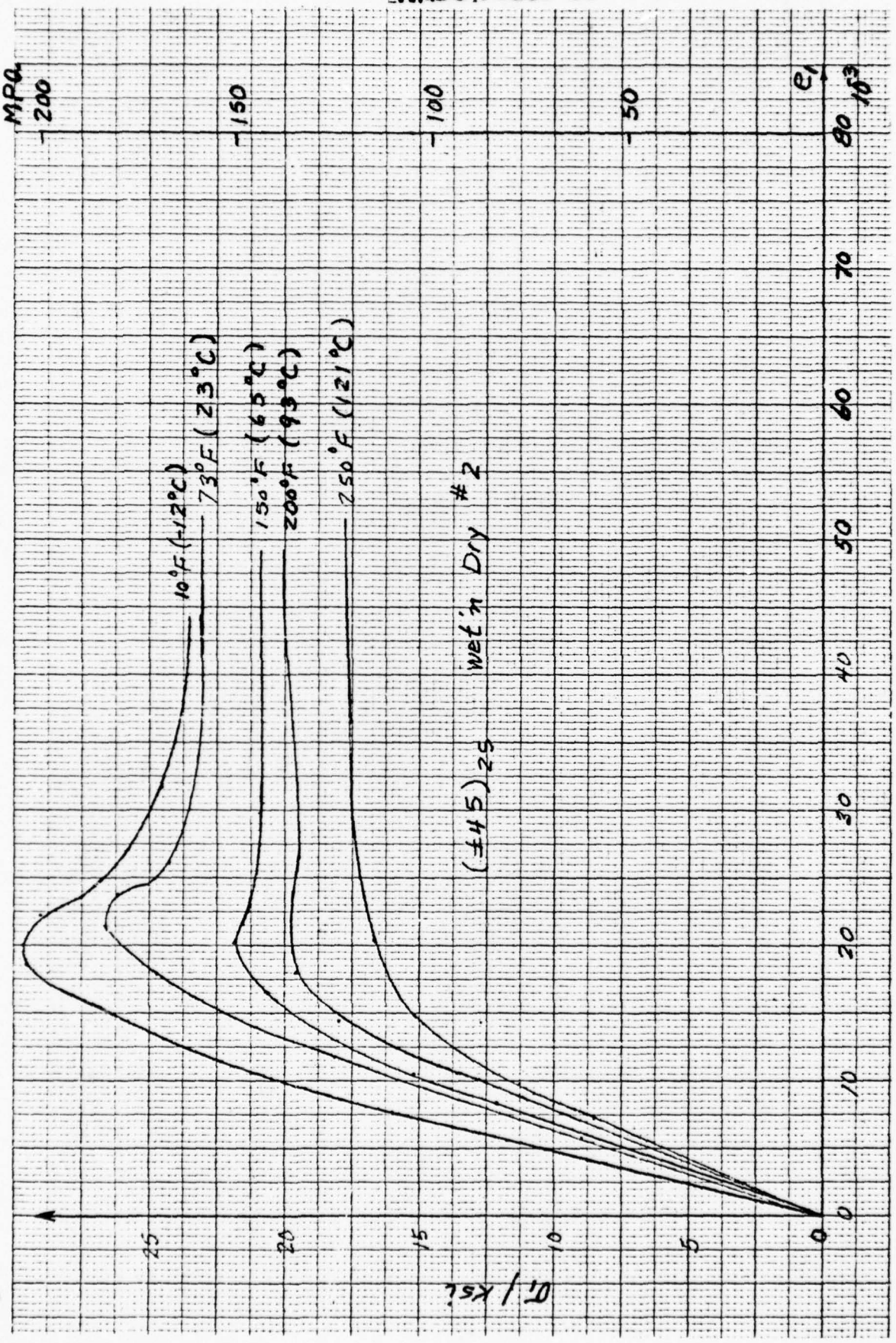

Fig. 15 Axial Stress-strain Curves for $(\pm 45)_{2s}$ Laminates Under Various Temperatures.

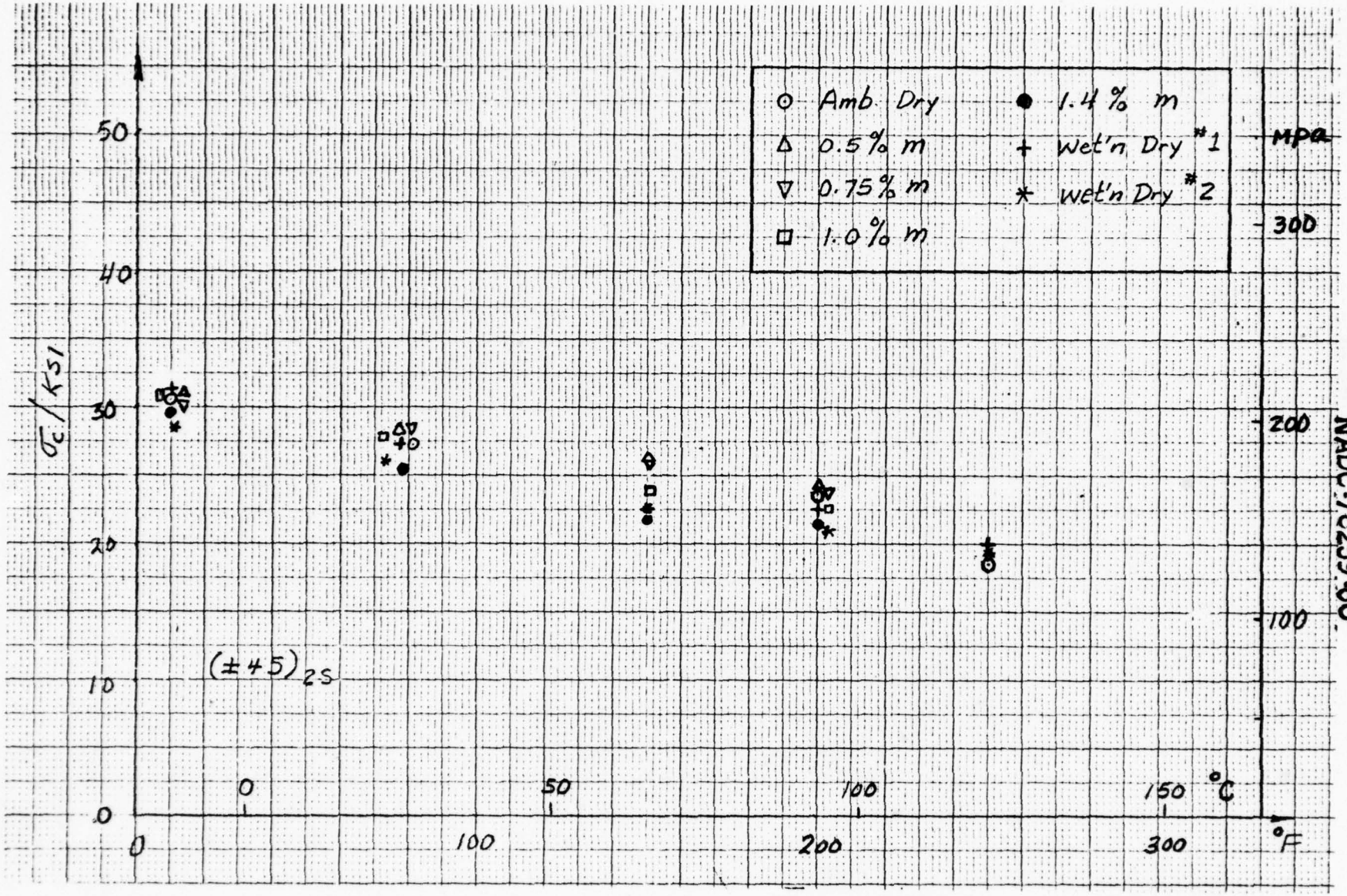

Fig. 16 Compressive Strength of $(\pm 45)_{2s}$ Laminates As Influenced by Temperature and Humidity

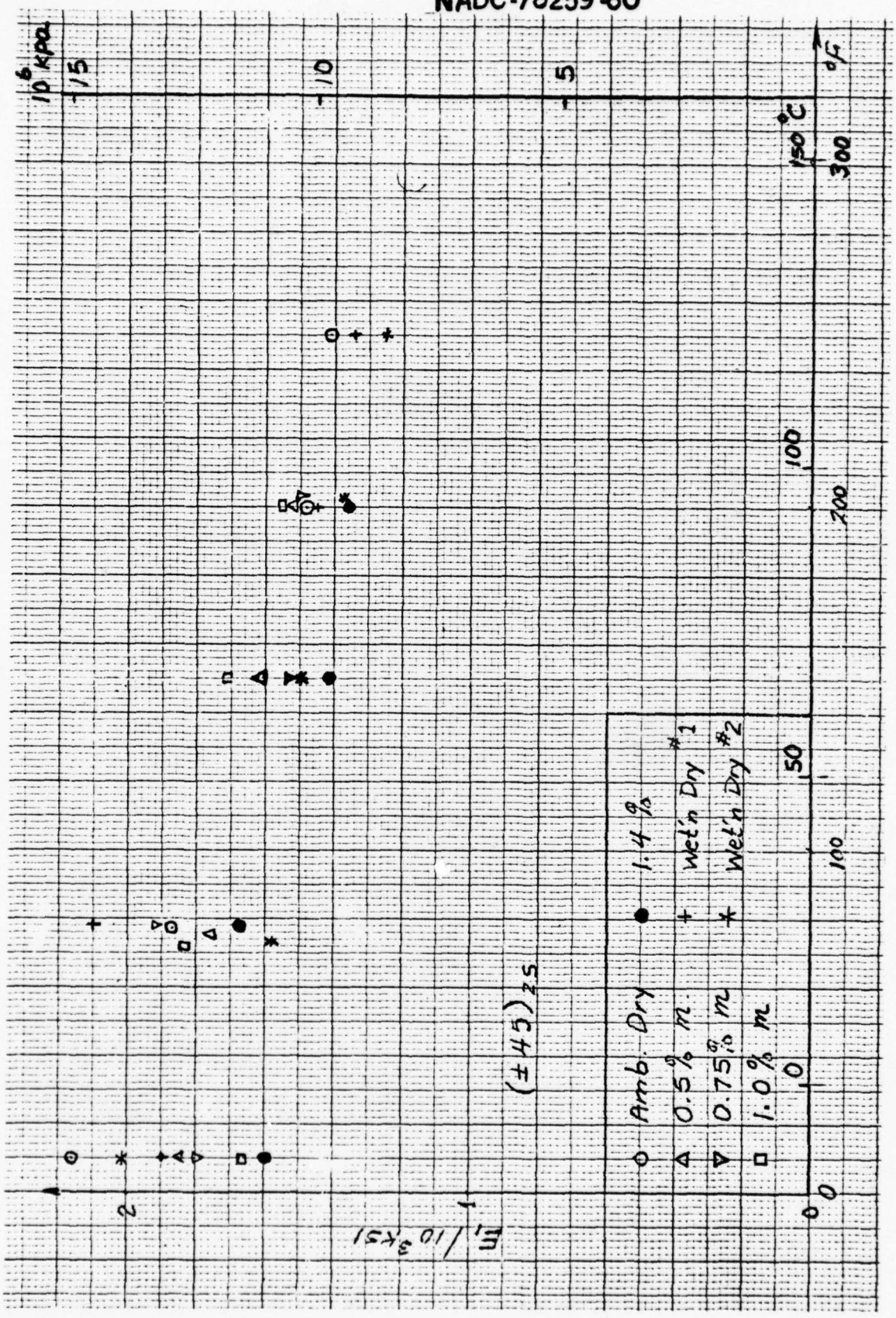

Fig. 17 Initial Axial Modulus of $(\pm 45)_{2s}$ Laminates As Influenced by Temperature and Humidity

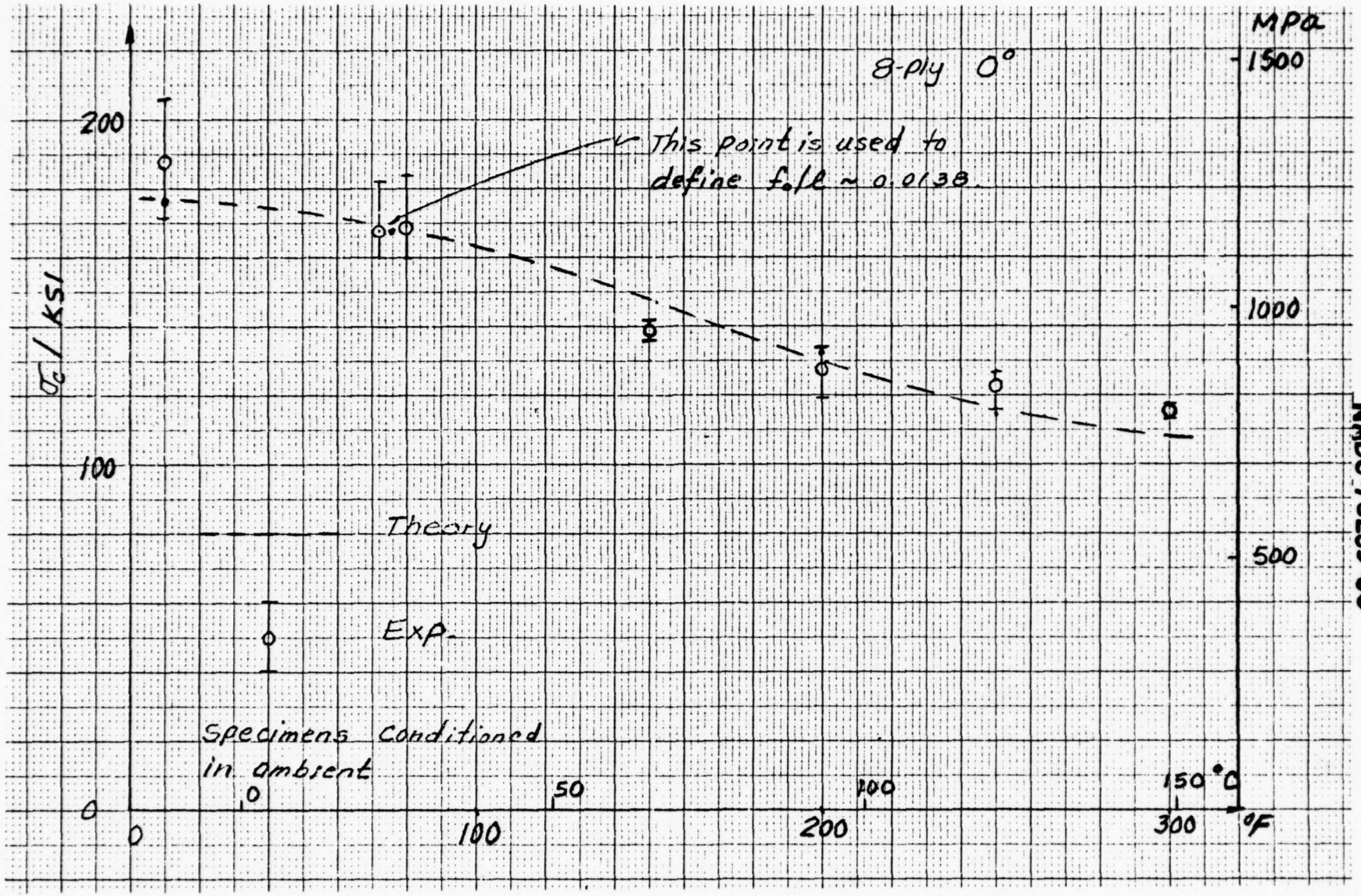

Fig. 18 Compressive Strength versus Temperature-- 0° Laminates.

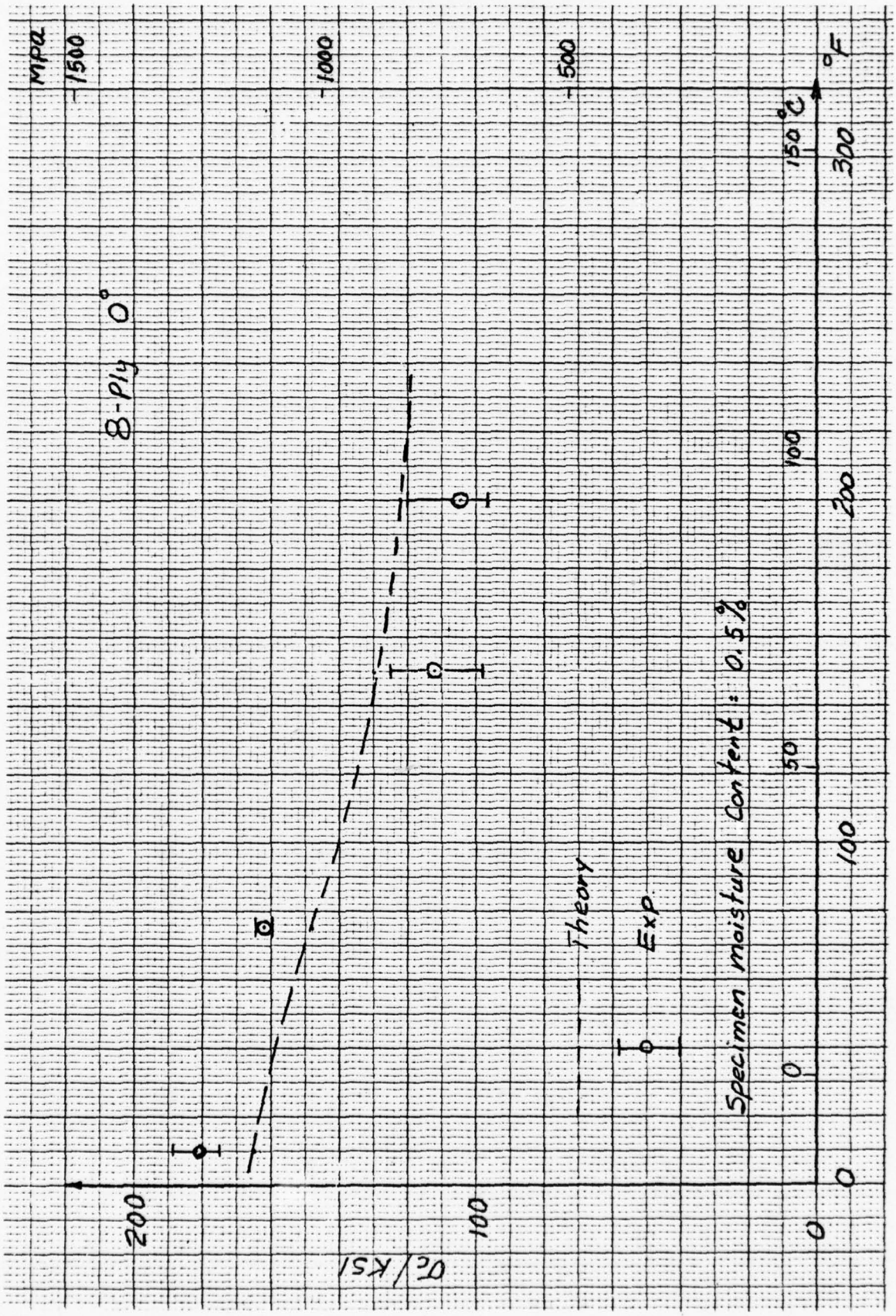

Fig. 19 Compressive Strength versus Temperature-- 0° Laminates.

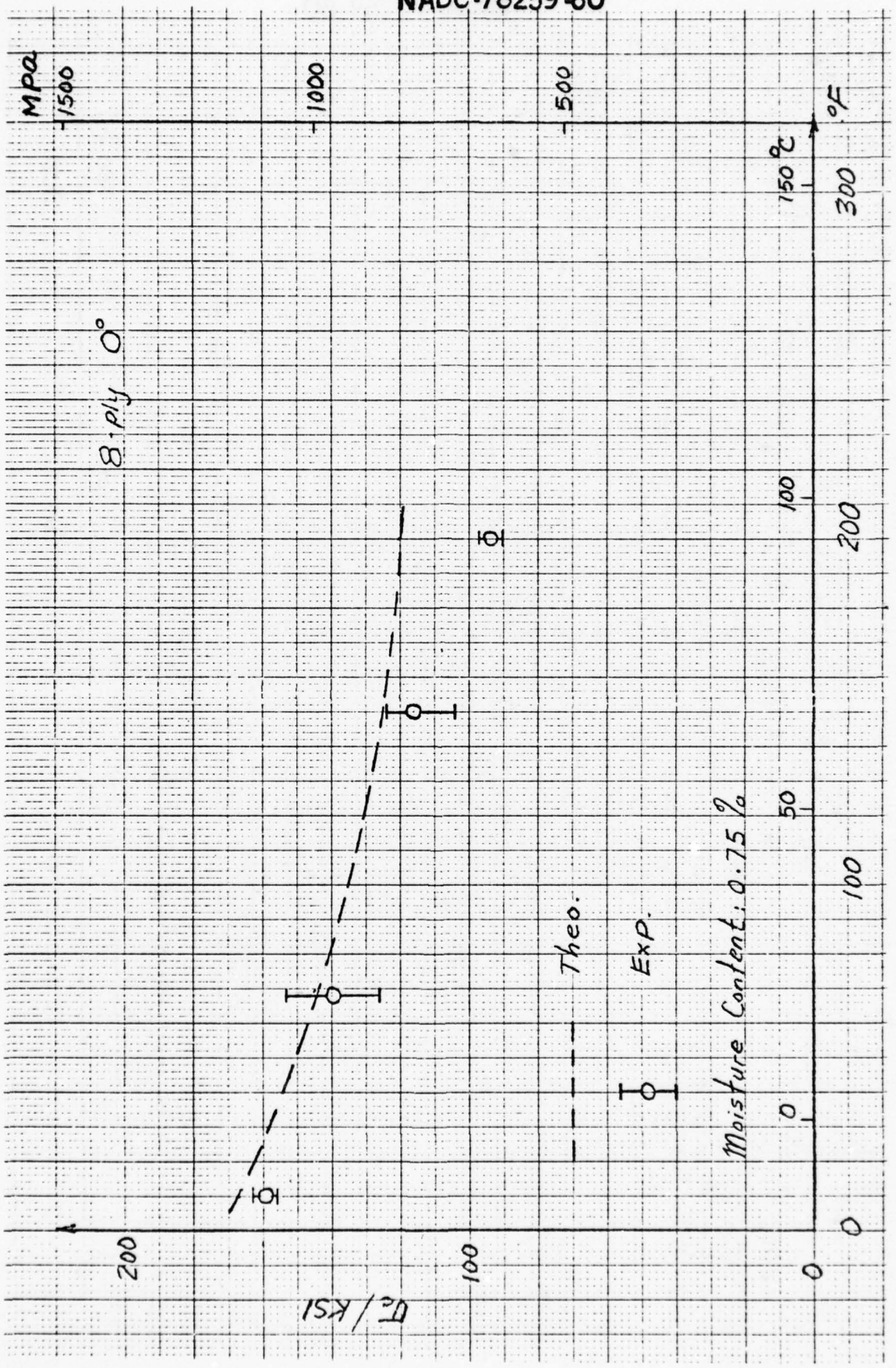

Fig. 20 Compressive Strength versus Temperature-- 0° Laminates.

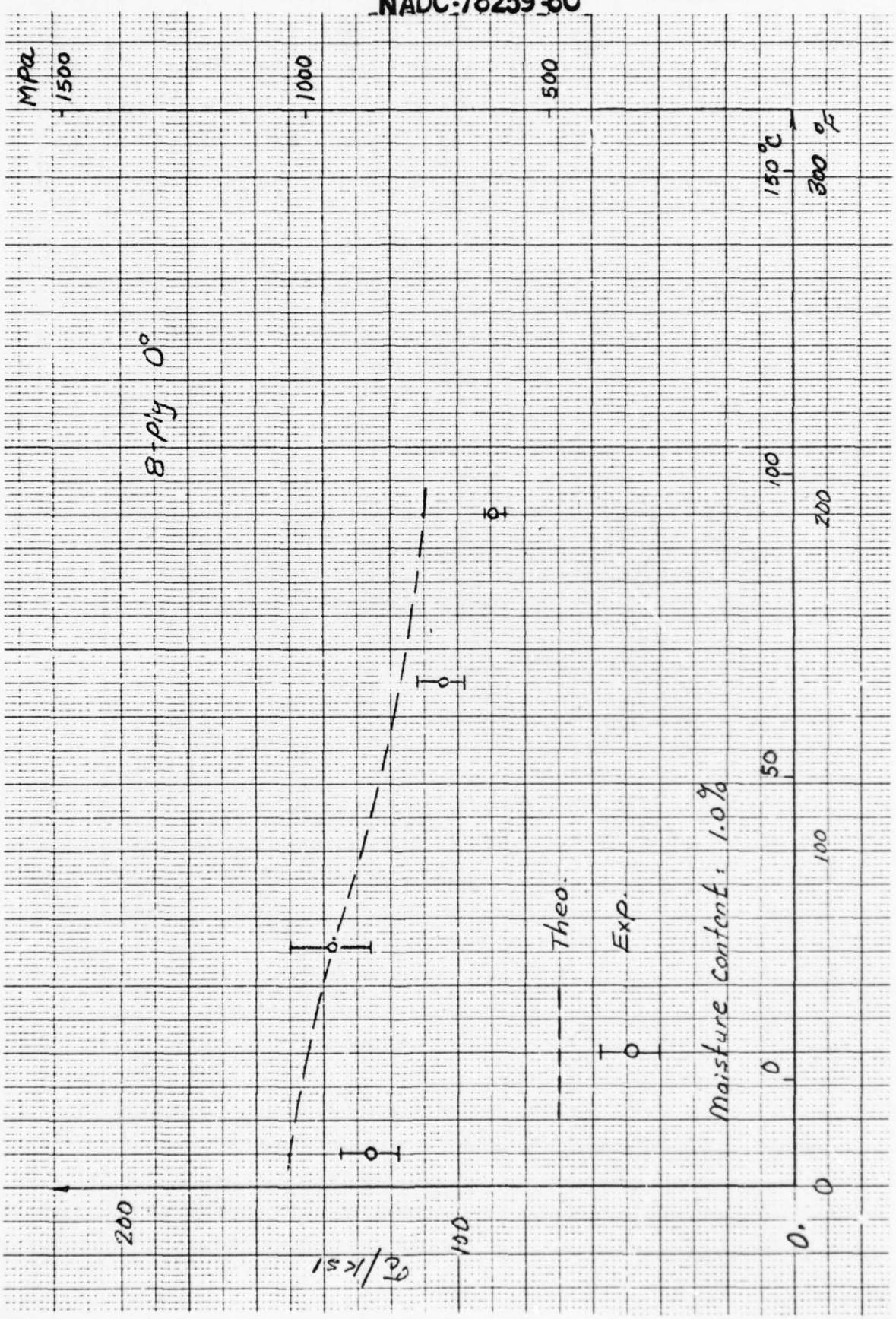

Fig. 21 Compressive Strength versus Temperature-- 0° Laminates.

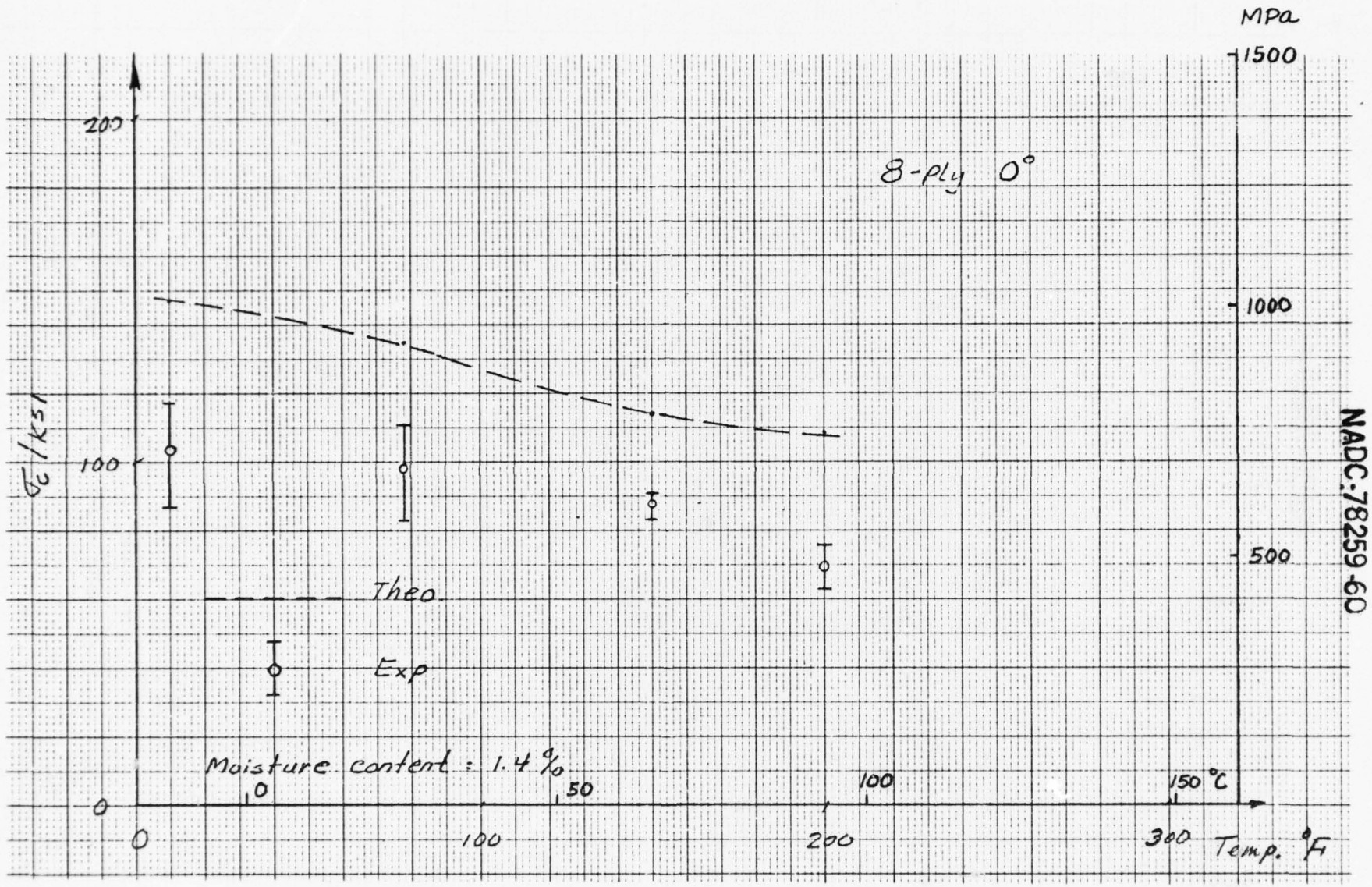

Fig. 22 Compressive Strength versus Temperature-- 0° Laminates.

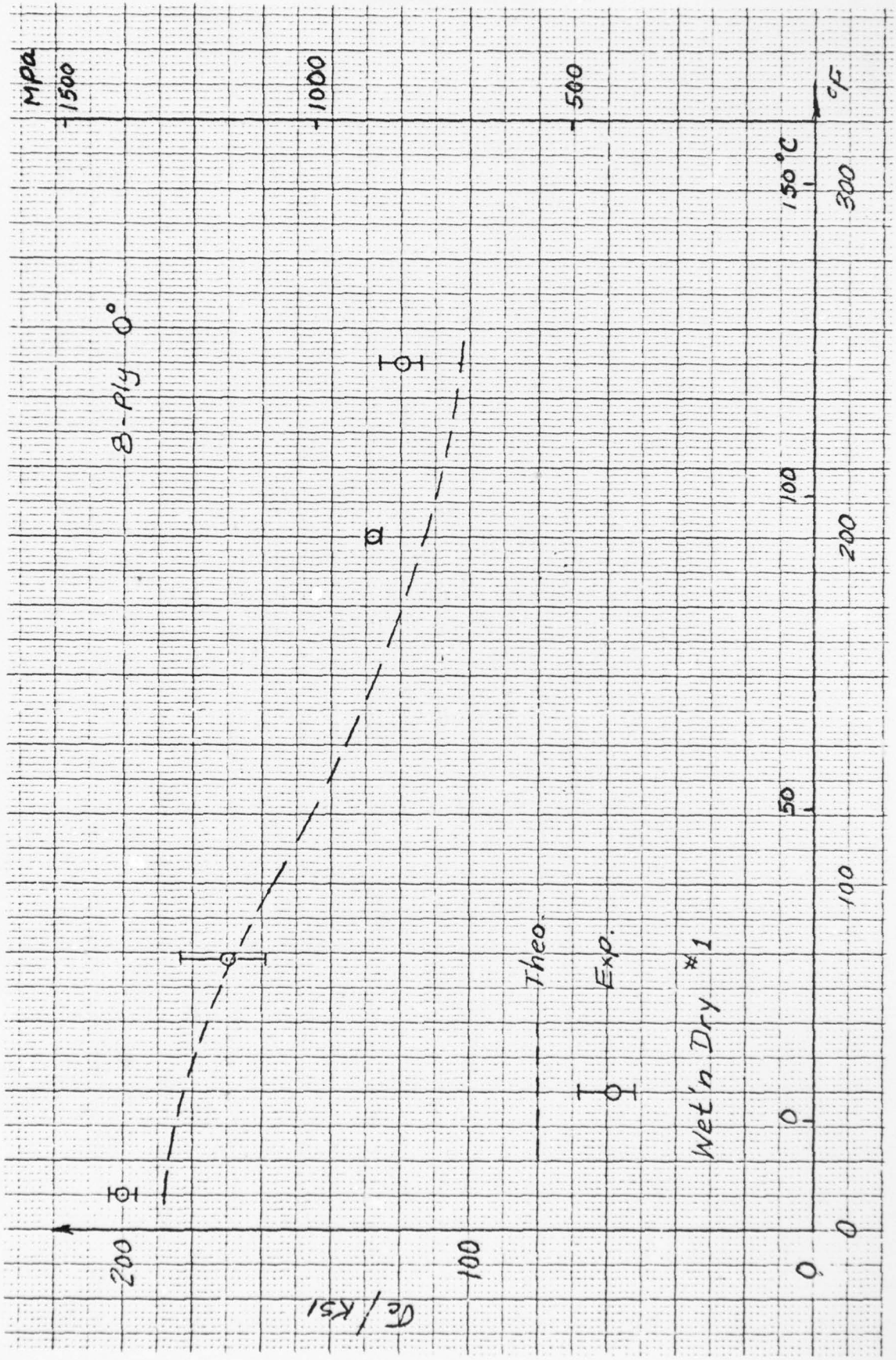

Fig. 23 Compressive Strength versus Temperature-- 0° Laminates.

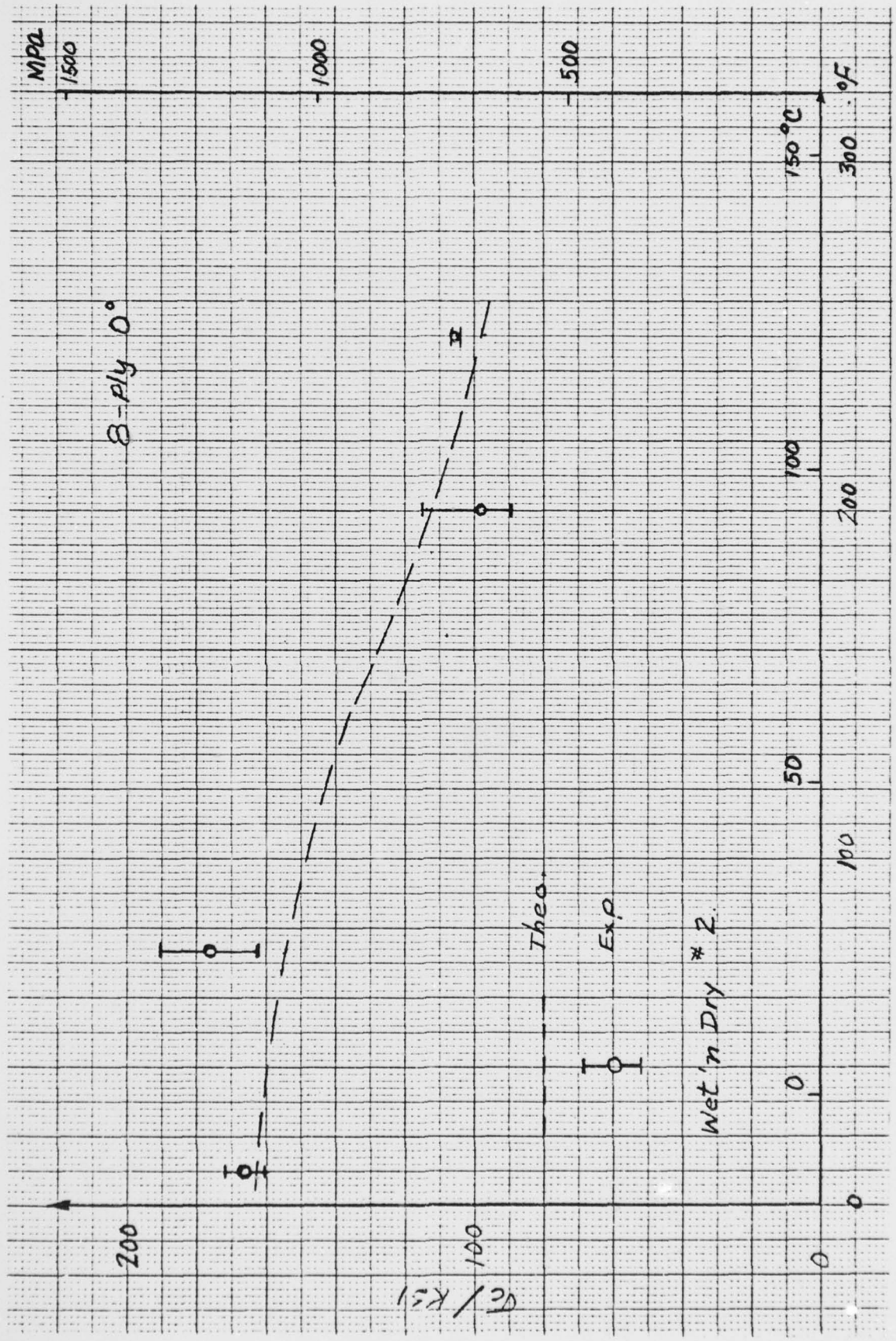

Fig. 24 Compressive Strength versus Temperature-- 0^{o} Laminates

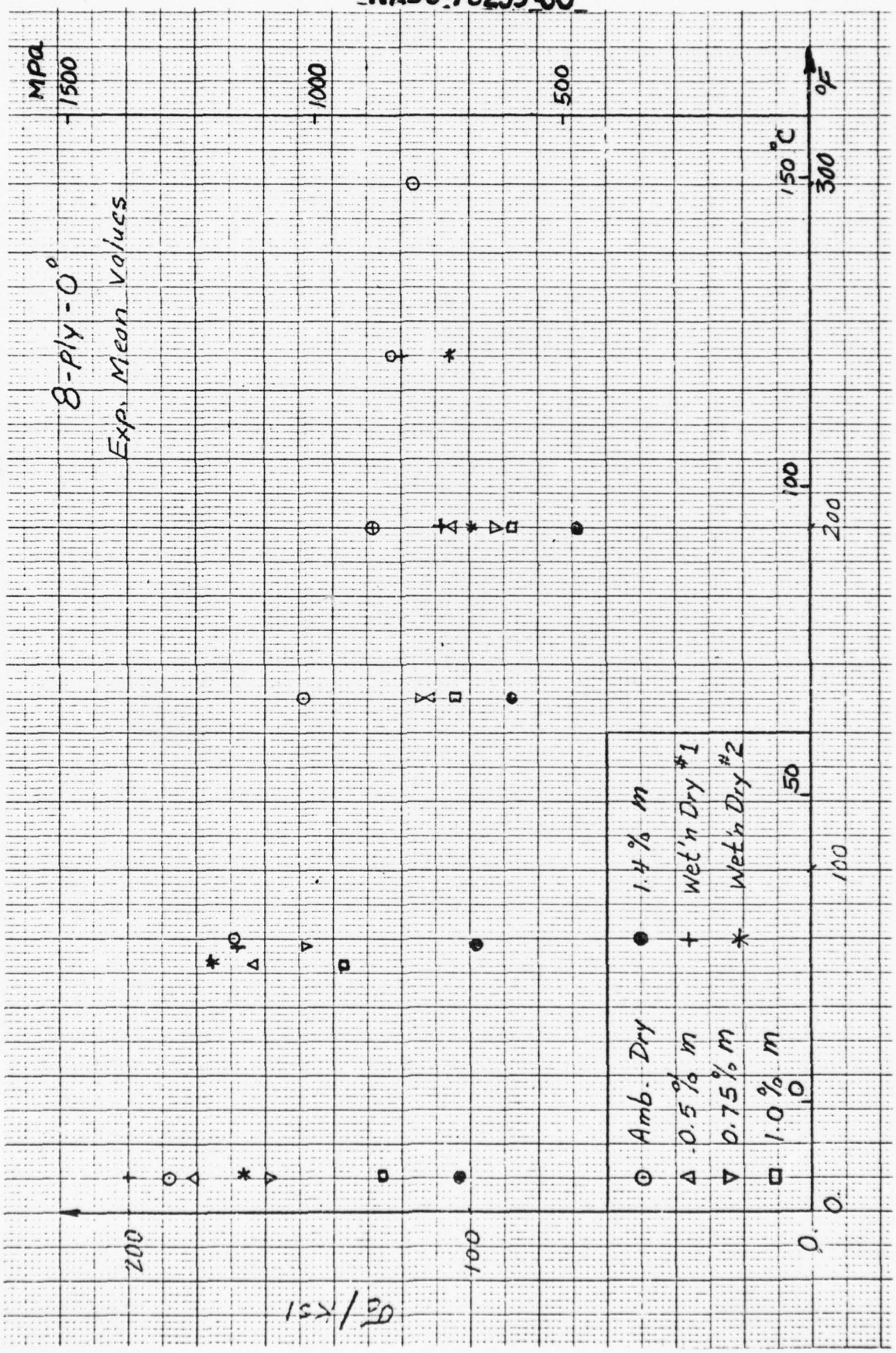

Fig. 25 Compressive Strength versus Temperature for All Moisture Conditions-- 0° Laminates.

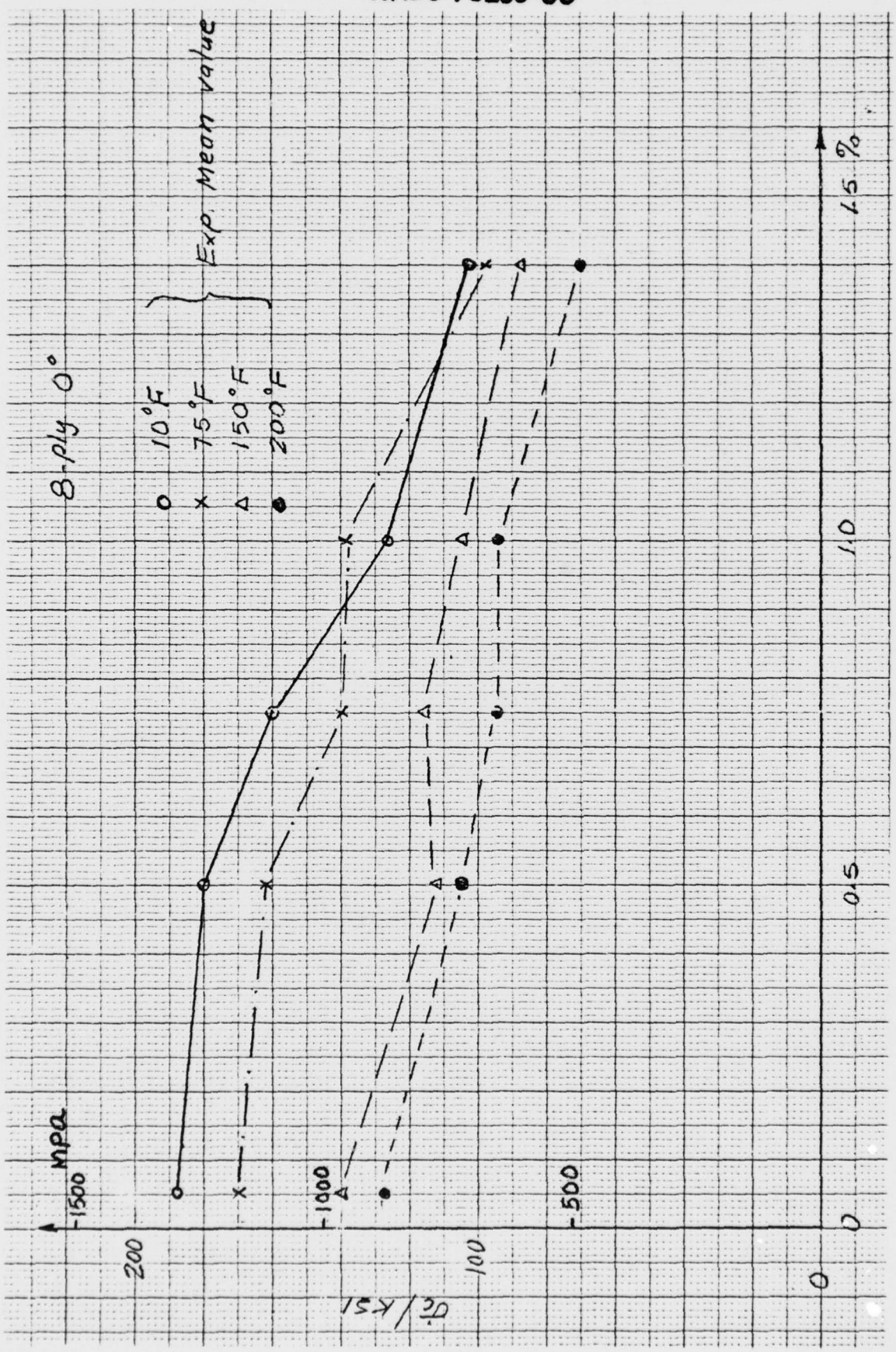

Fig. 26 Compressive Strength versus Moisture Content for All Temperatures-- 0° Laminates.

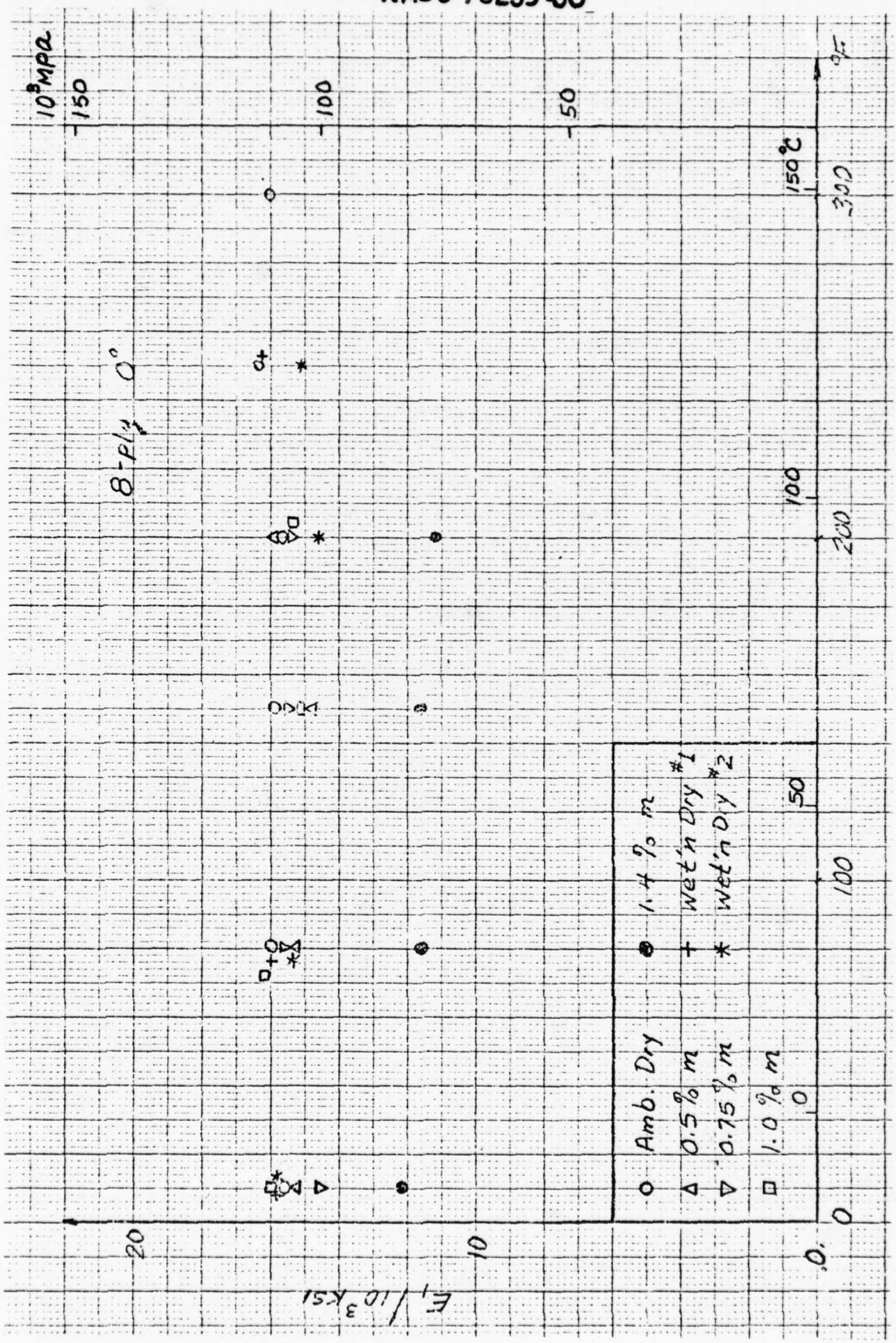

Fig. 27 Stiffness E_1 versus Temperature for All Moisture Conditions-- 0^o Laminates.

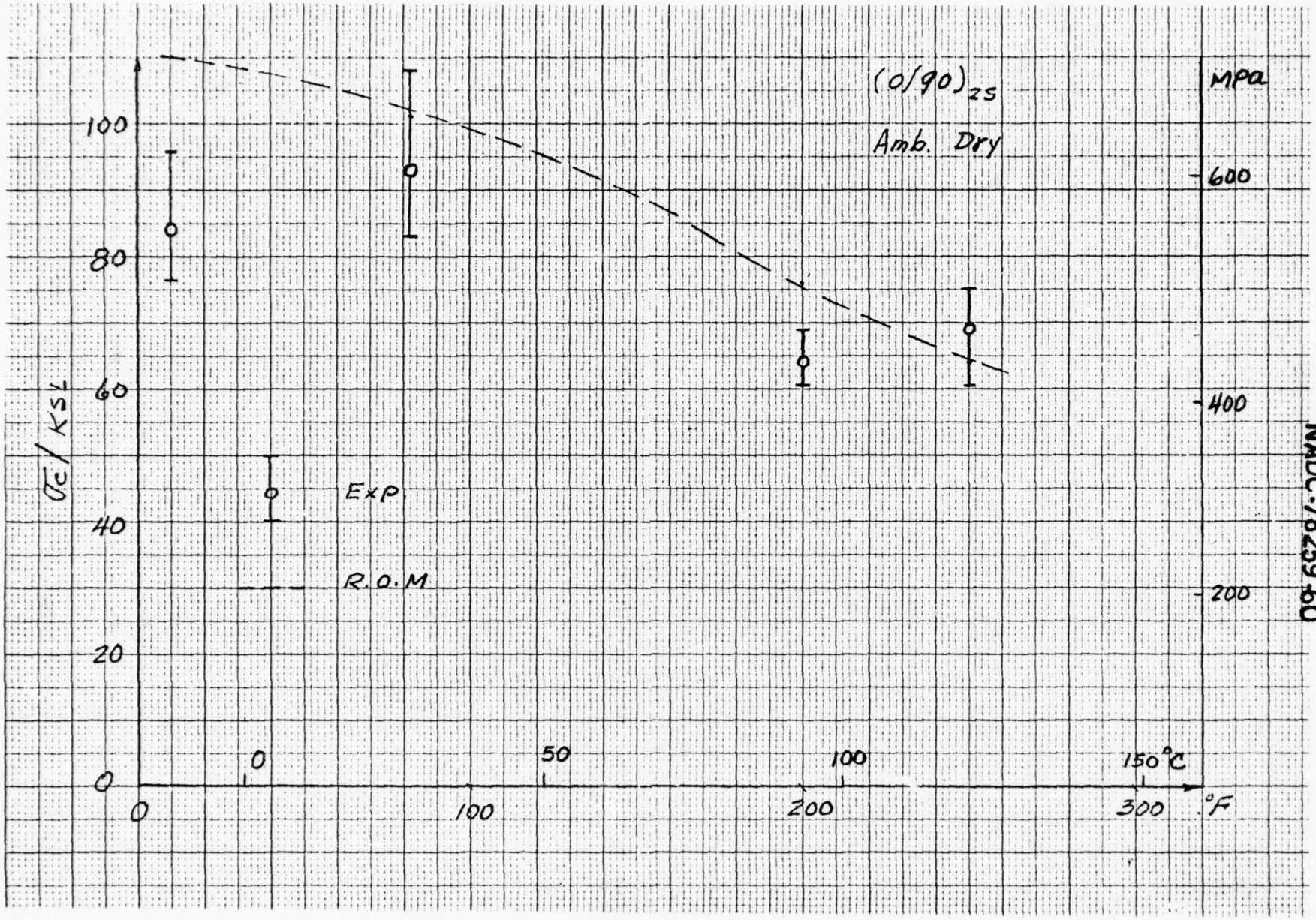

Fig. 28 Compressive Strength versus Temperature-- $(0/90)_{2s}$ Laminates.

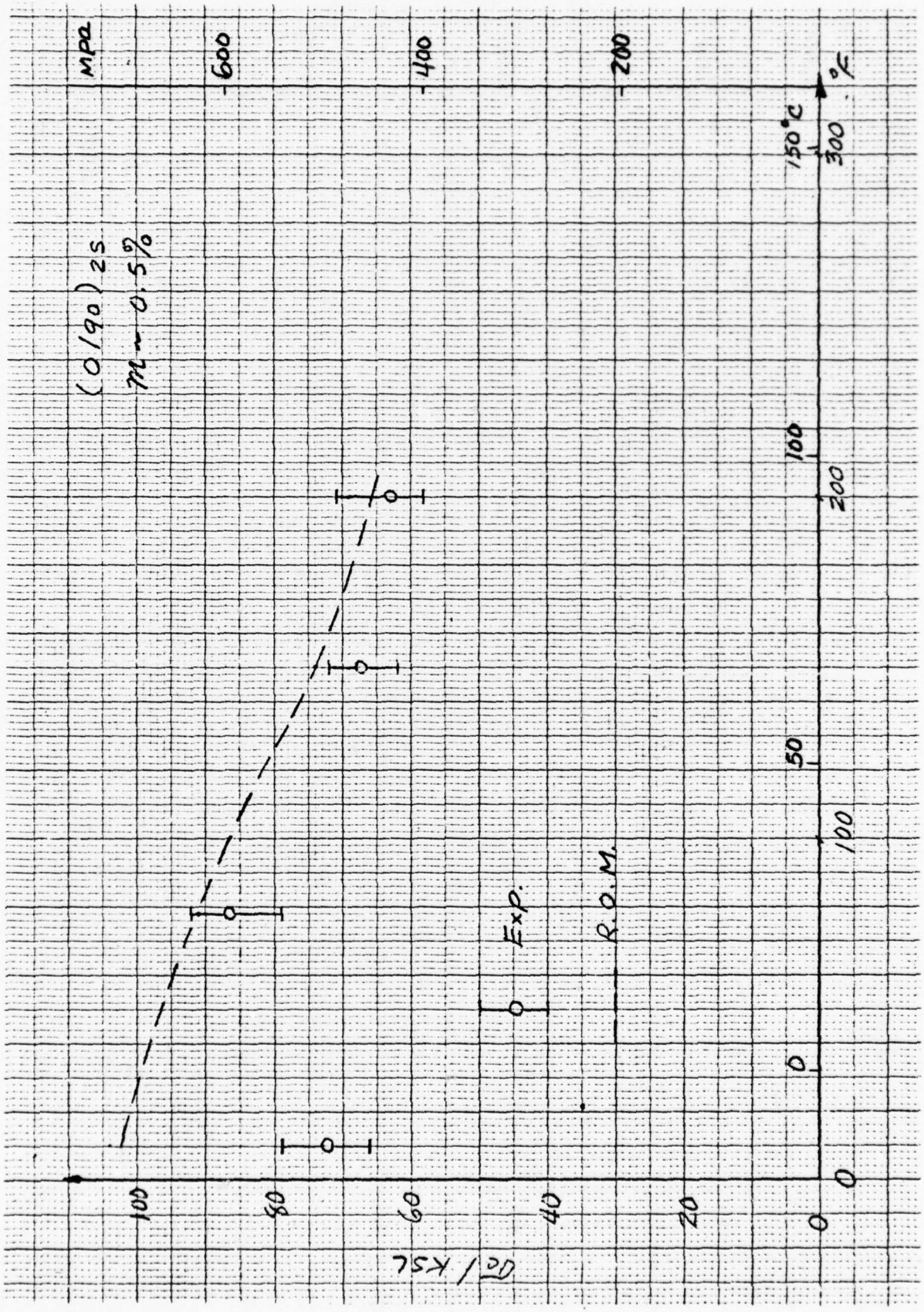

Fig. 29 Compressive Strength versus Temperature-- $(0/90)_{2s}$ Laminates.

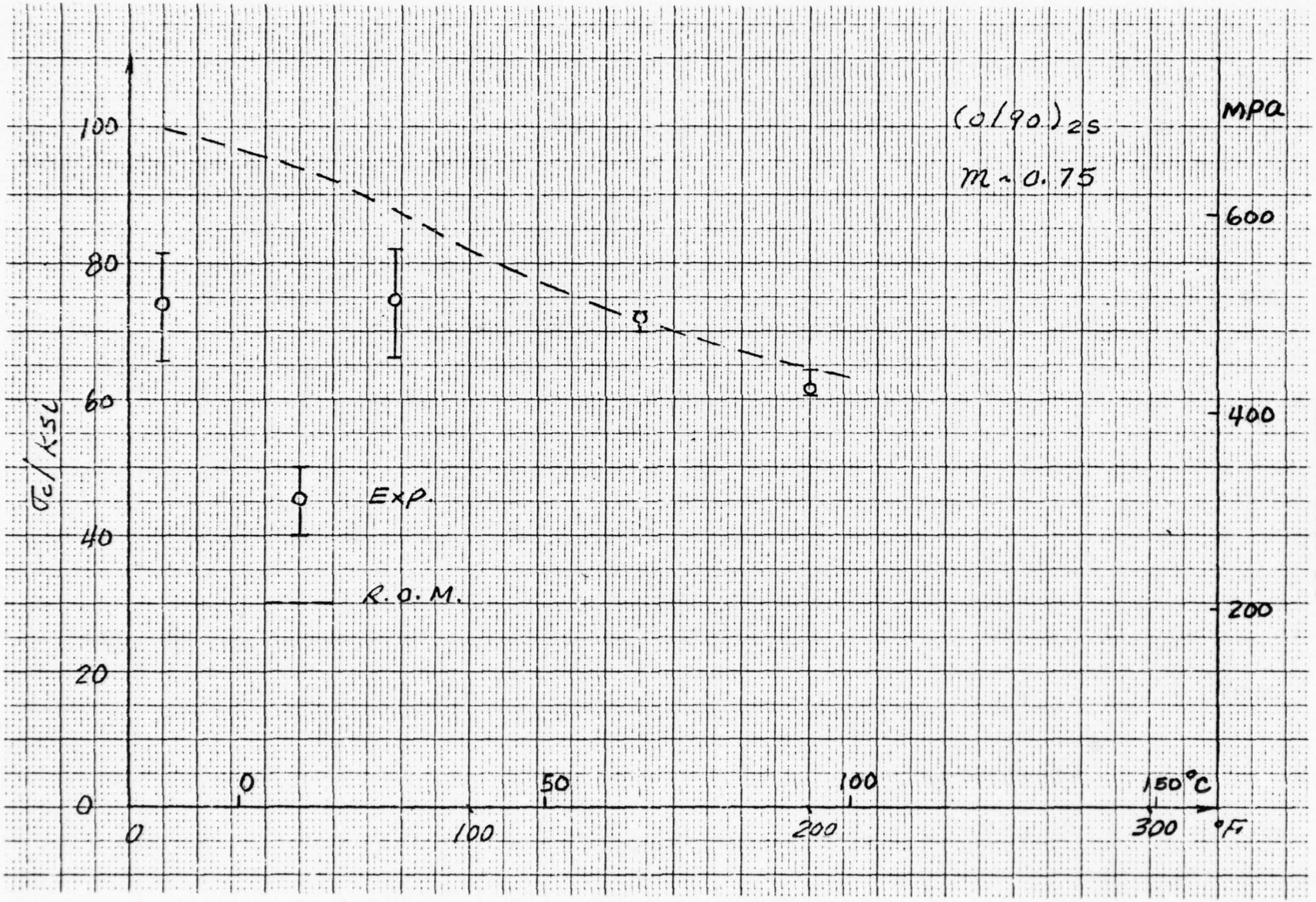

Fig. 30 Compressive Strength versus Temperature-- $(0/90)_{2s}$ Laminates.

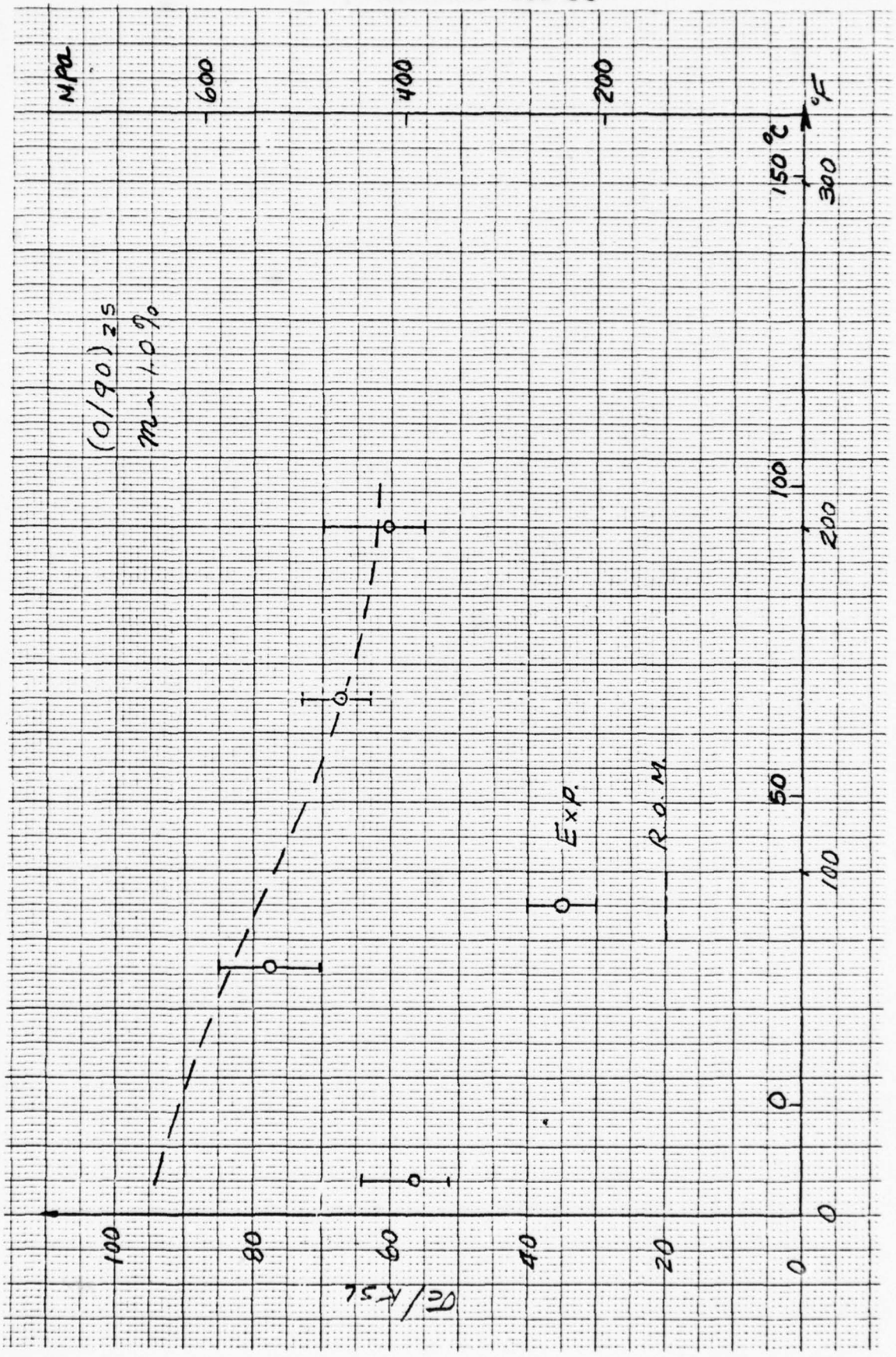

Fig. 31 Compressive Strength versus Temperature-- $(0/90)_{2s}$ Laminates.

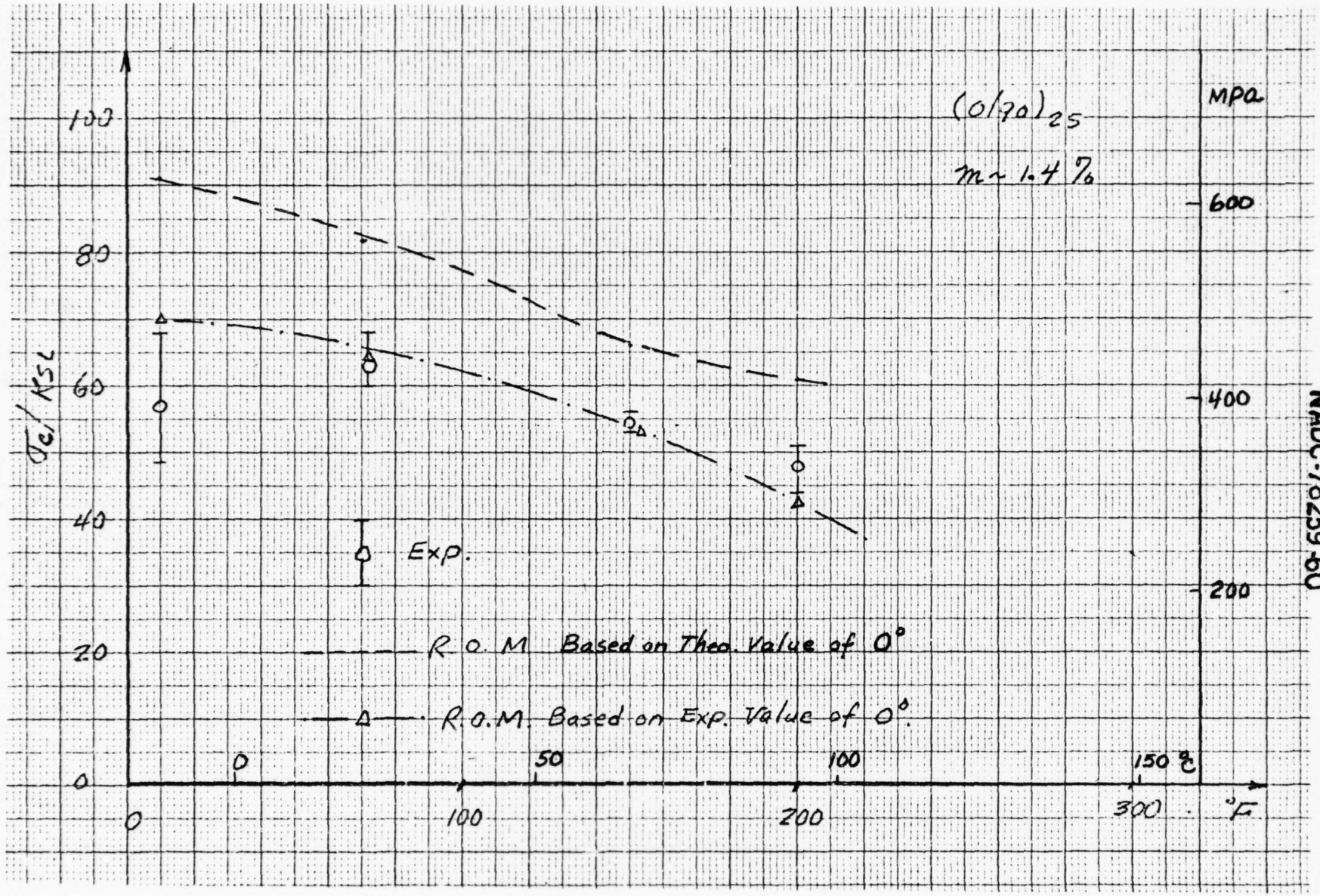

Fig. 32 Compressive Strength versus Temperature-- $(0/90)_{2s}$ Laminates.

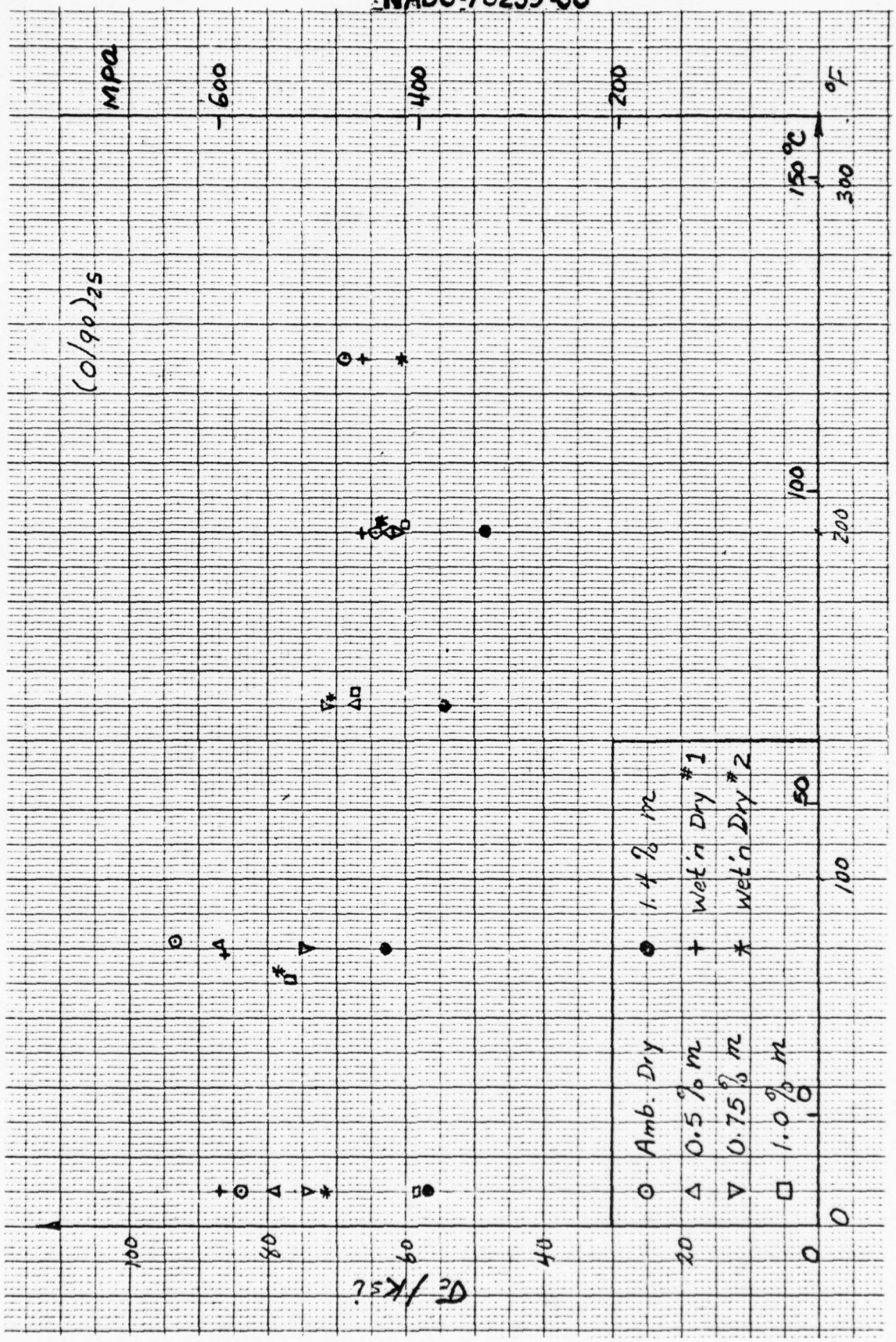

Fig. 33 Compressive Strength versus Temperature for All Moisture Conditions--$(0/90)_{2s}$ Laminates.

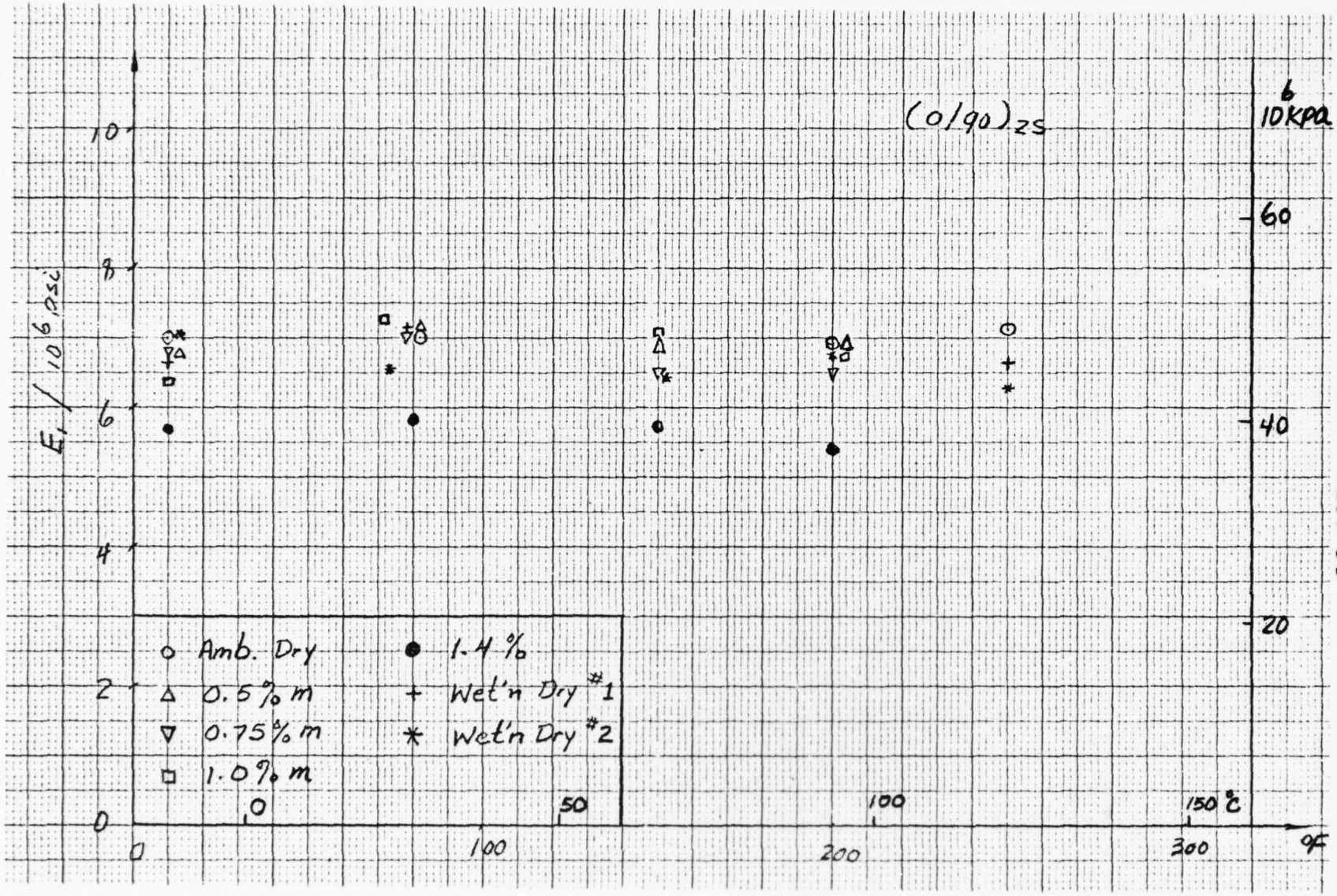

Fig. 34 Stiffness E_1 versus Temperature for all Moisture Conditions--$(0/90)_{2s}$ Laminates.

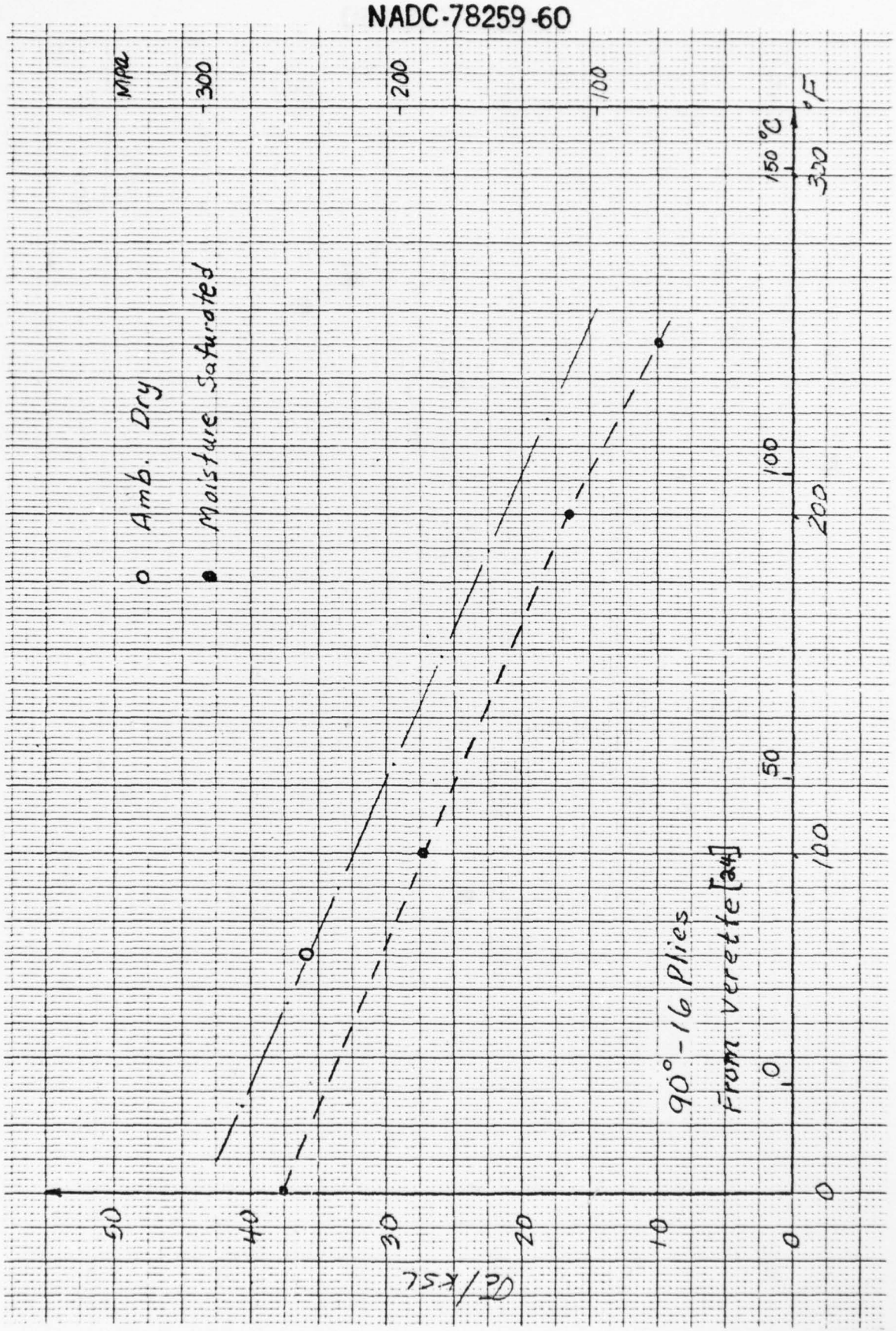

Fig. 35 Compressive Strength versus Temperature-- 90° Laminates.

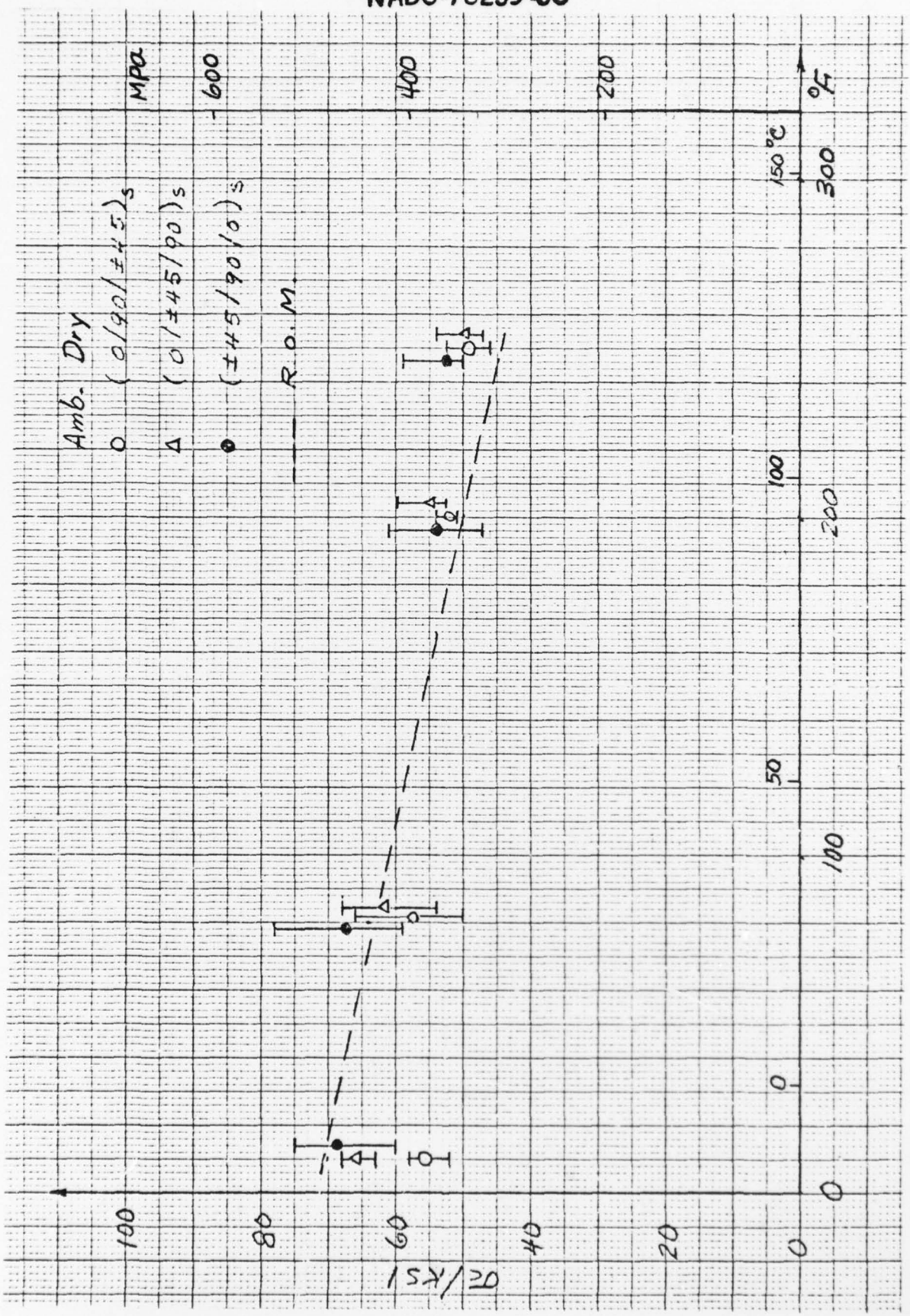

Fig. 36 Compressive Strength versus Temperature-- Quasi-isotropic Laminates.

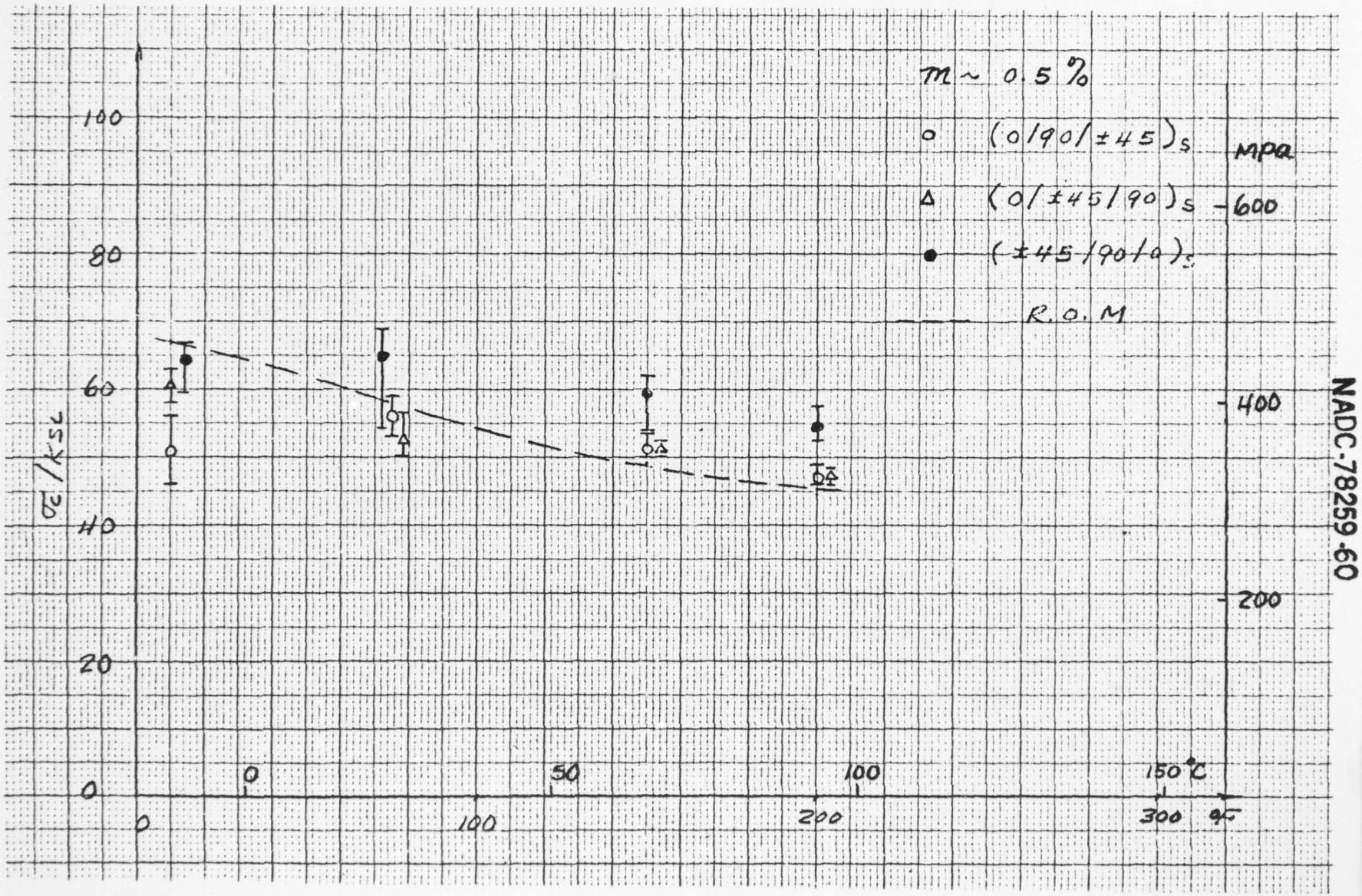

Fig. 37 Compressive Strength versus Temperature-- Quasi-isotropic Laminates.

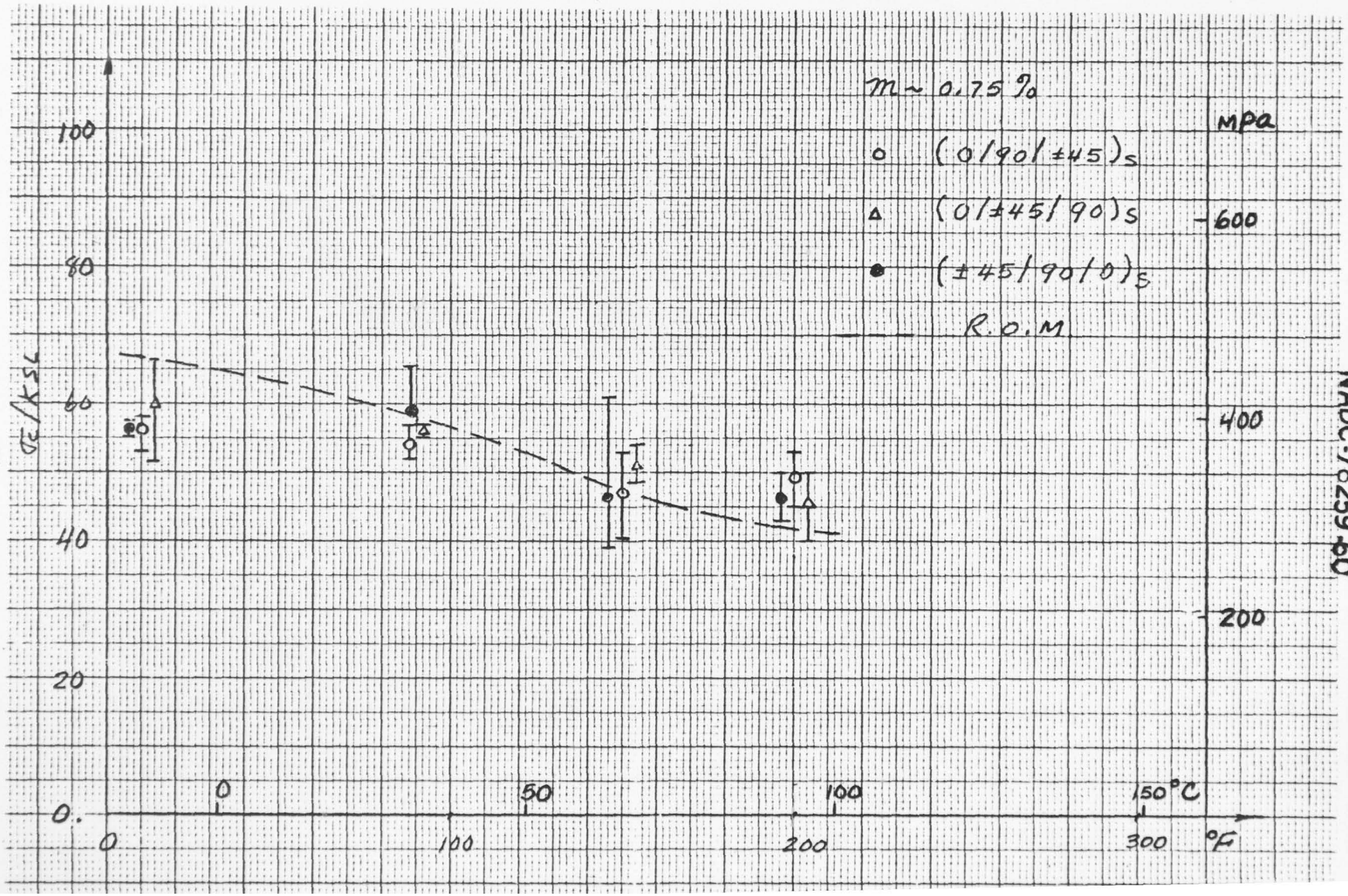
m ~ 0.75 %
MPa
○ (0/90/±45)s
△ (0/±45/90)s
● (±45/90/0)s
R.O.M.
100
80
60
40
20
0.
ksi
76
600
400
200
0
50
100
150 °C
0
100
200
300 °F

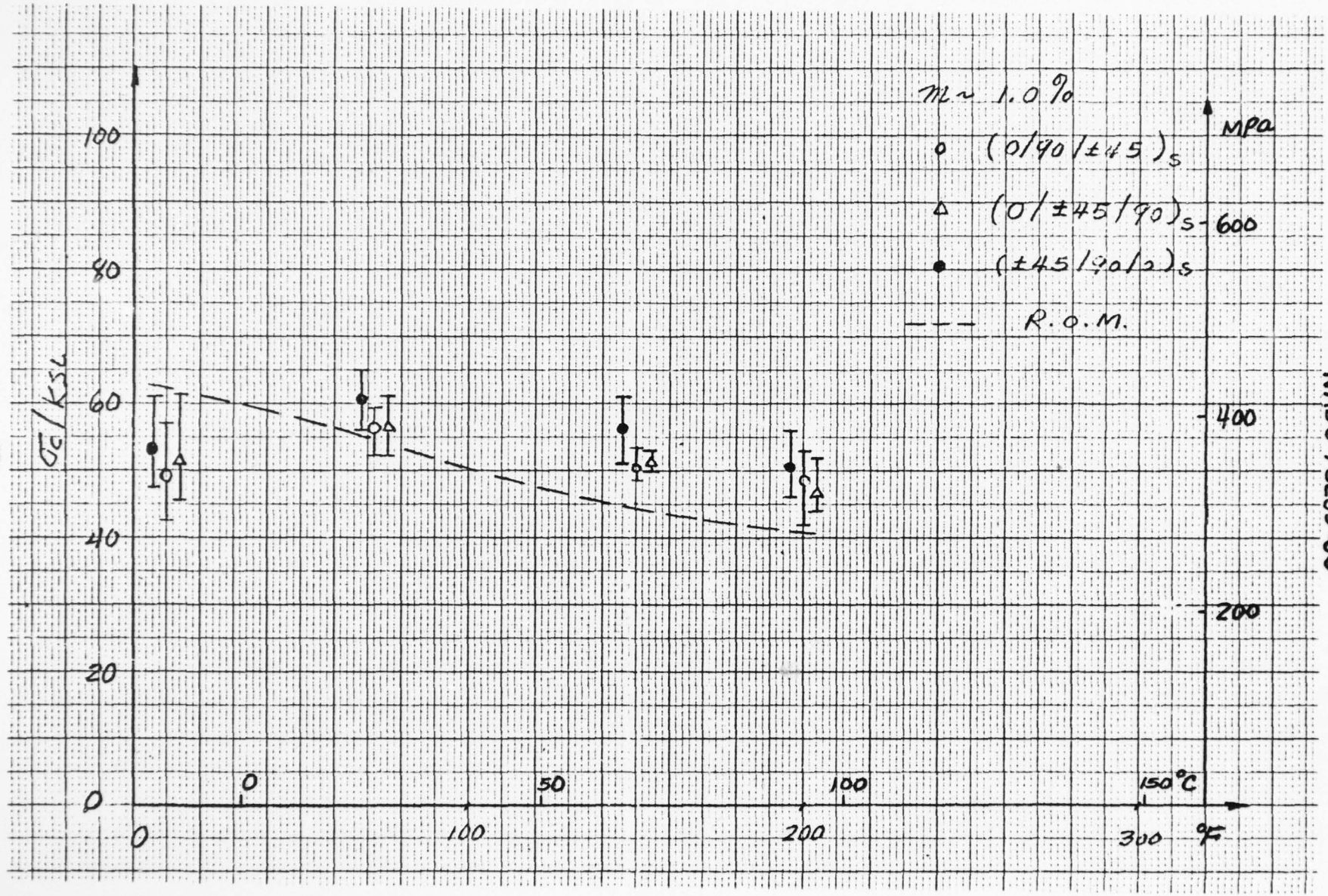

Fig. 39 Compressive Strength versus Temperature— Quasi-isotropic Laminates.

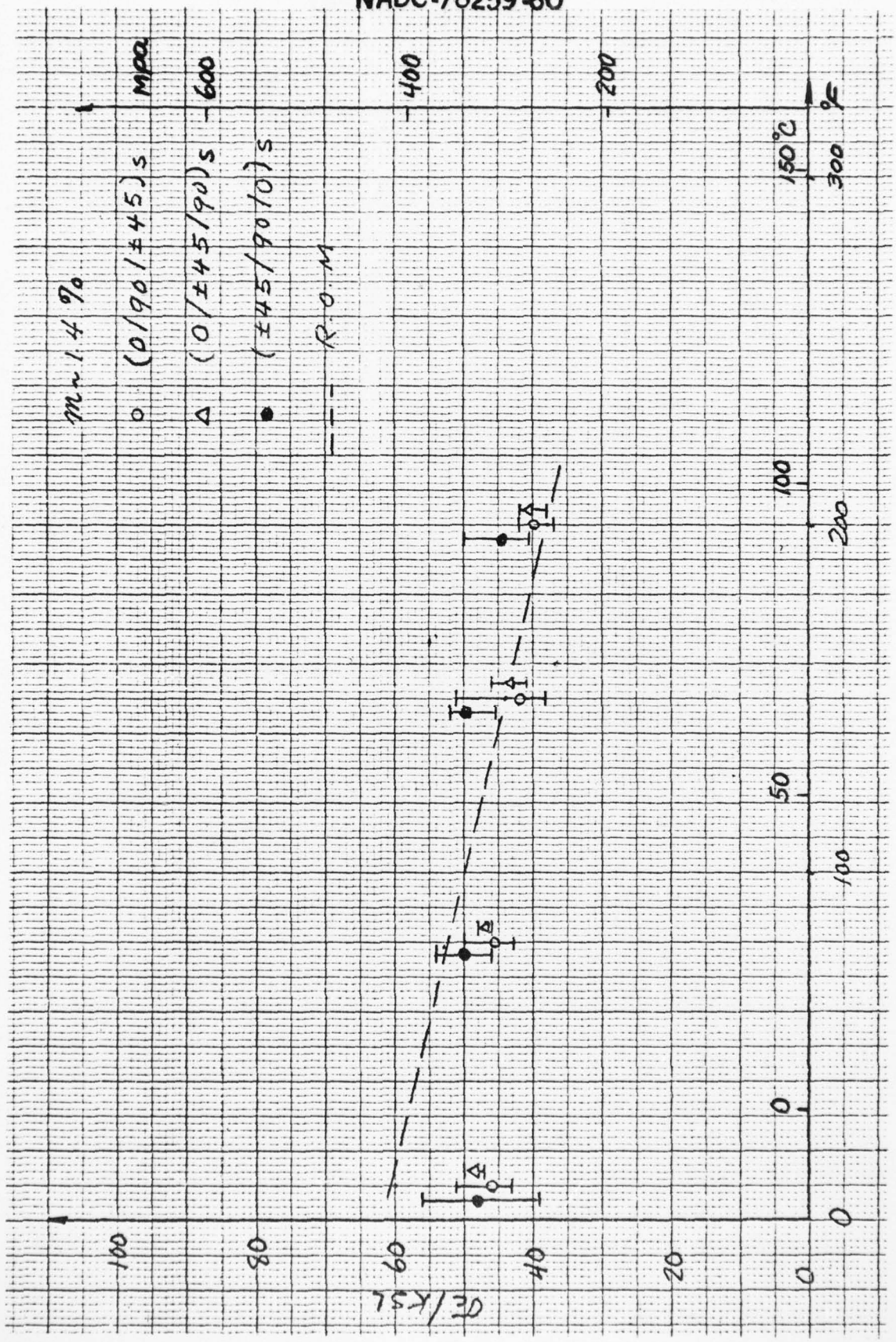

Fig. 40 Compressive Strength versus Temperature-- Quasi-isotropic Laminates.

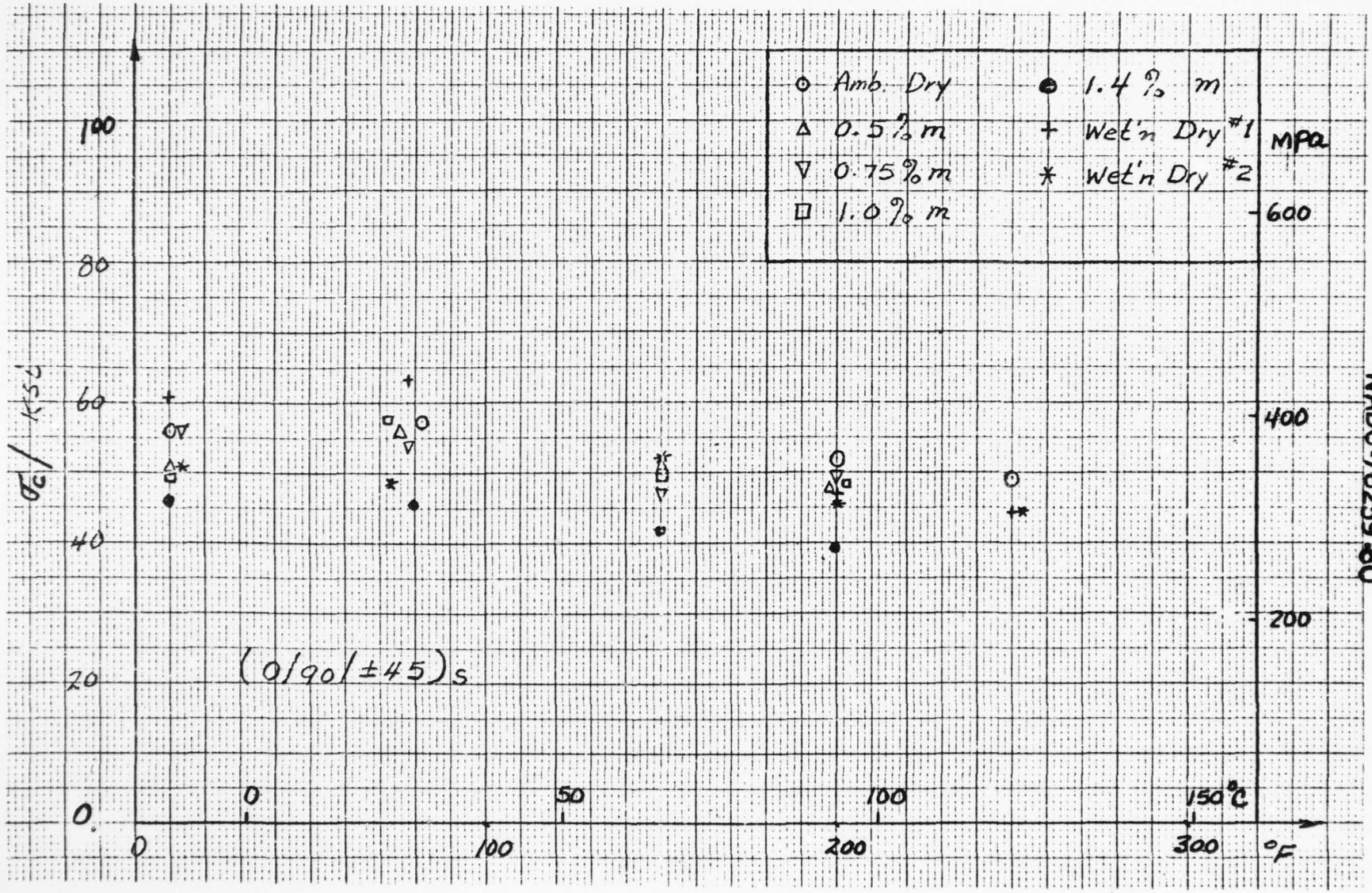

NADC-78259-60

Fig. 41 Compressive Strength versus Temperature for All Moisture Conditions--$(0/90/\pm 45)_s$

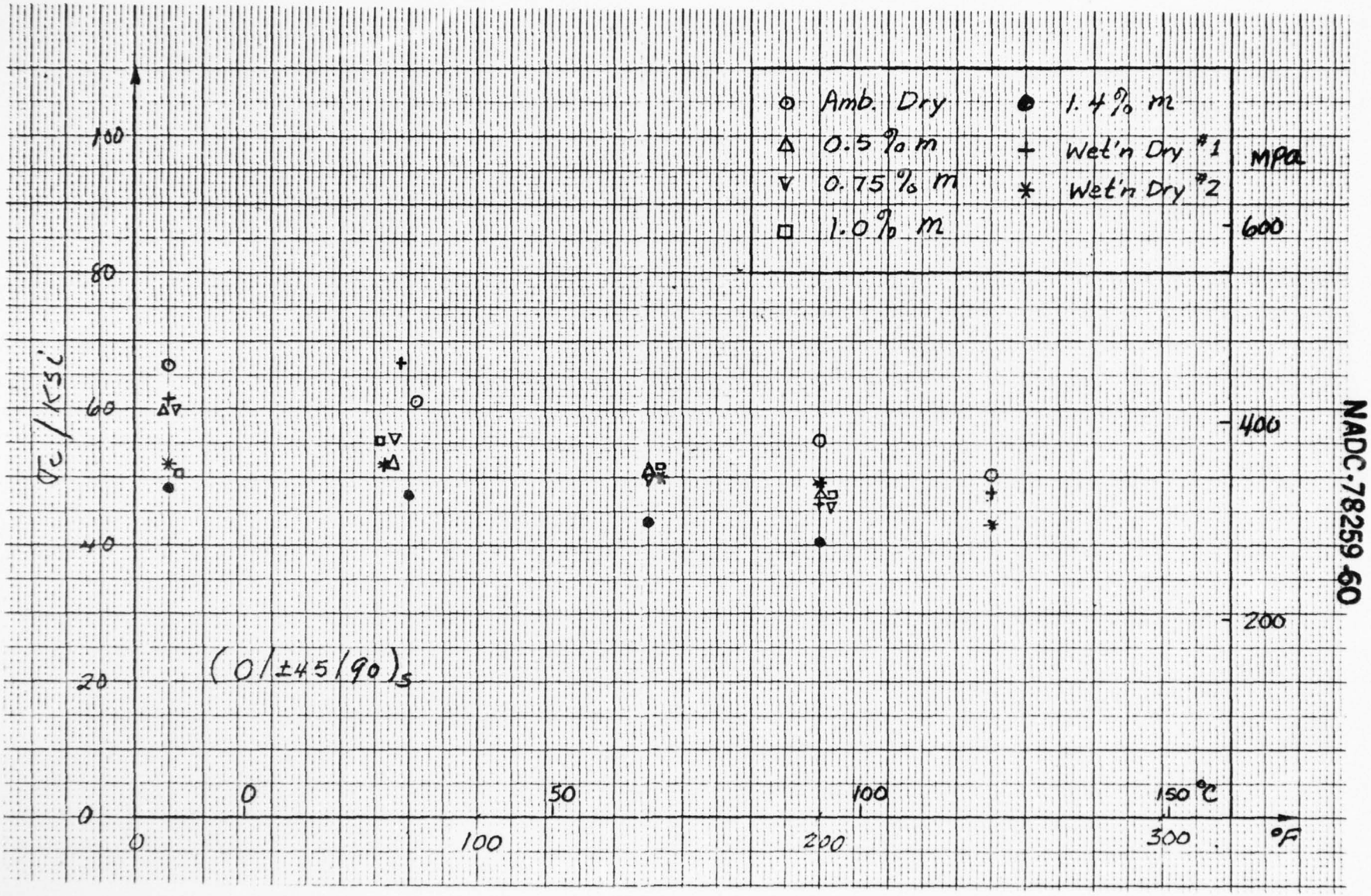

NADC-78259-60

Fig. 42 Compressive Strength versus Temperature for All Moisture Conditions--$(0/\pm45/90)_s$

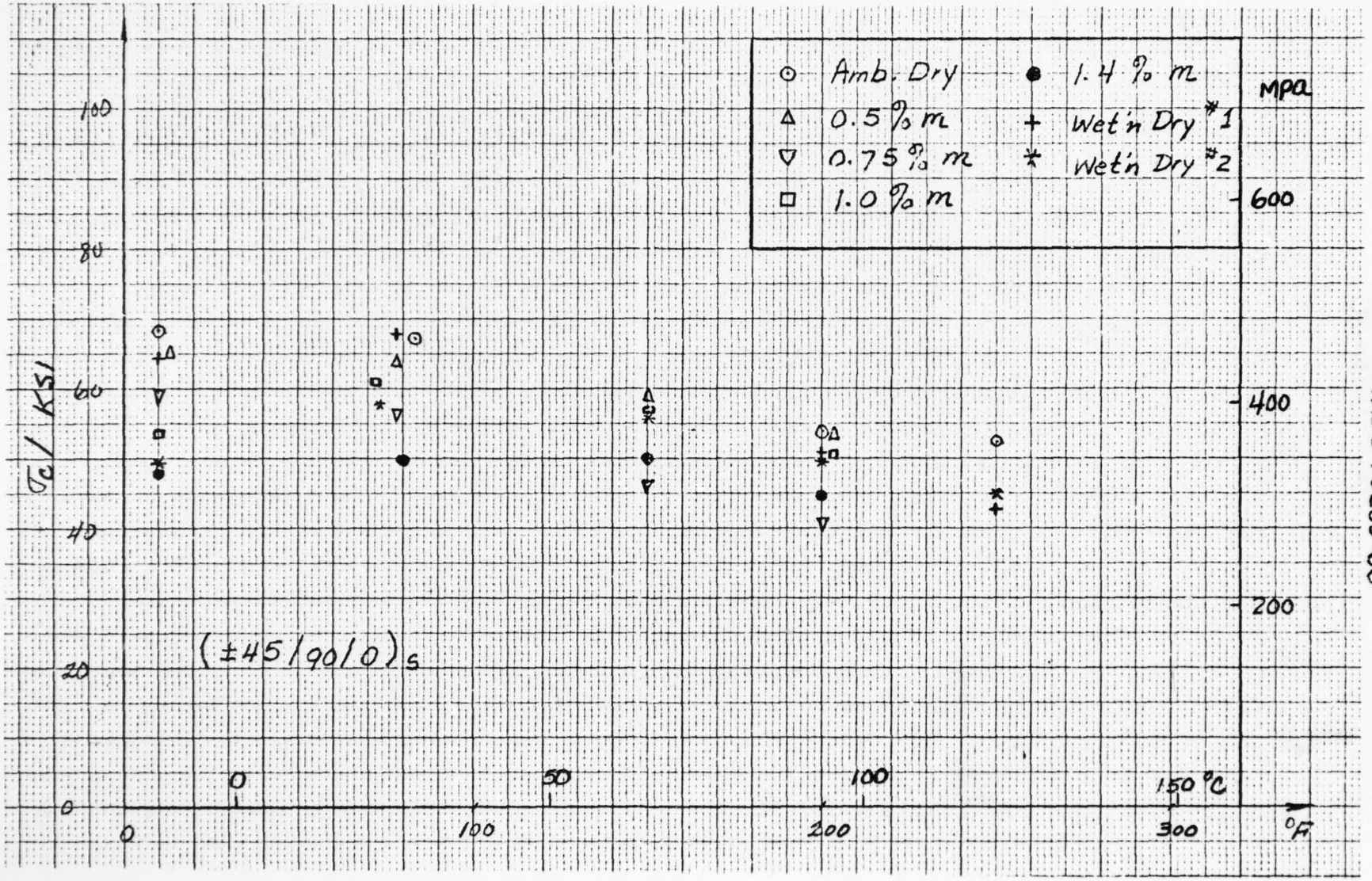

Fig. 43 Compressive Strength versus Temperature for All Moisture Conditions-- $(\pm 45/90/0)_s$

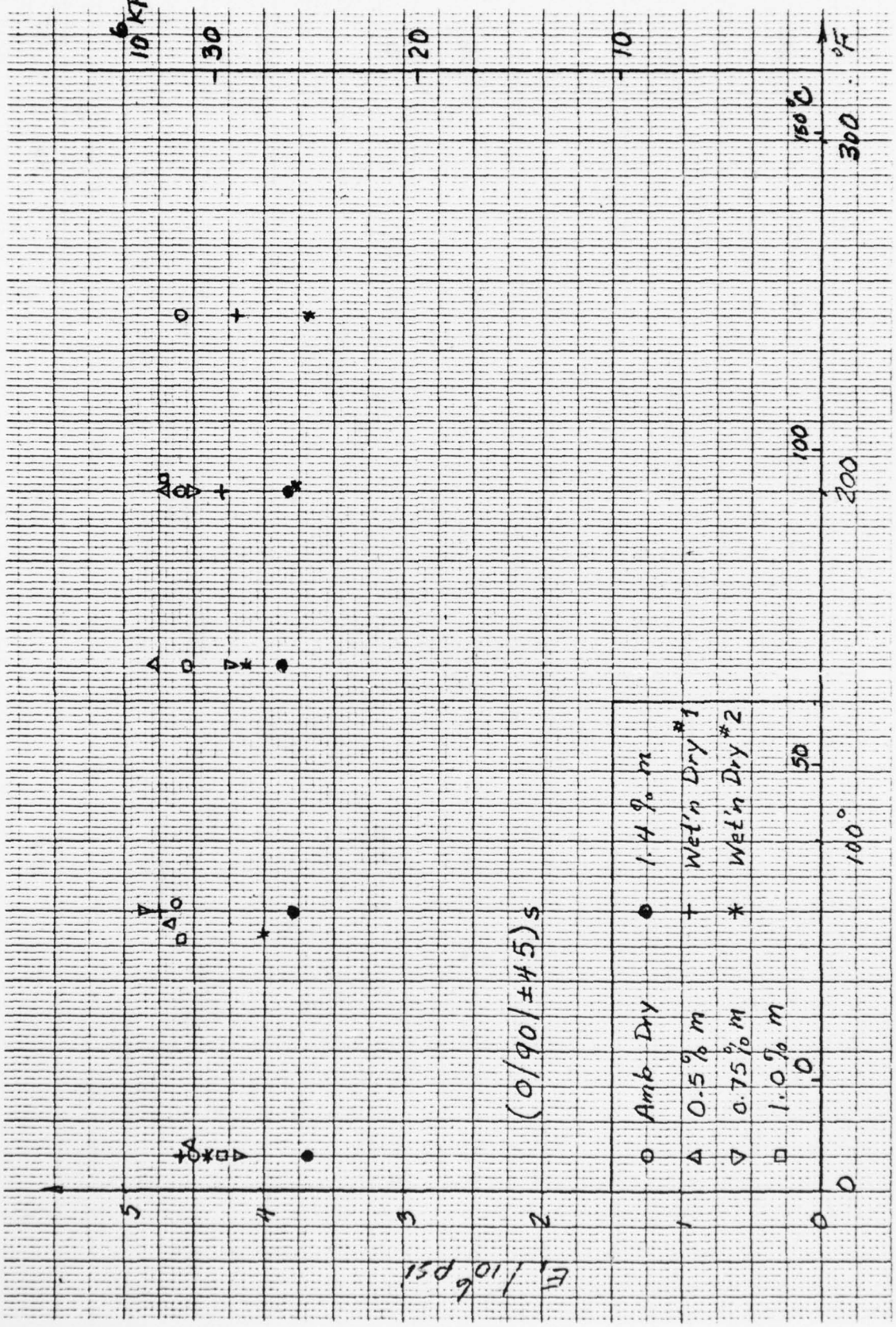

Fig. 44 Stiffness E_1 versus Temperature For All Moisture Conditions--$(0/90/\pm45)_s$

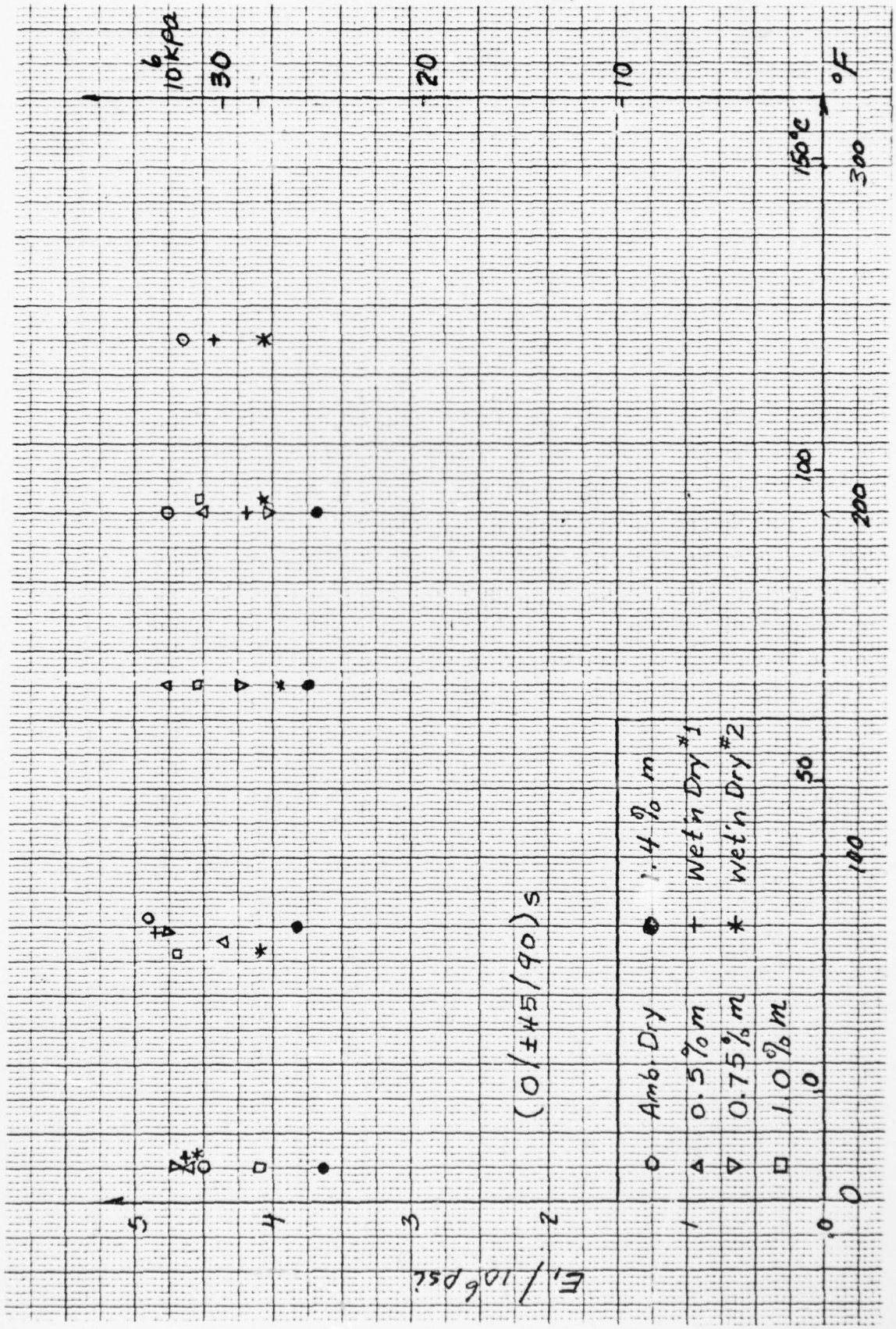

Fig. 45 Stiffness E_1 versus Temperature for All Moisture Conditions--(0/±45/90)$_s$

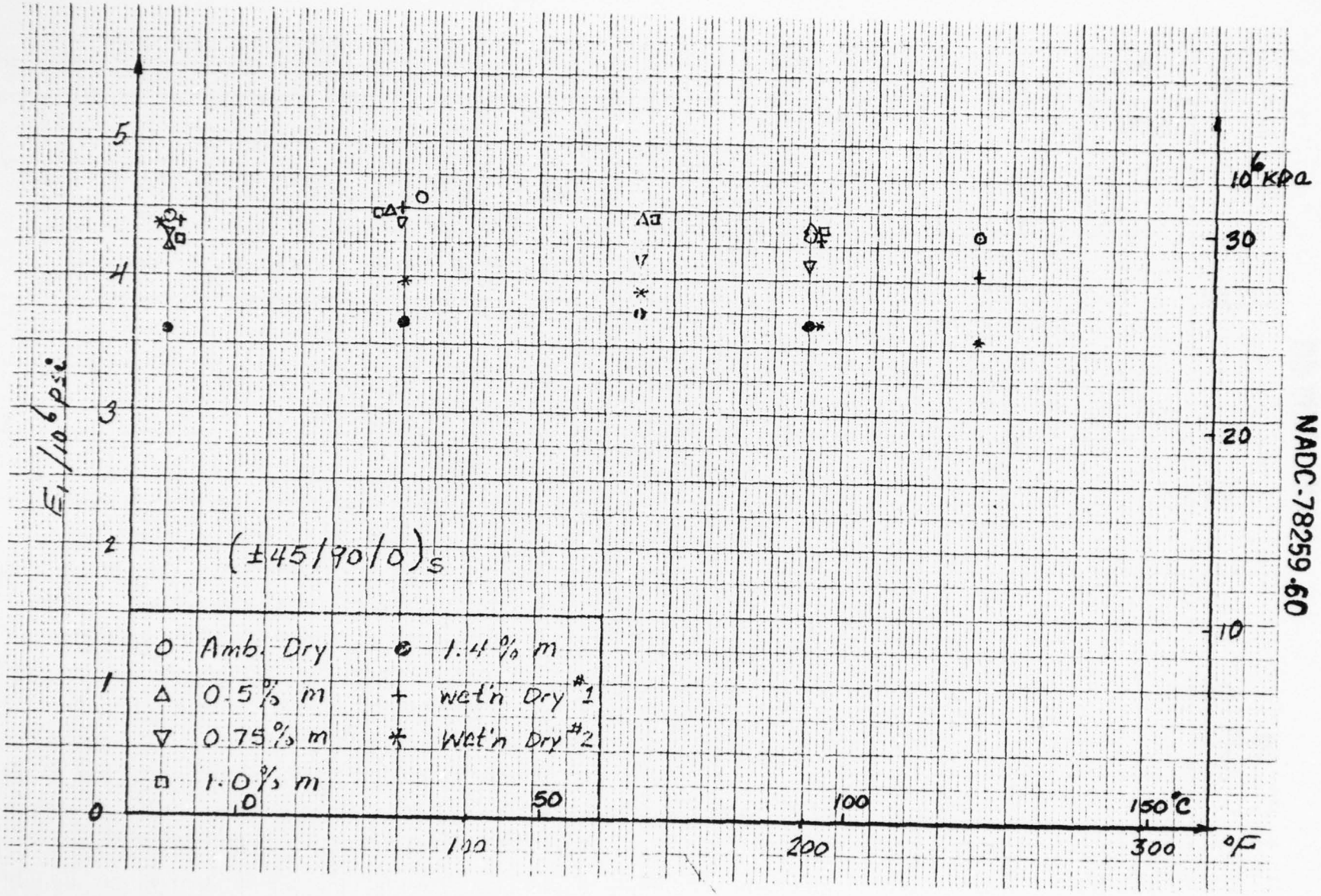

Fig. 46 Stiffness E_1 versus Temperature for All Moisture Conditions--$(\pm 45/90/0)_s$

DISTRIBUTION LIST

Government Activities

	No. of Copies
NAVAIRSYSCOM, AIR-954 (2 for retention), 2 for AIR-530, 1 for AIR-320B, AIR-52032D, AIR-5302, AIR-53021, AIR-530215).	9
AFFDL, WPAFB, OH 45433	
(Attn: FB/Mr. P. A. Parmley)	2
(Attn: FBC/Mr. C. Wallace)	1
(Attn: FBC/Mr. E. E. Zink)	1
AFML, WPAFB, OH 45433	
(Attn: LAM (Technical Library))	1
(Attn: LT-1/Mr. W. R. Johnston)	1
(Attn: LTF/Mr. T. Cordell)	1
(Attn: FBSC/Mr. L. Kelly)	1
(Attn: MAC/Mr. G. P. Peterson)	1
(Attn: MXA/Mr. F. J. Fechek)	1
(Attn: MBC/Mr. T. G. Reinhard, Jr.)	1
AFOSR, Washington, D.C. 20333	
(Attn: Mr. J. Pomerantz)	1
DDC	12
FAA, Airframes Branch, ES-120, Washington, D.C. 20553	
(Attn: Mr. J. Dougherty)	1
NASA (ADM), Washington, D.C. 20546	
(Attn: Secretary)	1
NASA, George C. Marshall Space Flight Center, Huntsville, AL 35812	
(Attn: S&E-ASTN-ES/Mr. E. E. Engler)	1
(Attn: S&E-ASTN-M/Mr. R. Schwinghamer)	1
(Attn: S&E-ASTM-MNM/Dr. J. M. Stuckey)	1
NASA, Langley Research Center, Hampton, VA 23365	
(Attn: Mr. J. P. Peterson, Mr. R. Pride, and Dr. M. Card)	3
NASA, Lewis Research Center, Cleveland, OH 44153	
(Attn: Technical Library, and M. Hershberg)	2
NAVPGSCHL, Monterey, CA 95940	
(Attn: Prof. R. Ball, Prof. M. H. Bank)	2
NAVSEASYSCOM, Washington, D.C. 20362	
(Attn: Code 035, Mr. C. Pohler)	1
NAVSEC, Hyattsville, MD 20782	
(Attn: Code 6101E03, Mr. W. Graner)	1
NAVSHIPRANDCEN, Bethesda, MD 20034	
(Attn: Code 173.2, Mr. W. P. Cauch)	1
NAVSHIPRANDCEN, Annapolis, MD 21402	
(Attn: Code 2870, Mr. H. Edelstein)	1
NOL, White Oak, MD 20910	
(Attn: Mr. F. R. Barnet)	1
NRL, Washington, D.C. 20375	
(Attn: Dr. I. Wolock)	1
ONR, Washington, D.C. 20362	
(Attn: Dr. N. Perrone)	1

Government Activities (Cont.)

PLASTEC, Picatinny Arsenal, Dover, NJ 07801
(Attn: Librarian, Bldg. 176, SARPA-FR-M-D and Mr. H. Pebly). . 2
Scientific & Technical Information Facility, College Park, MD
(Attn: NASA Representative). 1
USAAVMATLAB, Fort Eustis, VA 23603
(Attn: Mr. R. Beresford) 1
USAMATRESAG, Watertown, MA
(Attn: Dr. E. Lenoe) 1
USARESOFC, Durham, NC 27701 1

Non-Government Agencies

Avco Aero Structures Division, Nashville, TN 37202
(Attn: Mr. W. Ottenville). 1
Battelle Columbus Laboratories, Metals and Ceramics Information
Center, 505 King Avenue, OH 43201. 1
Bell Aerospace Company, Buffalo, NY 14240
(Attn: Zone I-85, Mr. F. M. Anthony) 1
Bell Helicopter Company, Fort Worth, TX 76100
(Attn: Mr. Charles Harvey) 1
Bendix Products Aerospace Division, South Bend, IN 46619
(Attn: Mr. R. V. Cervelli) 1
Boeing Aerospace Company, P.O. Box 3999, Seattle, WA 98124
(Attn: Code 206, Mr. R. E. Horton) 1
Boeing Company, Renton, Washington 98055
(Attn: Dr. R. June). 1
Boeing Company, Vertol Division, Phila., PA 19142
(Attn: Mr. R. L. Pinckney, Mr. D. Hoffstedt) 2
Boeing Company, Wichita, KS 67210
(Attn: Mr. V. Reneau/MS 16-39) 1
Cabot Corporation, Billerica Research Center, Billerica, MA
01821 1
Drexel University, Phila., PA 19104
(Attn: Dr. P. C. Chou) 1
E.I. DuPont Company, Wilmington, DE 19898
(Attn: Dr. Carl Zweben) Bldg. 262/Room 316 1
Fairchild Industries, Hagerstown, MD 21740
(Attn: Mr. D. Ruck). 1
Georgia Institute of Technology, Atlanta, GA
(Attn: Prof. W. H. Horton) 1
General Dynamics/Convair, San Diego, CA 92138
(Attn: Mr. D. R. Dunbar, W. G. Scheck) 2
General Dynamics, Fort Worth, TX 76101
(Attn: Mr. P. D. Shockey, Dept. 23, Mail Zone P-46). 1
General Electric Company, Phila., PA 19101
(Attn: Mr. L. McCreight) 1
Great Lakes Carbon Corp., N.Y., NY 10017
(Attn: Mr. W. R. Benn, Mgr., Markey Development) 1
Grumman Aerospace Corporation, Bethpage, L.I., NY 11714
(Attn: Mr. R. Hadcock, Mr. S. Dastin). 2

Non-Government Agencies (Cont.)

Hercules Powder Company, Inc., Cumberland, MD 21501
(Attn: Mr. D. Hug) 1
H. I. Thompson Fiber Glass Company, Gardena, CA 90249
(Attn: Mr. N. Myers) 1
ITT Research Institute, Chicago, IL 60616
(Attn: Mr. K. Hofar) 1
J. P. Stevens & Co., Inc., N.Y., NY 10036
(Attn: Mr. H. I. Shulock). 1
Kaman Aircraft Corporation, Bloomfield, CT 06002
(Attn: Tech. Library). 1
Lehigh University, Bethlehem, PA 18015
(Attn: Dr. G. C. Sih). 1
Lockheed-California Company, Burbank, CA 91520
(Attn: Mr. E. K. Walker, R. L. Vaughn) 2
Lockheed-Georgia Company, Marietta, GA
(Attn: Advanced Composites Information Center, Dept. 72-14, Zone 42). 1
LTV Aerospace Corporation, Dallas, TX 75222
(Attn: Mr. O. E. Dhonau/2-53442, C. R. Foreman). 2
Martin Company, Baltimore, MD 21203
(Attn: Mr. J. E. Pawken) 1
Materials Sciences Corp., Blue Bell, PA 19422 1
McDonnell Douglas Corporation, St. Louis, MO 63166
(Attn: Mr. R. C. Goran, O. B. McBee, C. Stenberg). 3
3 McDonnell Douglas Corporation, Long Beach, CA 90801
(Attn: H. C. Schjulderup, G. Lehman) 2
Minnesota Mining and Manufacturing Company, St. Paul, MN 55104
(Attn: Mr. W. Davis) 1
Northrop Aircraft Corp., Norair Div., Hawthorne, CA 90250
(Attn: Mr. R. D. Hayes, J. V. Noyes, R. C. Isemann). 3
Rockwell International, Columbus, OH 43216
(Attn: Mr. O. G. Acker, K. Clayton). 2
Rockwell International, Los Angeles, CA 90053
(Attn: Dr. L. Lackman) 1
Rockwell International, Tulsa, OK 74151
(Attn: Mr. E. Sanders, Mr. J. H. Powell) 2
Owens Corning Fiberglass, Granville, OH 43023
(Attn: Mr. D. Mettes). 1
Rohr Corporation, Riverside, CA 92503
(Attn: Dr. F. Riel and Mr. R. Elkin) 2
Ryan Aeronautical Company, San Diego, CA 92112
(Attn: Mr. R. Long). 1
Sikorsky Aircraft, Stratford, CT 06497
(Attn: Mr. J. Ray) 1
University of Oklahoma, Norman, OK 93069
(Attn: Dr. G. M. Nordby) 1
Union Carbide Corporation, Cleveland, OH 44101
(Attn: Dr. H. F. Volk) 1

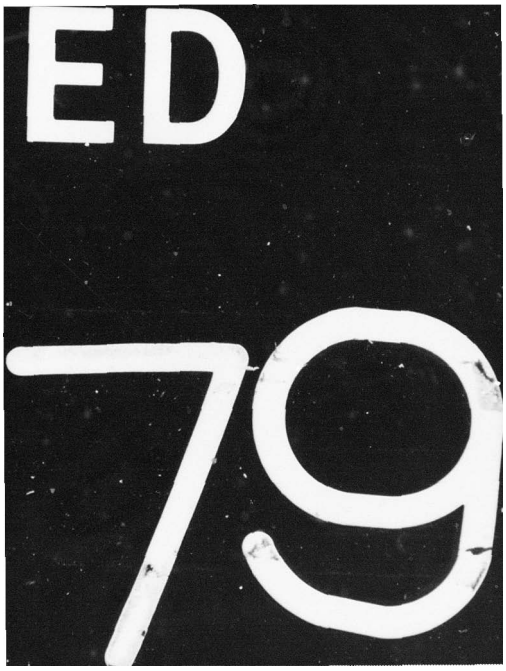
ED
79